

CAPITAL UNIVERSITY OF SCIENCE AND
TECHNOLOGY, ISLAMABAD



**Heat and Mass Transfer Analysis
in Newtonian and non-Newtonian
Fluids Using Finite Difference
Approach**

by

Naveed Akmal

A thesis submitted in partial fulfillment for the
degree of Doctor of Philosophy

in the

Faculty of Computing

Department of Mathematics

2021

Heat and Mass Transfer Analysis in Newtonian and non-Newtonian Fluids Using Finite Difference Approach

By

Naveed Akmal

(DMT 143009)

Dr. Mohammad Mehdi Rashidi, Professor

Tongji University, Shanghai, **China**

(Foreign Evaluator 1)

Dr. Oulwole Daniel Makinde, Professor

Stellenbosch University, Saldanha, **South Africa**

(Foreign Evaluator 2)

Dr. Muhammad Sagheer

(Supervisor)

Dr. Muhammad Sagheer

(Head, Department of Mathematics)

Dr. Muhammad Abdul Qadir

(Dean, Faculty of Computing)

**DEPARTMENT OF MATHEMATICS
CAPITAL UNIVERSITY OF SCIENCE AND TECHNOLOGY
ISLAMABAD**

2021

Copyright © 2021 by Naveed Akmal

All rights reserved. No part of this thesis may be reproduced, distributed, or transmitted in any form or by any means, including photocopying, recording, or other electronic or mechanical methods, by any information storage and retrieval system without the prior written permission of the author.

Dedicated to my Parents, wife and children



**CAPITAL UNIVERSITY OF SCIENCE & TECHNOLOGY
ISLAMABAD**

Expressway, Kahuta Road, Zone-V, Islamabad
Phone: +92-51-111-555-666 Fax: +92-51-4486705
Email: info@cust.edu.pk Website: <https://www.cust.edu.pk>

CERTIFICATE OF APPROVAL

This is to certify that the research work presented in the thesis, entitled “**Heat and Mass Transfer Analysis in Newtonian and Non-Newtonian Fluids using Finite Difference Approach**” was conducted under the supervision of **Dr. Muhammad Sagheer**. No part of this thesis has been submitted anywhere else for any other degree. This thesis is submitted to the **Department of Mathematics, Capital University of Science and Technology** in partial fulfillment of the requirements for the degree of Doctor in Philosophy in the field of **Mathematics**. The open defence of the thesis was conducted on **June 01, 2021**.

Student Name : Naveed Akmal (DMT143009)



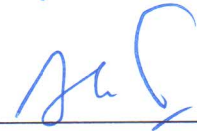
The Examining Committee unanimously agrees to award PhD degree in the mentioned field.

Examination Committee :

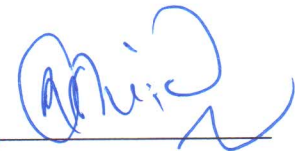
(a) External Examiner 1: Dr. Qazi Mahmood
Associate Professor
University of Wah, Wah Cantt




(b) External Examiner 2: Dr. Ahmer Mahmood,
Associate Professor
IIU, Islamabad




(c) Internal Examiner : Dr. Rashid Ali
Associate Professor
CUST, Islamabad



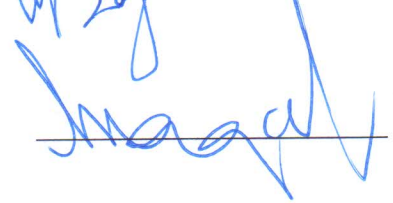
Supervisor Name : Dr. Muhammad Sagheer
Professor
CUST, Islamabad



Name of HoD : Dr. Muhammad Sagheer
Professor
CUST, Islamabad



Name of Dean : Dr. Muhammad Abdul Qadir
Professor
CUST, Islamabad



AUTHOR'S DECLARATION

I, **Naveed Akmal (Registration No. DMT-143009)**, hereby state that my PhD thesis entitled, '**Heat and Mass Transfer Analysis in Newtonian and Non-Newtonian Fluids using Finite Difference Approach**' is my own work and has not been submitted previously by me for taking any degree from Capital University of Science and Technology, Islamabad or anywhere else in the country/ world.

At any time, if my statement is found to be incorrect even after my graduation, the University has the right to withdraw my PhD Degree.



(Naveed Akmal)

Dated: June, 2021

Registration No : DMT-143009

PLAGIARISM UNDERTAKING

I solemnly declare that research work presented in the thesis titled “**Heat and Mass Transfer Analysis in Newtonian and Non-Newtonian Fluids using Finite Difference Approach**” is solely my research work with no significant contribution from any other person. Small contribution/ help wherever taken has been duly acknowledged and that complete thesis has been written by me.

I understand the zero tolerance policy of the HEC and Capital University of Science and Technology towards plagiarism. Therefore, I as an author of the above titled thesis declare that no portion of my thesis has been plagiarized and any material used as reference is properly referred/ cited.

I undertake that if I am found guilty of any formal plagiarism in the above titled thesis even after award of PhD Degree, the University reserves the right to withdraw/ revoke my PhD degree and that HEC and the University have the right to publish my name on the HEC/ University Website on which names of students are placed who submitted plagiarized thesis.



(Naveed Akmal)

Dated: June, 2021

Registration No : DMT-143009

List of Publications

It is certified that the following publication(s) have been made out of the research work that has been carried out for this thesis:-

1. **N. Akmal**, M. Sagheer, and S. Hussain, “Numerical study focusing on the entropy analysis of MHD squeezing flow of a nanofluid model using Cattaneo–Christov theory,” *AIP Advances*, vol. 8(5), pp. 055201, 2018.
2. **N. Akmal**, M. Sagheer, S. Hussain and A. Kamran “Study of micropolar nanofluids with power-law spin gradient viscosity model by the Keller box method,” *Canadian Journal of Physics*, vol. 98(1), pp. 16–27, 2020.
3. **N. Akmal**, M. Sagheer, S. Hussain and A. Kamran “Investigation of free convection in micropolar nanofluid with induced magnetic field,” *The European Physical Journal Plus*, vol. 235(5), pp. 1–12, 2019.

Naveed Akmal

(DMT 143009)

Acknowledgement

First and foremost, I would like to thank Almighty **Allah Talah** for giving me the strength, knowledge, ability and opportunity to undertake this research study and to persevere and complete it satisfactorily. Without his blessings, this achievement would not have been possible. Peace and blessings to **Hazrat Muhammad (SAW)** who guides us the right path, who is forever a torch of guidance and knowledge for the mankind.

I am grateful to and acknowledge the efforts of my erudite supervisor **Dr. Muhammad Sagheer** for his valuable suggestions and guidance during the PhD research work. His experience, tremendous cooperation and valuable comments enabled me to complete my dissertation successfully. I would appreciate the painstaking attitude of my supervisor. I am also thankful and pay my gratitude to **Dr. Shafqat Hussain** who always guided through his valuable technical suggestions to improve the quality of the research work.

I am grateful to all my PhD fellows who helped me in my work, especially **Mr. Abid Kamran** who helped me a lot in my PhD work, without which it would not be possible for me to complete it.

I express my devoted affection to all my family members for creating a delightful atmosphere and excusing me from family duties in order to complete the research.

Abstract

This dissertation is an attempt to analyze the heat and mass transfer in Newtonian and non-Newtonian nanofluids flowing in different physical channels and sheets. The non-Newtonian nanofluid models of micropolar fluids are employed to highlight the thermal transportation in such fluids. Single phase nanofluid model; Tiwari-Das and Buongiorno nanofluid models are used in the study. Water is used as the base fluid in single phase models and the nanoparticles used are Cu and Al_2O_3 . Magnetic field is used to influence the nanofluid flow and its impact on the heat transfer is observed. The application of magnetic field prompts Joule heating effect which is added to the mathematical modeling of the models. Also viscous dissipation effect is considered in all the three problems to find out the internal heat generated during the movement of the fluid. An additional equation of angular momentum is used to observe the impact of microstructures present in the micropolar fluid. The Maxwell equations of electromagnetism are included to tackle the induced magnetic field effects. Other aspects of the study involve convective boundary conditions and the induced magnetic field effects. The governing equations of mathematical models are nondimensionalized into the ordinary differential equations by applying suitable similarity transformations. The system of ordinary equations are then solved by a valuable finite difference scheme called the Keller box method. The Matlab code for Keller box method is developed and its verification is done by reproducing the work already published in different journals. The numerical results are analyzed by variation in important parameters using line, 3D graphs and tables of numerical values.

It is observed that an increase in the volume fraction of nanoparticles decreases the temperature of the nanofluid flowing between two parallel plates with upper plate moving vertically and lower plate stretching horizontally. Greater Brownian motion of the nanoparticles rises the temperature but decreases the concentration of the nanofluids, in a flow of micropolar nanofluid pertaining over a stretching sheet. However for a flow of micropolar nanofluid between parallel plates, the linear as well as the angular velocity of the nanofluid diminishes with a rise in the

rotational viscosity parameter.

Key Words:

Nanofluids, Tiwari-Das and Buongiorno nanofluid models, viscous dissipation, magnetohydrodynamics, parallel plates, Keller box method.

Contents

Author’s Declaration	v
Plagiarism Undertaking	vi
List of Publications	vii
Acknowledgement	viii
Acknowledgement	viii
Abstract	ix
List of Figures	xiv
List of Tables	xvii
Symbols	xviii
1 Introduction	1
1.1 Motivation	1
1.2 Advent of Nanofluids	2
1.3 Experimental Verses Mathematical Approach for Nanofluids	3
1.4 Single Verses Two Phase Nanofluid Models	6
1.5 Role of Magnetohydrodynamics in Heat Transfer Enhancement	7
1.6 Non-Newtonian Fluids	8
1.7 Heat Transfer in Boundary Layer Flow	9
1.8 Objective of the Thesis	9
1.9 Chapter-wise Breakdown of Thesis	10
2 Preliminaries and Solution Methodology	11
2.1 Fluid	11
2.2 Nanofluid	13
2.3 Micropolar Fluid	14
2.4 Heat Transfer	15
2.4.1 Conduction	16
2.4.2 Convection	16

2.4.3	Radiation	17
2.5	Differential Operators	18
2.6	Substantial Derivative	19
2.7	Equations of Motion for Flow Model	21
2.7.1	Equation of Continuity	21
2.7.2	Momentum Equation	21
2.7.3	Energy Equation	22
2.8	Second Law of Thermodynamics	23
2.9	Cattaneo–Christov Theory	24
2.10	Body Forces	25
2.10.1	Squeezing Flow	25
2.10.2	Magnetohydrodynamics (MHD)	25
2.10.3	Free Convection	26
2.11	Single Phase Nanofluid Models	26
2.11.1	Buongiorno Model	27
2.11.2	Tiwari–Das Model	28
2.12	Thermal Dispersion Model	29
2.13	Boundary Layer Flow	30
2.14	Entropy	30
2.15	Physical Quantities	31
2.15.1	Hartmann Number	31
2.15.2	Rotational Viscosity Parameter	31
2.15.3	Reynolds Number	32
2.15.4	Prandtl Number	32
2.15.5	Eckert Number	32
2.15.6	Thermophoresis Parameter	32
2.15.7	Brownian Motion Parameter	33
2.15.8	Bejan Number	33
2.15.9	Skin Friction Coefficient	34
2.15.10	Nusselt Number	34
2.15.11	Sherwood Number	34
2.16	Keller Box Method	34
3	MHD Squeezing Flow of a Nanofluid Model Using Cattaneo–Christov Theory	40
3.1	Introduction	40
3.2	Mathematical Formulation	41
3.3	Solution Methodology	45
3.4	Discussion on Results	46
3.5	Conclusion	59
4	Study of Micropolar Nanofluids with Power-law Spin Gradient Viscosity Model	61
4.1	Introduction	61
4.2	Mathematical Formulation	62

4.3	Solution Methodology	65
4.4	Discussion on Results	71
4.5	Conclusion	86
5	Investigation of Free Convection in Micropolar Nanofluid with Induced Magnetic Field	87
5.1	Introduction	87
5.2	Mathematical Formulation	88
5.3	Solution Methodology	91
5.4	Discussion on Results	94
5.5	Conclusion	113
6	Conclusion and Future Work	114
6.1	Conclusion	114
6.2	Future Work	116
	Bibliography	117

List of Figures

2.1	Shear stress for three types of fluids that is Pseudoplastic($n > 1$), Newtonian($n = 1$) and Dilatants($n < 1$)	12
2.2	Conduction, convection and radiation	17
2.3	Motion of particle in flow field	19
2.4	Cornet Engine	24
2.5	Flow model of the problem	38
3.1	Schematic diagram of flow model	41
3.2	Impact of sq on f'	50
3.3	Impact of $-sq$ on f'	51
3.4	Impact of sq on θ	51
3.5	Impact of sq on Ng	52
3.6	Impact of $-sq$ on Ng	52
3.7	Impact of sq on Be	53
3.8	Impact of $-sq$ on Be	53
3.9	Impact of β_e on θ	54
3.10	Impact of Ec_x on θ	54
3.11	Impact of Ec_x on Ng	55
3.12	Impact of Ec_x on Be	55
3.13	Impact of M on f'	56
3.14	Impact of M on θ	56
3.15	Impact of M on Ng	57
3.16	Impact of M on Be	57
3.17	Impact of ϕ_1 on θ	58
3.18	Impact of ϕ_1 on Ng	58
3.19	Impact of ϕ_1 on Be	59
4.1	Flow model of the problem	63
4.2	Flow Chart: Keller box method	66
4.3	Variation in θ subject to Nb	75
4.4	Variation in ϕ subject to Nb	75
4.5	Variation in θ subject to Nt	76
4.6	Variation in ϕ subject to Nt	76
4.7	Variation in θ subject to Pr	77
4.8	Variation in ϕ subject to Pr	77
4.9	Variation in ϕ subject to Sc	78

4.10	Variation in f' subject to K .	78
4.11	Variation in R subject to K .	79
4.12	Variation in θ subject to K .	79
4.13	Variation in ϕ subject to K .	80
4.14	Variation in f' subject to n .	80
4.15	Variation in R subject to n .	81
4.16	Variation in θ subject to n .	81
4.17	Variation in ϕ subject to n .	82
4.18	Variation in θ subject to Ec .	82
4.19	Stream lines for $n = 0.75$.	83
4.20	Stream lines for $n = 0.85$.	83
4.21	Stream lines for $n = 1.0$.	84
4.22	Stream lines for $K = 0.0$.	84
4.23	Stream lines for $K = 0.5$.	85
4.24	Stream lines for $K = 1.0$.	85
5.1	Schematic diagram of the flow model	88
5.2	Impact of Brownian motion parameter Nb on Sherwood number	98
5.3	Impact of Thermophoresis parameter Nt on Sherwood number	98
5.4	Impact of Schmidt number Sc on Sherwood number	99
5.5	Impact of Hartmann number M on the velocity.	99
5.6	Impact of Hartmann number M on the angular momentum.	100
5.7	Impact of Hartmann number M on the induced magnetic field.	100
5.8	Impact of rotation parameter K on the velocity.	101
5.9	Impact of rotation parameter K on the angular momentum.	101
5.10	Impact of rotation parameter K on the induced magnetic field.	102
5.11	Impact of buoyancy ratio Br on the velocity.	102
5.12	Impact of buoyancy ratio Br on the angular momentum.	103
5.13	Impact of buoyancy ratio Br on the induced magnetic field.	103
5.14	Impact of magnetic Prandtl number Pm on the velocity.	104
5.15	Impact of magnetic Prandtl number Pm on the momentum.	104
5.16	Impact of magnetic Prandtl number Pm on the induced magnetic field.	105
5.17	Impact of Schmidt number Sc on the temperature.	105
5.18	Impact of Schmidt number Sc on the concentration.	106
5.19	Impact of suction parameter V_0 on the velocity.	106
5.20	Impact of suction parameter V_0 on the angular momentum.	107
5.21	Impact of suction parameter V_0 on the induced magnetic field.	107
5.22	Impact of suction parameter V_0 on the temperature.	108
5.23	Impact of Brownian motion parameter Nb on the temperature.	108
5.24	Impact of Brownian motion parameter Nb on the concentration.	109
5.25	Impact of thermophoresis parameter Nt on the velocity.	109
5.26	Impact of thermophoresis parameter Nt on the angular momentum.	110

5.27	Impact of thermophoresis parameter Nt on the induced magnetic field.	110
5.28	Impact of thermophoresis parameter Nt on the concentration.	111
5.29	Skin friction as a function of Pm and K for $Pr = 10$, $M = 5$, $V_0 = 1$, $Nt = 0.1$, $Br = 1$, $Sc = 1$	111
5.30	Skin friction as a function of Pm and V_0 for $Pr = 10$, $M = 5$, $K = 1$, $Nt = 0.1$, $Br = 1$, $Sc = 1$	112
5.31	Nusselt number as a function of Pr and V_0 for $Pm = 1$, $M = 5$, $K = 1$, $Nt = 0.1$, $Br = 1$, $Ec = 0.4$, $Sc = 1$	112

List of Tables

2.1	Thermophysical properties of the base fluid and nanoparticles. . . .	29
3.1	Thermophysical properties of the base fluid and nanoparticles. . . .	45
3.2	For different values of S and for fixed values of $Pr = Ec = 1$ and $\delta = 0.1$	46
3.3	Reduced Nusselt number and skin friction coefficient for copper–water and alumina–water when $Pr = 6.2$	47
4.1	Values of Nusselt and Sherwood numbers for different values of h and η_∞	66
4.2	Nusselt number for different values of Nt, M, α and Pr and for the fixed values of parameters $\gamma = 0.25, Nb = 0.5$ and $Sc = 10$	71
4.3	Nusselt number and Sherwood number corresponding to different values of parameters.	72
5.1	Values of reduced Nusselt number, skin friction coefficient and Sherwood number corresponding to different values of step size	91
5.2	Comparison of the present skin friction coefficient results to the previous results	93
5.3	Impact of pertinent parameters on the Nusselt number with $M = 5, Pm = 0.8, K = 1, Br = 1$	94
5.4	Impact of pertinent parameters on the skin friction with $Ec = 0.4, Nb = 0.1, Nt = 0.1, Sc = 1, Pr = 10$	95

Symbols

∇	nabla
α	thermal diffusivity (m ² /sec)
β	thermal expansion coefficient (1/K)
β_c	concentration expansion coefficient
β_e	non-dimensional form of relaxation time of heat flux
γ	spin gradient viscosity (m ² /sec)
δ_E	relaxation time of heat flux
δ_{el}	electrical conductivity (S/m)
η	dimensionless coordinate
θ	nondimensional temperature
κ^*	rotation viscosity (rad/sec)
κ	thermal conductivity of the fluid (W/(m.K))
λ_0	thermal relaxation time (sec)
λ_E	diffusive parameter (m ² /sec)
μ_f	plastic dynamic viscosity of fluid (kg/(m.sec))
μ_e	magnetic permeability (N/A ²)
$\mu_0 N ^{n-1}$	apparent dynamic viscosity (kg/(m.sec))
ν_{nf}	kinetic viscosity of nanofluid (m ² /sec)
ν	kinetic viscosity ((m ² /sec)
ρ	fluid density (kg/m ³)
σ	dimensional constant (1/sec)
τ_1	fraction of nanoparticles effective heat capacity to that of material in the base fluid

ϕ	dimensionless concentration
ϕ_1	volumetric fraction of nanoparticles
Ψ	stream function
Ω	dimensionless temperature difference
b_0	constant magnetic field (tesla)
b_G	buoyancy force (N)
b_x	dimensional induced magnetic field (tesla)
c_p	specific heat at constant pressure (J / (kg.K))
f'	dimensionless velocity
j	micro inertia per unit mass (m ²)
k_{nf}	thermal conductivity of nanofluid (W/(m.K))
k	flow consistence
$k_0 N ^{n-1}$	vortex viscosity (m ² /sec)
n	power-law index
p	pressure (Pa)
q_m	mass flux (Kg/sec)
q_w	heat flux (W/m ²)
sq	squeezing parameter
\vec{u}	dimensional velocity vector (m/sec)
u	component of velocity in x direction (m/sec)
v_0	dimensional suction velocity (m/sec)
v	component of velocity in y direction (m/sec)
\mathbf{B}	magnetic field vector
Br	buoyancy ratio
B_x	nondimensional induced magnetic field
C	concentration of nano-particles (mg/L)
C_{fx}	local skin friction
C_f	skin friction
C_w	concentration of fluid on the sheet
C_∞	ambient concentration
D_B	coefficient of Brownian diffusion (mg/L)

D_T	thermophoretic diffusion coefficient
Ec	Eckert number
Ec_x	local Eckert number
J	current density (A/m ²)
M	Hartmann number
K	dimensionless viscosity ratio
N	angular velocity in xy plane (rad/sec)
Nb	Brownian motion parameter
Ng	entropy generation number
Nt	thermophoresis parameter
Nu	reduced Nusselt number
Pm	magnetic Prandtl number
Pr	Prandtl number
R	dimensionless angular velocity
Re	Reynolds number
Re_x	local Reynolds number
S_0'''	characteristic entropy generation (J/(mol.K))
S_{gen}'''	actual entropy generation rate (J/(mol.K))
S_1	thermal stratification
Sh_x	local Sherwood number
Sh	Sherwood number
T	fluid temperature (K)
T_∞	ambient temperature (K)
T_w	temperature on lower plate (K)
T_h	temperature on upper plate (K)
U	dimensionless velocity
U_w	characterized velocity
V	velocity of fluid (m/sec)
V_h	velocity of upper plate (m/sec)
V_0	suction velocity (m/sec)
Y	dimensionless variable

Chapter 1

Introduction

In this chapter, we have expounded different basic terms relevant to this thesis, following the motivation implications of advent of nanofluids on the industry and other disciplines. A discussion on the experimental and mathematical approach of the nanofluid models is also presented. Some single and two phase models of the nanofluids are discussed. The role of magnetohydrodynamics (MHD) in heat transfer enhancement is explained. The non-Newtonian fluids' importance is elaborated in detail in the chapter. The importance of boundary layer theory and the heat transfer in it is narrated as well. The chapter is concluded with an explanation of the objectives and deliberation of the structure of the thesis.

1.1 Motivation

Enhancing the rate of heat transfer in the mechanical processes has always been considered as a big deal. As it is very important for the whole system that heat radiates rapidly into the space as soon as it is generated to safeguard the system, several methods, like application of heat sinks, use of conventional fluids like oil, ethylene glycol and water are used to make the system cool.

In the present work rate of heat transfer is discussed which is the need of time and is of great deal of importance. Three different articles are presented in this

dissertation to discuss the transfer of heat exchange in micropolar and nano fluids. Different results are presented for radiating the heat from the system which justifies the impotence of present work. Many experiments have been performed and these experiments reveal that higher thermal conductivity of the solids make them feasible for addition to such fluids. Solids are scaled down to nano scale to construct a class of heat transfer fluids called the nanofluids. With the advent of nanofluids in the 1995, nanofluids have revolutionized the heat exchange rate of the system.

1.2 Advent of Nanofluids

The idea of adding the solid particles to the liquids is very old. It was Maxwell who first introduced this idea in 1881. He added micro/millimeter sized particles in the base fluids in order to enhance the capability of the base fluids. Since those solid particles were large in size so they settled down at the bottom of the container and caused clogging, erosion, high pressure drop and sedimentation, hence the idea failed.

The idea could only be implemented if the size of solid particles was to be smaller than the micrometer size. Work started on development of the nanosized particles of the heat conducting solid elements in the industry. Many researchers used nanoparticles of the solid metals to produce the fluids with nanosized particles of the metals.

In 1993, Masuda *et al.* [1] measured the thermal conductivity and viscosity of the water based suspension of Al_2O_3 , SiO_2 and TiO_2 nanoparticles. It is found that the thermal conductivity as well as the viscosity of the water increases with the addition of these three type of nanoparticles. In 1995, Choi *et al.* [2] performed an experiment in the Argonne laboratory and prepared such fluids by mixing copper nanoparticles to water and named it as nanofluids. It was the Choi who first called these fluids as nanofluids. After the manufacturing of nanofluids, many researches have been performed on these type of fluids with the focus on swift cooling in the

industry.

1.3 Experimental Verses Mathematical Approach for Nanofluids

Experimentally nanofluids are prepared in the laboratory. Nanofluids can be prepared by two different methods [3]. One of them is called single while the other is two-step method. In single step method direct evaporation technique is used on the nanofluid to disperse the metal nanoparticles. Under vacuum conditions vaporization of the source metal is taking place. In two step method first of all in the presence of inert gas or chemical deposition is used to produce the nanotubes or nanoparticles as the dry powder. Then in the second step the dry nanoparticles are mixed in the base fluid. To minimize the accumulation of particles surfactants are added or ultrasonic techniques are used.

Peyghambarzadeh *et al.* [4] performed the experimental work on the car radiator in order to investigate the cooling effect of Fe_2O_3 and CuO nanofluids as compared with the conventional fluids like water and they found that the thermal conductivity enhances with the use of these fluids. In the formation of the nanofluids they did not use any kind of surfactants and in order to make the fluids stable they keep the PH of the fluids constant at 11.1 and 10.1 respectively. Under the laminar flow regime, Naraki *et al.* [5] did the experimentation on CuO -water and found that the thermal heat conductivity was enhanced. In order to obtain a stable nanofluid, a Surfactant was used. The highest stability was achieved with 0.2 wt% sodium dodecyl sulfonate and 10.1 PH among all the prepared solutions. Due to a decrease in the specific heat of fluid, the heat transfer coefficient was decreased. An experimental study was performed on a car radiator to enhance the heat transfer rate by Ali *et al.* [6, 7] using MgO -water and ZnO -water nanofluids. Surfactant was added to the nanofluids with a ratio of 1 : 5 of particles in order to maintain their stability. Till the optimum value of flow rate is reached, the heat transfer rate increases beyond which stickiness of the particles with wall made the

heat transfer rate decreased.

Elias *et al.* [8] studied the physical and thermal properties of nanofluids having Al_2O_3 nanoparticles mixed in a mixture of 50 : 50 ethylene glycol and water. Due to an increase in the Brownian motion of the particles, the thermal conductivity was increased. A rise in the number of the nanoparticles lead to a higher thermal conductivity, density and viscosity of the nanofluid. Tomar and Tripathi [9] studied the impact of a mixture of water-ethylene glycol (50 : 50) with nanoparticles Al_2O_3 and found that with an increase in the volume concentration, fluid circulation required more power for pumping due to higher density. Ebrahimi *et al.* [10] studied the enhancement of the heat transfer in car radiator when nanofluid of SiO_2 -water was used. They concluded that an augmentation in the number of nanoparticles, Reynolds number and the inlet fluid temperature the value of Nusselt number is enhanced.

Many theoretical studies have been made on nanofluids after its development. Many researchers have written a very big number of articles on nanofluids. Mehryan *et al.* [11] observed the micropolar nanofluid flow under the effect of natural convection with porous media. By solving the problem numerically with the Galerkin finite element method, conclusion was made that an increment in the rotation of micro particles was observed due to an upsurge in the Darcy-Rayleigh number. Hussanan *et al.* [12] analyzed five different oxides, those of copper, titanium, aluminum, iron and graphene, added in three different types of base fluids, engine oil, kerosene and water and concluded that the temperature of Go-water nanofluid is higher than the oxide nanoparticle based nanofluids and Go-engine oil or Go-kerosene. Hashemi *et al.* [13] pondered on the Cu-micropolar nanofluid with hot porous medium. Darcy model was considered to observe the macroscopic flow and the Galerkin method with non-uniform mesh was used to solve the problem. The conclusion of investigation was that with a hike in the Darcy number, there is a decline in the strength of the fluid flow.

Hsiao [14] observed the repercussion of viscous dissipation and magnetic field upon the micropolar nanofluid flowing on a stretching sheet. He came up with the

conclusion that by increasing the magnetic parameter, heat transfer rate and flow velocity decreases whereas the temperature, concentration and the couple stress at surface tend to increase. Mehmood *et al.* [15] observed the effects of Lorentz forces on mixed convection in lid-driven square cavity filled with $\text{Al}_2\text{O}_3 - \text{H}_2\text{O}$ nanofluid. Hussain *et al.* [16] computationally examined flow properties of water-alumina nanofluid considering the inclined magnetic field effect in a square cavity. For further reading of similar nature, [17–22] can be consulted.

Xuan and Li [23] used the nano-particles of copper to measure the thermal conductivity of the nanofluid by using the hot wire apparatus. Some parameters like the volume fraction and the shape of the particles were discussed and concluded that the size, shape and volume fraction of the nanoparticles affect the heat transfer rate. Sekhar *et al.* [24], under the constant heat flux at boundary, investigated the heat transfer rate of the fluid in the horizontal circular pipe under the low Reynolds number. The effects of different concentrations of Al_2O_3 on the heat transfer rate of the nanofluid were observed. Due to the increasing concentration of the nanoparticles, the heat transfer rate was observed to increase.

Albadr *et al.* [25], experimentally studied the heat rate effect of Al_2O_3 nanofluid for different concentrations of the nanoparticles in a horizontal shell under the turbulent flow conditions. It was observed that by keeping the inlet temperature and flow rate fixed, the heat transfer rate of the nanofluid is much greater than that of the base fluid. Dharmalingam *et al.* [26], experimentally and mathematically studied the heat transfer of the nanofluids and their physical and chemical properties and found that the heat transfer rate of the nanofluids is much greater than the ordinary fluids.

Raju *et al.* [27] observed the heat and mass transfer rate of magneto-nanofluids over a rotating cone with the heat source and temperature difference viscosity. Two types of nanofluids were taken under consideration with titanium and Ti-alloy as nanoparticles and Ti-water nanofluid was noticed to have less heat transfer rate as compared with that of the Ti-alloy-water nanofluid. Moreover, the fluid particle interaction was observed to be greater in Ti-water as compared with that

in the Ti-alloy-water. The importance of the nanofluids is discussed in [28–32].

1.4 Single Verses Two Phase Nanofluid Models

Immanently, a nanofluid is a two-phase fluid. After taking some suitable assumptions like thermal balance and velocity, of the nanoparticles and the base fluid as same, we can consider it as a single-phase or homogeneous solution. As the nanofluid is a suspension of nano-particles in the base fluid, so we can consider that the nano-particles are dispersed in the base fluid homogeneously. Constitutive equations of continuity, momentum and enthalpy used for the conventional fluids can also be utilized in the nanofluids. In the single-phase case, we can only find the thermophysical properties (mass, volume and density) of the nanofluids [33]. When we consider a nanofluid in the single-phase model, it would have some limitations.

For example, when the Nusselt number is calculated by single-phase model, it has less values as compared with the values calculated in the two-phase models [33]. The ground basis for this may be the factors like gravity, Brownian motion, solid/liquid interface and friction forces. Ding and Wen [34] studied a theoretical model for the migration of a particle in the suspension of nanofluid due to shear rate, viscosity and Brownian motion. Hence, the authors were of the opinion that single-phase models of nanofluids cannot always be considered. Therefore, considering the chaotic movement of nanoparticles and selecting suitable thermophysical properties to some extent have limitations.

The slip mechanism like, gravity, Brownian motion, fluid friction and thermophoresis makes a nanofluid as two-phase fluid. Hence a solid-liquid two-phase general theory can be employed to these fluids. In this model, base fluid and nanoparticles are assumed to have different temperatures and velocities. The results drawn by two phase theory are more accurate to those obtained from single-phase models [35]. In comparison with the single-phase model, the two phase models have a high computational cost. Lagrangian-Eulerian and Eulerian-Eulerian are the dif-

ferent approaches for the two-phase models [36]. Fluid is assumed to obey the continuum theory so that the time average form of the Navier-Stokes equations can be used while the solid particles are accommodated using Lagrangian frame in Lagrangian-Eulerian model. Moreover, correlation between the base fluid and nanoparticles are added to energy and momentum equations. Eulerian-Eulerian model is an alternative branch of two-phase models. Since nanofluid contains a large number of ultrafine particles, so this model is recommended.

In many studies of the nanofluids a single-phase model is employed. It is found that the results obtained by single-phase model has errors. These errors can be removed by using the temperature dependent thermo-physical properties. Buongiorno and thermal dispersion models which are preferred due to their low computational cost.

1.5 Role of Magnetohydrodynamics in Heat Transfer Enhancement

When a magnetic field is applied outside a system on electrically conducting fluid, it reduces the velocity of flow and hence the temperature of system increases. Electrically conducting fluid subjected to the magnetic field, experiences a force that results in a current generation in the fluid. This is known as magnetohydrodynamics (MHD). Its applications can be seen in astrophysics, geophysics [37–44] and many other industrial processes such as magnetohydrodynamic generators, pumps, bearings etc. Mabood *et al.* [45] investigated the boundary layer flow with thermal radiation and Lorentz forces over an exponentially stretched sheet. In this study, they observed the effects of magnetic and radiation parameters on the flow field. It was observed that as the magnetic field gets stronger, temperature is increased inside the boundary layer and the velocity is reduced. Rashidi *et al.* [46] analyzed the effect of MHD on the entropy generation of Newtonian fluid passed over a stretching surface. They used OHAM to solve the mathematical model analytically. The study revealed that with an augmentation in the Hartmann number, the velocity is reduced while temperature and entropy of system

are increased. Rapits [47] discussed the MHD driven viscous and incompressible fluid flow over a porous sheet and observed the effects of the thermal radiation. Conclusion states that with a stronger magnetic field, the velocity of the fluid is decreased.

Kandasamy *et al.* [48] studied the MHD influenced nanofluid past over a vertical sheet. They concluded that the temperature as well as the concentration profile decreases with a rise in the thermal and solutal stratification. Reddy *et al.* [32] discussed the Williamson nanofluid flowing over a nonuniform thick stretching sheet under the influence of MHD. Furthermore, the thermal conductivity of the fluid was not uniform. The spectral quasi-linearisation method was employed to solve the ODEs. One of the conclusions declares that the temperature and nanoparticle volume fraction increase and the velocity declines for greater magnetic number. Öztop *et al.* [49] inspected the effects of MHD on nanofluid filled lid-driven cavity with wavy walls and partial heating. Finite volume method was employed to find solution of the problem. The results concluded that due to a decrease in the nanoparticles as well as the Hartmann number, the heat transfer rate through the fluid is decreased.

1.6 Non-Newtonian Fluids

Fluids are mainly classified as Newtonian and non-Newtonian. In Newtonian fluids, shear stress (the force per unit area applied to fluid) is linearly related to shear rate (also called the deformation rate) but in case of non-Newtonian flow this linear relationship does not hold. Most of the suspensions, mixtures, surfactants, solution of polymer materials are of the non-Newtonian in nature, used in our daily life. In industries like paints, chemicals, food products and manufacturing of plastic goods, the application of heat exchange characteristics can be observed. In industry, laminar flow for non-Newtonian fluids is observed because of their high viscosity. For a thorough and complete analysis of the non-Newtonian fluids and their properties, the interested readers are referred to Skelland [50].

1.7 Heat Transfer in Boundary Layer Flow

At the solid-liquid interface, a thin layer of fluid is formed due to the viscous effects which is called the boundary layer. Flow is laminar in the upstream and it becomes turbulent in the down stream. If there is a temperature gradient present between the surface and the fluid, then there will be boundary layers of velocity and temperature. In 1905, Prandtl [51] was the one who introduced the concept of this layer for the first time. When the fluid moves along the solid surface, some of its part is stuck along the surface due to the viscosity in the vicinity of the surface. As compared with the length of the surface, these viscous layers are very thin for the greater value of the Reynolds number from the initial edge.

1.8 Objective of the Thesis

The dilemma of the heat transfer processes has been the finding of the best way to remove heat from the system efficiently. Although there has been a substantial work already done in this field but the search for a more effective nanofluid has not stopped.

The main aim of this thesis is to enhance the established research in the field of the computational heat transfer in nanofluids. This objective is scrutinized with the help of the use of single phase models of nanofluids.

Besides this another objective was to observe the role of microstructures on the heat transfer rate and the skin friction coefficient of the nanofluids at the surface. Many non-Newtonian fluids used in industries obey the power law model. In one of the study carried out in the thesis, the spin gradient viscosity model of micropolar power law fluid is pondered upon numerically. A subsidiary objective is to test and compare different nanoparticles with different base fluids to try to hunt down the best possible nanofluid mixture in a particular engineering situation. The core objective is to pave the way for future researches in the search of finding better heat transfer exponents in the field of heat transfer through nanofluids.

1.9 Chapter–wise Breakdown of Thesis

In the **Chapter 2**, some basic terms like heat transfer, nanofluids, applications of nanofluids, boundary layer flow and objectives of the thesis are explained and discussed.

Numerical study utilizing the second law of thermodynamics on the squeezing magnetohydrodynamics flow using Cattaneo–Christov theory is pondered upon in the **Chapter 3**. The heat transfer in a fluid squeezed between two plates is described with the help of Cattaneo–Christov theory in the presence of the magnetic field. In addition to this, entropy is also discussed by neglecting the time relaxation effect. A detailed discussion on the results is presented. Contents of this chapter are published in AIP Advances, vol. 8, no. 5, p. 055201, 2018.

In the **Chapter 4**, micropolar nanofluids with power-law spin gradient viscosity model is interpreted. Micropolar fluid with nanoparticles with the spine gradient viscosity is considered. The governing system of PDEs, obtained after application of similarity transformations of ODEs, are solved by using the Keller box method. Discussion on the useful results is done and conclusions are made a part of the chapter at the end. The contents of this chapter are published in the Canadian Journal of Physics vol. 98, no. 1, p. 16–27, 2020.

Chapter 5 comprises of an investigation of free convection in micropolar nanofluid with induced magnetic field. Micropolar nanofluid is considered under the effect of the magnetic field. The induced magnetic field is also dealt within this chapter. After solving the system a set of PDEs is obtained, which is then converted into ODEs after applying the resemblance transformations. These ODEs are solved by using the Keller box method and conclusions are made at the end of the chapter. The contents of this chapter are published in The European Physical Journal Plus, vol. 134, no. 5, p. 235, 2019.

The complete summary of this thesis is discussed in **Chapter 6**.

Chapter 2

Preliminaries and Solution

Methodology

In this chapter, some of the basic terminologies of fluid dynamics and solution methodology are discussed. The Keller-box method, in particular, is explained with the help of an example.

2.1 Fluid

A substance which is unable to resist the tangential stress, and continuously deforms, no matter how small the shear stress may be, is called a fluid. Greater the viscosity of the fluid, larger the stress required to deform the fluid. There are fluids for which the viscosity is zero. Such fluids are called ideal or inviscid fluids. All real fluids exhibit viscosity. Many fluids show negligible viscosity effects in many engineering applications and can be considered as inviscid fluids. The magnitude of resistance to this gradual deformation is characterized by the fluid viscosity which relates the velocity gradient to the shear stress by a linear relationship of the form

$$\tau = \mu_f \frac{du}{dy}, \quad (2.1)$$

where, τ is the stress tensor which is different for different fluids, $\frac{du}{dy}$ is known as the gradient, and μ_f represents the plastic dynamic viscosity of the fluid.

The expression given in equation (2.1) is known as Newton's law of viscosity for the incompressible fluids. The fluids that follow the law expressed by equation (2.1), are known as Newtonian fluids such as air, oil, water etc. There are many mathematical models in which the Newtonian fluids are taken into account due to their physical properties. There exists a class of materials which have a complex structure, so they don't obey the Newton's law, rather they obey the power-law, that is

$$\tau = k \left(\frac{du}{dy} \right)^n . \quad (2.2)$$

Examples of such materials are polymer solutions, greases and certain oils, solid suspensions, synthetic fibers, plastic, soap and detergents, certain biological and pharmaceutical fluids. Here in equation (2.2), k denotes the flow consistency, n is the flow behaviour index or power-law index. Equation (2.2) represents shear thinning for $n < 1$, Newtonian for $n = 1$ and shear thickening fluids for $n > 1$ as shown in the Figure 2.1 [52].

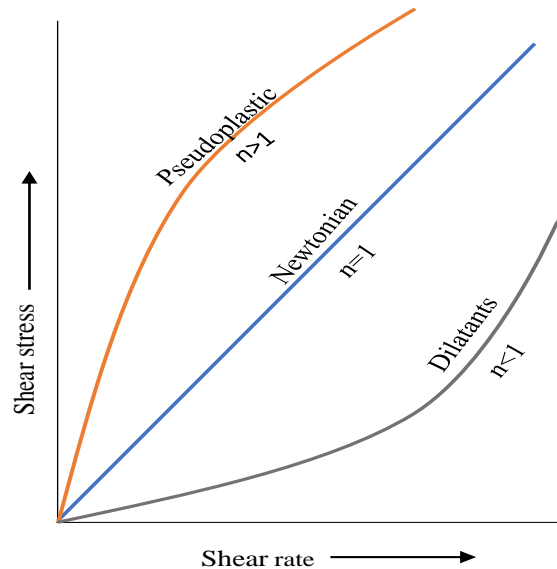


FIGURE 2.1: Shear stress for three types of fluids that is Pseudoplastic($n > 1$), Newtonian($n = 1$) and Dilatants($n < 1$)

The fluids on which when shear stress is applied, their viscosity becomes low like tooth paste, tomato Ketchup etc are known as shear thinning fluids.

In the second class of fluids when shear stress is applied its viscosity does not change such fluids are known as Newtonian fluids.

In the other class when pressure is applied they become hard like cornstarch and quick sand are known as shear thickening fluids.

There are a number of applications of non-Newtonian fluids in many branches of science, engineering and industrial technology which justify the need to further explore the rheological effects in various phenomena in these fields.

The classification that separates non-Newtonian fluids from Newtonian, are categorized on the basis of their behaviors in shear. In continuum or fluid mechanics, an incompressible flow is one for which the density is constant within the fluid parcel and isotropic, when its physical properties remain uniform throughout, for example air and water flow.

A fluid is said to be viscous if its viscosity is substantially greater than that of water whereas the ideal fluids have zero viscosity. When there is no effect of time on the fluid flow, it is called a steady flow.

2.2 Nanofluid

A suspension or mixture of base fluid with nanosized particles having size ranges from 1-100 nanometers is known as nanofluid. The science behind preparing the nanofluids is that to enhance the thermal capability of the base fluids. The common solid additives in the form of nanoparticles are composed by down-sizing metals and their oxides, ceramics and their oxides, carbides and composites of metals, whose thermal conductivity is very high. Of the base fluids, water is the most commonly used while engine oil, kerosene oil, ethylene glycol and composition of water and engine oil are also used. Nanofluids can be studied in the processes of heat transfer [35].

2.3 Micropolar Fluid

The fluid flow that involves the microscopic characteristics of the local structure and the micro rotation of the fluid particles is characterized by the spin mass inertia and named as the micropolar fluid. The shear stress tensor describing the micropolar fluids is asymmetric and deformation of the fluid particles is neglected. This fluid is used to discuss motion of liquid crystal and the animal blood circulation. Micropolar fluid falls under the class of non-Newtonian fluids for which the nonlinearity occurs due to the microrotation of atoms within the constitutive fluid resulting in a rotation viscosity.

An insight to the introductory theory of micropolar fluids can be seen in the work of Eringen [53]. Contemporary to Eringen theory, the idea of coupled stresses in the fluids was given by Stokes [54] which was helpful in a meaningful understanding of the stresses in the micropolar fluids. The claim of the usefulness of the micropolar theory can be supported by its applications in science and engineering. It has been used to describe liquid crystal behavior [55, 56]. Similarly, the low concentration suspension flows in connection with blood rheology have been investigated by using the micropolar theory [57–59].

Micropolar fluids have been discussed by many researchers in their articles. Some of them are, Shu and Lee [60] discussed the two and three dimensional Oseen and unbounded Stokes flows. They derived the solutions known as the micropolar Stokes couplet, micropolar Oseenlet and micropolar Oseen couplet. For a translating circular cylinder and solid sphere in the micropolar fluid, the above solutions were used to calculate the drag coefficients at low Reynolds numbers and a comparison was presented with that of the Newtonian fluid. It was concluded that the drag coefficients in the Newtonian fluid are smaller than those calculated in the micropolar fluids. With a variation in the radius of the outer tube, in an annular region with constriction, Muthu *et al.* [61] investigated the flow of the micropolar fluid. Perturbation method was used to solve the nonlinear equations of the problem with the conclusion that there is a significant mean pressure drop in the steady streaming analysis even if the mean flow rate is zero.

Chen *et al.* [62] observed the dynamics of the micropolar fluid and used the time-centered split method (TCSM) incorporated with Chorin's projection method to solve the nonlinear equations of the micropolar fluid model. They developed a computational code for the solution of the micropolar fluid flow by considering the multiple meshes and discretizing the scheme to the second-order accuracy.

Haque *et al.* [63] studied the effect of MHD on steady micropolar fluid flow in a porous medium. A numerical scheme Nachtsheim-Swigert shooting method was employed, to solve the nonlinear boundary value problem. They concluded that the skin friction and temperature have small values for heavier particles.

Animasaun [64] investigated the effects of the micropolar fluid on the melting horizontal surface. The thermal conductivity and dynamic viscosity were considered as a function of temperature, while taking the vortex viscosity as constant. The effects of the heat source, velocity ratio, variable viscosity and thermal conductivity on the flow field were observed.

It was concluded that with an increase in temperature the Nusselt number, Sherwood number and the skin friction coefficient decrease.

2.4 Heat Transfer

Heat is always transferred from hot body to the cold. It is a molecular activity. Heat can be transferred from system to surrounding or vice versa according as where the molecular activity is greater. If the molecules of wall of a system are more active than the surrounding molecules then energy is transferred from the system. Since this is a molecular activity, so it can be observed microscopically. As the energy is transferred, the body which absorbs energy, experiences a rise in temperature. Hence macroscopically, it can be observed with the change in temperature.

There are three different ways of transfer of heat that is, conduction, convection and radiation.

2.4.1 Conduction

In the absence of the velocity gradient, **conduction** is the processes of heat transfer due to the random motion of the molecules. So it can take place in all three phases that is liquid, solid and gasses. Since the molecules of solids are tightly packed, so it is more pronounced in solids. The rate of heat transfer and temperature are related by the **Fourier's law**. The one dimensional case of Fourier's law states as follows:

$$q = -k \frac{dT}{dx}, \quad (2.3)$$

where q is the heat flux density, k is the conductivity of material and $\frac{dT}{dx}$ is the temperature gradient applied to the body. The thermal conductivity of the material is commonly taken as constant.

2.4.2 Convection

Transfer of energy from solid to fluid is known as **convection**. In this form of energy transfer, heat transfer takes place in both the ways that is the random molecular motion (conduction) and bulk transfer of the molecules (advection). In case of liquid and gases, as molecules are free to move from place to place so convection can be seen in these phases of matter. If the wall of container has temperature T and temperature of the liquid at surface is T_∞ then heat flux according to Newton's law of cooling is given as:

$$q = h(T - T_\infty), \quad (2.4)$$

Convection can be classified in three types that is the free or natural, forced and mixed convection. Natural convection occurs due to temperature difference between the surface of liquid at free stream and with the solid, hence it occurs slowly, whereas forced convection occurs faster as some force is applied on it. Hence in case of forced convection the value of h is large. In mixed convection,

both type of convection are taken at the same time. If both the free and the forced convection are acting in the same direction, the convection is laminar but if they are acting in opposite direction the convection will be turbulent.

2.4.3 Radiation

Heat transfer that requires no medium is termed as radiation. This form of transfer of heat energy is different from conduction and convection. The body which emits the heat radiation is often called a black body. The heat radiation emitted by the black body is given as

$$q = \sigma(T^4 - T_{\infty}^4), \quad (2.5)$$

where q represents the heat radiation, T and T_{∞} represent the absolute and ambient temperatures and σ is the Stefan-Boltzmann constant. The Figure 2.2 represent the how the conduction, convection and radiation take place.

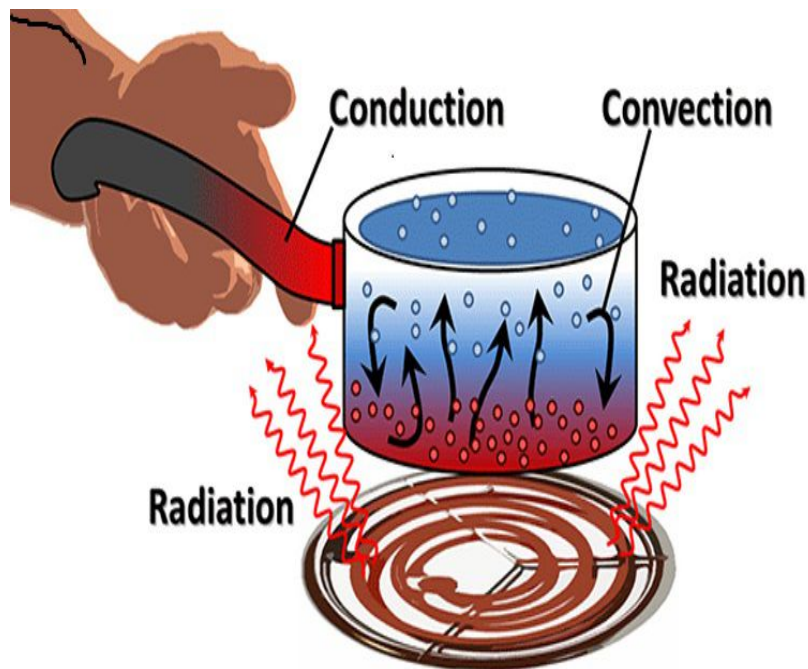


FIGURE 2.2: Conduction, convection and radiation

2.5 Differential Operators

The differential operator ∇ , called nabla or del, is defined as

$$\nabla = \frac{\partial}{\partial x}i + \frac{\partial}{\partial y}j + \frac{\partial}{\partial z}k.$$

It behaves like vector so it is called vector differential operator.

If Φ is a scalar point function then **gradient** of the function is defined as:

$$\nabla\Phi = \frac{\partial\Phi}{\partial x}i + \frac{\partial\Phi}{\partial y}j + \frac{\partial\Phi}{\partial z}k.$$

The gradient of a scalar function is a vector which represents direction as well as the magnitude of maximum space rate of increase. If \mathbf{V} is a vector point function that is

$$\mathbf{V} = ui + vj + wk,$$

then **divergence** of the vector function is defined as:

$$\nabla \cdot \mathbf{V} = \left(\frac{\partial}{\partial x}i + \frac{\partial}{\partial y}j + \frac{\partial}{\partial z}k \right) \cdot (ui + vj + wk)$$

$$\nabla \cdot \mathbf{V} = \frac{\partial u}{\partial x}i + \frac{\partial v}{\partial y}j + \frac{\partial w}{\partial z}k.$$

The **Curl** of the vector function is defined as:

$$\nabla \times \mathbf{V} = \begin{vmatrix} i & j & k \\ \frac{\partial}{\partial x} & \frac{\partial}{\partial y} & \frac{\partial}{\partial z} \\ u & v & w \end{vmatrix}$$

$$\nabla \times \mathbf{V} = \left(\frac{\partial w}{\partial y} - \frac{\partial v}{\partial z} \right) i - \left(\frac{\partial w}{\partial x} - \frac{\partial u}{\partial z} \right) j + \left(\frac{\partial v}{\partial x} - \frac{\partial u}{\partial y} \right) k.$$

Physically Curl of a vector function represents the rotation of the fluid.

The **Laplacian** operator is defined as:

$$\nabla \cdot \nabla = \nabla^2 = \frac{\partial^2}{\partial x^2} + \frac{\partial^2}{\partial y^2} + \frac{\partial^2}{\partial z^2}.$$

The **Laplacian** of scalar point function Φ is given as:

$$\nabla^2\Phi = \frac{\partial^2\Phi}{\partial x^2} + \frac{\partial^2\Phi}{\partial y^2} + \frac{\partial^2\Phi}{\partial z^2}.$$

The **Laplacian** of vector function \mathbf{V} is given as:

$$\nabla^2\mathbf{V} = \frac{\partial^2 u}{\partial x^2} + \frac{\partial^2 v}{\partial y^2} + \frac{\partial^2 w}{\partial z^2}.$$

Operator $\mathbf{V} \cdot \nabla$ is

$$\mathbf{V} \cdot \nabla = u \frac{\partial}{\partial x} + v \frac{\partial}{\partial y} + w \frac{\partial}{\partial z}.$$

2.6 Substantial Derivative

“Consider a particle moving in a velocity field. At time t , the particle is at the position $P(x, y, z)$ and has a velocity,

$$\left. \mathbf{V}_P \right]_t = \mathbf{V}(x, y, z, t).$$

At $t + dt$, the particle has moved to a new position, with coordinates $x + dx, y + dy, z + dz$, and has a velocity given by

$$\left. \mathbf{V}_P \right]_{t+dt} = \mathbf{V}(x + dx, y + dy, z + dz, t + dt).$$

This is shown pictorially in Fig. 2.3.

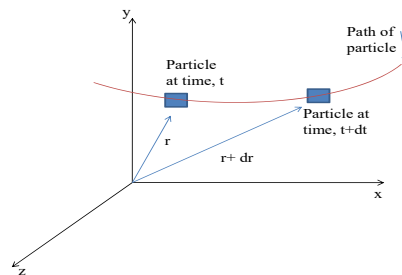


FIGURE 2.3: Motion of particle in flow field

The particle velocity at time t is given by $\mathbf{V}_P \Big|_t = \mathbf{V}(x, y, z, t)$. Then $d\mathbf{V}_P$, the change in the velocity of the particle, in moving from location r to $r + dr$, in time dt , is given by the chain rule,

$$d\mathbf{V}_P = \frac{\partial \mathbf{V}}{\partial x} dx_P + \frac{\partial \mathbf{V}}{\partial y} dy_P + \frac{\partial \mathbf{V}}{\partial z} dz_P + \frac{\partial \mathbf{V}}{\partial t} dt.$$

The total acceleration of the particle (at some point P) is given by

$$\mathbf{a}_P = \frac{d\mathbf{V}_P}{dt} = \frac{\partial \mathbf{V}}{\partial x} \frac{dx_P}{dt} + \frac{\partial \mathbf{V}}{\partial y} \frac{dy_P}{dt} + \frac{\partial \mathbf{V}}{\partial z} \frac{dz_P}{dt} + \frac{\partial \mathbf{V}}{\partial t}.$$

Since

$$\frac{dx_P}{dt} = u, \quad \frac{dy_P}{dt} = v, \quad \frac{dz_P}{dt} = w,$$

we have

$$\mathbf{a}_P = \frac{d\mathbf{V}_P}{dt} = u \frac{\partial \mathbf{V}}{\partial x} + v \frac{\partial \mathbf{V}}{\partial y} + w \frac{\partial \mathbf{V}}{\partial z} + \frac{\partial \mathbf{V}}{\partial t}.$$

To emphasize on the calculations of the acceleration of a fluid particle in a velocity field a special derivative with notation $\frac{DV}{Dt}$ used in the literature. Thus

$$\frac{DV}{Dt} = \mathbf{a}_P = \frac{d\mathbf{V}_P}{dt} = u \frac{\partial \mathbf{V}}{\partial x} + v \frac{\partial \mathbf{V}}{\partial y} + w \frac{\partial \mathbf{V}}{\partial z} + \frac{\partial \mathbf{V}}{\partial t}. \quad (2.6)$$

The derivative, $\frac{D}{Dt}$, defined by Eq. (2.6), is commonly called the substantial derivative [65]. Often it is called the material derivative or particle derivative.

The physical significance of the terms in Eq. (2.6) is

$$\underbrace{\frac{DV}{Dt}}_{\text{Total acceleration of particle}} = \underbrace{u \frac{\partial \mathbf{V}}{\partial x} + v \frac{\partial \mathbf{V}}{\partial y} + w \frac{\partial \mathbf{V}}{\partial z}}_{\text{Convective acceleration}} + \underbrace{\frac{\partial \mathbf{V}}{\partial t}}_{\text{Local acceleration}}$$

From Eq. (2.6), it can be recognized that a fluid particle moving in a flow field may undergo acceleration for either of two reasons. In a steady flow the motion of a fluid particle is completely described with convective acceleration, while if the flow

field is unsteady, the fluid particle will undergo an additional local acceleration because the velocity field is a function of time. The convective acceleration may be written as a single vector expression using the gradient operator ∇ in the form

$$\mathbf{a}_{con} = u \frac{\partial \mathbf{V}}{\partial x} + v \frac{\partial \mathbf{V}}{\partial y} + w \frac{\partial \mathbf{V}}{\partial z} = (\mathbf{V} \cdot \nabla) \mathbf{V}$$

Thus Eq. (2.6) may be written as

$$\frac{D\mathbf{V}}{Dt} = \mathbf{a}_P = (\mathbf{V} \cdot \nabla) \mathbf{V} + \frac{\partial \mathbf{V}}{\partial t}. \quad (2.7)$$

2.7 Equations of Motion for Flow Model

The equation of motion for the flow of nanofluids are the laws of conservation of mass, momentum and energy. These equations are described as follows

2.7.1 Equation of Continuity

The law of conservation of mass is given by the equation of continuity.

$$\frac{\partial \rho_f}{\partial t} + \nabla \cdot \rho_f \mathbf{V} = 0, \quad (2.8)$$

This equation is same for the fluids and the Buongiorno model. For Tiwari Das model replace ρ_f with ρ_{nf} . For incompressible fluids this equation is written as

$$\nabla \cdot \mathbf{V} = 0. \quad (2.9)$$

2.7.2 Momentum Equation

Momentum equation for incompressible fluid is given by

$$\rho_f \left(\frac{\partial \mathbf{V}}{\partial t} + (\mathbf{V} \cdot \nabla) \mathbf{V} \right) = \rho_f \nu_f \nabla^2 \mathbf{V} + b, \quad (2.10)$$

where b is the body force. For common fluids and Buongiorno model this equation remains the same but for the Tiwari and Das model ρ_f and v_f are replaced with ρ_{nf} and v_{nf} .

2.7.3 Energy Equation

First law of thermodynamics: rate of change of energy of a fluid particle is equal to the rate of heat addition plus the rate of work done [65].

- Rate of increase of energy is $\rho \frac{DE}{Dt}$.
- Energy $E = i + \frac{1}{2}(u^2 + v^2 + w^2)$, where i is the internal (thermal) energy and $\frac{1}{2}(u^2 + v^2 + w^2)$ is the kinetic energy.
- Potential energy (gravitation) is usually treated separately and included as a source term.
- We will derive the energy equation by setting the total derivative equal to the change in energy as a result of work done by viscous stresses and the net heat conduction.
- Next we will subtract the kinetic energy equation to arrive at a conservation equation for the internal energy.

The total rate of work done by surface stresses is calculated by adding all work done along x , y and z -components.

Work done per unit volume by surface stresses is given by

$$\begin{aligned} & -div(p\vec{u}) + \frac{\partial(u\tau_{xx})}{\partial x} + \frac{\partial(u\tau_{yx})}{\partial y} + \frac{\partial(u\tau_{zx})}{\partial z} + \frac{\partial(v\tau_{xy})}{\partial x} \\ & + \frac{\partial(v\tau_{yy})}{\partial y} + \frac{\partial(v\tau_{zy})}{\partial z} + \frac{\partial(w\tau_{xz})}{\partial x} + \frac{\partial(w\tau_{yz})}{\partial y} + \frac{\partial(w\tau_{zz})}{\partial z} \end{aligned}$$

The net rate of heat transfer to the fluid particle per unit volume is given by

$$\frac{-\partial q_x}{\partial x} - \frac{\partial q_y}{\partial y} - \frac{\partial q_z}{\partial z} = -div\mathbf{q}$$

Fouriers law of heat conduction relates the heat flux to the local temperature gradient:

$$q_x = -k \frac{\partial T}{\partial x}, \quad q_y = -k \frac{\partial T}{\partial y}, \quad q_z = -k \frac{\partial T}{\partial z}.$$

In vector form is

$$\mathbf{q} = -k \text{ grad } T.$$

Thus, energy flux due to conduction is

$$- \text{div} \mathbf{q} = \text{div}(k \text{ grad } T).$$

Setting the total derivative for the energy in a fluid particle equal to the previously derived work and energy flux terms, results in the following energy equation:

$$\begin{aligned} \rho \frac{DE}{Dt} = & - \text{div}(p\vec{u}) + \frac{\partial(u\tau_{xx})}{\partial x} + \frac{\partial(u\tau_{yx})}{\partial y} + \frac{\partial(u\tau_{zx})}{\partial z} + \frac{\partial(v\tau_{xy})}{\partial x} \\ & + \frac{\partial(v\tau_{yy})}{\partial y} + \frac{\partial(v\tau_{zy})}{\partial z} + \frac{\partial(w\tau_{xz})}{\partial x} + \frac{\partial(w\tau_{yz})}{\partial y} + \frac{\partial(w\tau_{zz})}{\partial z} \\ & + \text{div}(k \text{ grad } T) + S_E \end{aligned}$$

Note that a source term S_E that includes sources (potential energy, sources due to heat production from chemical reactions, etc.).”

2.8 Second Law of Thermodynamics

The entropy of the universe is always increasing is the statement for the second law of thermodynamics. The example of the second law is the cornet engine, which operates between the two reservoirs. One of the reservoir is at hot temperature, where the engine absorbs heat energy and do the useful work and some of the energy is released into the other reservoir which is at lower temperature than the engine. Thus in this way the engine perform work repeatedly so that all the heat energy of the hot reservoir is consumed such that the temperature of the two reservoirs become equal. Hence there is no useful energy is left behind to perform any more work.

The figure of the cornet engine [66] is shown below.

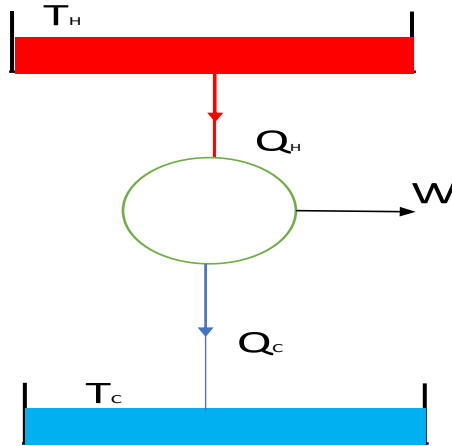


FIGURE 2.4: Carnot Engine

2.9 Cattaneo–Christov Theory

$$\mathbf{q} = -k\nabla T, \quad (2.11)$$

is known as the Fourier law of heat exchange [67]. According to this law, if one end of a metal rod is heated then heat is felt instantly on the other end which means heat travels with the speed of light, which is not possible. In order to rectify this flaw in the Fourier law, Cattaneo [68] purposed his theory as

$$\left(1 + \lambda_0 \frac{\partial}{\partial t}\right) \mathbf{q} = -k\nabla T, \quad (2.12)$$

where λ_0 is thermal relaxation time. When temperature gradient is applied across a volume element λ_0 is the time lag to achieve the steady state solution.

Christov [68] replaced the time derivative with the upper convective to modify the theory of Cattaneo. The main objective was to remove the paradoxical feature of the thermal waves in a moving frame. Thus the Cattaneo-Christov model became

$$\lambda_0 \left[\frac{\partial \mathbf{q}}{\partial t} + \mathbf{V} \cdot \nabla \mathbf{q} - \mathbf{q} \cdot \nabla \mathbf{V} + (\nabla \cdot \mathbf{V}) \mathbf{q} \right] + \mathbf{q} = -k\nabla T. \quad (2.13)$$

2.10 Body Forces

2.10.1 Squeezing Flow

Squeezing flow is the flow of a fluid between the two plates, which occurs when the plates move towards or away from each other. As the fluid is present between the plates and when plates come towards each other, the fluid is compressed and hence it moves away. Otherwise when the plates move away from each other then in that case a space is generated and to cover this space fluid moves inside.

2.10.2 Magnetohydrodynamics (MHD)

When a magnetic field is applied on an electrically conducting fluid, it produces the current in fluid and create forces on the fluid. The application of magnetic field normal to the flow of the fluid produces a magnetic force on the fluid particles called the Lorentz forces and is calculated by the equation:

$$b_{Mag} = \mathbf{J} \times \mathbf{B}. \quad (2.14)$$

\mathbf{J} is given as:

$$\mathbf{J} = \delta_f(\mathbf{E} + \mathbf{V} \times \mathbf{B}), \quad (2.15)$$

is known as the generalized Ohms law, where δ_f is the electrical conductivity, \mathbf{E} is the electric field and \mathbf{B} is the strength of the magnetic field that is the applied magnetic field \mathbf{B}_0 and the induced magnetic field \mathbf{b} . In order to find the MHD term we have to consider the Maxwell equations given as:

$$\nabla \cdot \mathbf{E} = 0, \quad (2.16)$$

$$\nabla \times \mathbf{B} = \mu_m \mathbf{J}, \quad (2.17)$$

$$\nabla \times \mathbf{E} = -\frac{\partial \mathbf{B}}{\partial t}. \quad (2.18)$$

Assumptions are electric field is zero and the Reynolds number for the flow is small so that the induced magnetic field is zero. In the absence of electric field Eq. (2.15) becomes:

$$\mathbf{J} = \delta_f \mathbf{V} \times \mathbf{B}_0, \quad (2.19)$$

$$\mathbf{J} \times \mathbf{B} = \delta_f (\mathbf{V} \times \mathbf{B}_0) \times \mathbf{B}_0, \quad (2.20)$$

$$= \delta_f [(\mathbf{V} \cdot \mathbf{B}_0) \mathbf{B}_0 - (\mathbf{B}_0 \cdot \mathbf{B}_0) \mathbf{V}], \quad (2.21)$$

since \mathbf{V} and \mathbf{B}_0 are perpendicular to each other so, $\mathbf{V} \cdot \mathbf{B}_0 = 0$, hence

$$\mathbf{J} \times \mathbf{B} = -\delta_f \mathbf{B}_0^2 \mathbf{V}, \quad (2.22)$$

which is the required term for the magnetic field. If the magnetic Prandtl number is nearly equal or greater than “1” then the induced magnetic effect must be considered and is given mathematically by the equation as

$$\frac{\partial \mathbf{B}}{\partial t} = \nabla \times (\mathbf{V} \times \mathbf{B}) + \mu_e \nabla^2 \mathbf{B}. \quad (2.23)$$

2.10.3 Free Convection

Free or natural convection occurs in the fluids with different densities due to different temperature gradients. The natural convection can only take place in gravitational field. Hence it acts as the body force known as buoyancy force given by the equation:

$$b_G = g\beta(T - T_0). \quad (2.24)$$

2.11 Single Phase Nanofluid Models

Generally nanofluid is considered as the two phase fluid. That is, one is the solid phase comprising of nanoparticles and the other is the liquid phase. Since

the the size of the particles added to the base fluid is very very small, so the mixture can be considered as a single phase fluid. In fluid mechanics, single phase models can be divided into three main approaches, which are Buongiorno, Tiwari-Das(homogeneous) and thermal dispersion models.

2.11.1 Buongiorno Model

Buongiorono nanofluid model [69] is a combination of dispersion and homogeneous models. The abnormal convective heat transfer enhancement observed in the nanofluids has been explained in this model. This model is mainly focused on two main factors that is the thermophoresis and Brownian diffusion. This model explains the role of nanoparticles diffusion effect in the nanofluid heat transfer near the wall for the turbulent flows.

The flow equations for the fluid are given by the continuity, momentum, energy and the concentration as follows:

$$\nabla \cdot \mathbf{V} = 0, \quad (2.25)$$

$$\rho_{nf} (\mathbf{V} \cdot \nabla) \mathbf{V} = -\nabla p + \mu_{nf} \nabla^2 \mathbf{V} + b, \quad (2.26)$$

$$\mathbf{V} \cdot \nabla T = \alpha_{nf}^* \nabla^2 T + \tau^* \left[D_B (\nabla T \cdot \nabla C) + \frac{D_T}{T_\infty} (\nabla T \cdot \nabla T) \right], \quad (2.27)$$

$$\mathbf{V} \cdot \nabla C = D_B \nabla^2 C + \frac{D_T}{T_\infty} \nabla^2 T. \quad (2.28)$$

This model for the nanofluids has been used in Chapters 4 and 5 of this thesis.

If we are working on the micropolar fluid then its momentum and angular momentum equations will be of the form [70].

$$u \frac{\partial u}{\partial x} + v \frac{\partial u}{\partial y} = \left(\frac{\mu_f + \kappa^*}{\rho} \right) \frac{\partial}{\partial y} \left(|N|^{n-1} \frac{\partial u}{\partial y} \right) + \frac{\kappa^*}{\rho} \frac{\partial}{\partial y} (|N|^{n-1} N), \quad (2.29)$$

$$\rho j \left(u \frac{\partial N}{\partial x} + v \frac{\partial N}{\partial y} \right) = \frac{\partial}{\partial y} \left(\gamma \frac{\partial N}{\partial y} \right) - \kappa^* |N|^{n-1} \left(2N + \frac{\partial u}{\partial y} \right). \quad (2.30)$$

2.11.2 Tiwari–Das Model

Tiwari and Das model [71], considered a two-sided-lid-driven differentially heated square cavity filled with nanofluid. The experiment was performed for three different cases.

In case I, left wall (cold) was moving upward and the right wall (hot) was in the downward direction, while case II was vice a versa and in the third case both of the walls were moving in the upward direction, whereas the upper and lower walls were insulated. The major parameters discussed were Richardson number Ri and volume fraction ϕ' . Both the Richardson number and the motion of walls effect the heat transfer rate. It was observed that when nanosized solid particles of Copper are added in the range $0\% < \phi' < 20\%$ to the base fluid, they enhanced the thermal conductivity of the fluid dramatically. This effect is more pronounced with the increasing volume fraction of the solid particles. The range of the Richardson number is taken from 0.1 to 100. The value of the Grashoff number is fixed at 10^4 for different values of the Richardson number. The values of the Reynolds number are identical to both sides of the cavity. It was witnessed that for case I, the values of the Nusselt number increase abruptly after a certain volume fraction of the nanoparticles for $Ri = 1.0$. For the third case the heat transfer rate is reduced for $Ri = 0.1, 1$ and 10 as compared to the other two cases. When the nanoparticles of solid are added to the base fluid they change the natural convection of the fluid to the forced convection. For the forced convection in which $Ri < 1$, the Nusselt number showed greater values for case II, as compared to case I and III. For volume fraction at 0.16 and 0.20 the Nusselt has greatest value in case III as compared with case I & II.

The governing equations of continuity, momentum and energy for this nanofluid model are given as:

$$\nabla \cdot \mathbf{V} = 0, \quad (2.31)$$

$$\rho_{nf} (\mathbf{V} \cdot \nabla) \mathbf{V} = -\nabla p + \mu_{nf} \nabla^2 \mathbf{V} + b, \quad (2.32)$$

$$\mathbf{V} \cdot \nabla T = \alpha_{nf} \nabla^2 T. \quad (2.33)$$

The physical properties of the nanofluid have the following relation as

$$\rho_{nf} = \phi_1 \rho_p + (1 - \phi_1) \rho_f, \quad (2.34)$$

$$(\rho c_p)_{nf} = \phi_1 (\rho c_p)_p + (1 - \phi_1) (\rho c_p)_f, \quad (2.35)$$

$$\mu_{nf} = \frac{\mu_f}{(1 - \phi_1)^{2.5}}, \quad (2.36)$$

$$k_{nf} = k_f \left[\frac{(k_p + 2k_f) - 2\phi_1 (k_f - k_p)}{(k_p + 2k_f) + \phi_1 (k_f - k_p)} \right], \quad (2.37)$$

and the effective electric conductivity of the nanofluid $(\delta_{el})_{nf}$ is proposed by Maxwell [72] as:

$$(\delta_{el})_{nf} = \left[1 + \frac{3 \{(\delta_{el})_p - (\delta_{el})_f\} \phi_1}{\{(\delta_{el})_p + 2(\delta_{el})_f\} - \{(\delta_{el})_p - (\delta_{el})_f\} \phi_1} \right] (\delta_{el})_f. \quad (2.38)$$

Table 2.1 provides the thermophysical properties of the nanoparticles and base fluids that are used in the present study [73]. This model is applied in the Chapter 3 of this thesis.

	ρ Kg m^{-3}	c_p $\text{J Kg}^{-1}\text{K}^{-1}$	κ $\text{W m}^{-1}\text{K}^{-1}$	δ_{el} $(\Omega\text{m})^{-1}$
Pure water (H ₂ O)	997.1	4179	0.6130	0.05
Copper (Cu)	8933	385.0	401.00	5.96×10^7
Alumina (Al ₂ O ₃)	3970	765.0	40.000	1×10^{-10}

TABLE 2.1: Thermophysical properties of the base fluid and nanoparticles.

2.12 Thermal Dispersion Model

By modifying the single phase model the Xuan and Roetzel [74] changed it into the thermal dispersion model. They consider the random or irregular motion of nanoparticles due to which velocity and the temperature of the fluid arises. The velocity and the temperatuer is given by

$$\mathbf{V} = \bar{V} + V', \quad (2.39)$$

$$\mathbf{T} = \bar{T} + T', \quad (2.40)$$

where V' and T' represent the velocity and temperature variations due to irregular movement of the nanoparticles also \bar{V} and \bar{T} represents the average velocity and temperature. The energy equation is given by after neglecting the boundary surface between the nanoparticles and base fluid as

$$\nabla \cdot \left[(\rho c_p)_{nf} \bar{V} \bar{T} \right] = \nabla \cdot (k_{nf} \nabla \bar{T}) + \nabla \cdot \left[(\rho c_p)_{nf} \overline{V' T'} \right] \quad (2.41)$$

2.13 Boundary Layer Flow

Flows for very high Reynolds numbers behaves like as inviscid flows, because for these cases the effect of viscosity is almost negligible. The flows with high Reynolds numbers can be divided into two regions. The region which is narrow and near to the boundary wall is called boundary layer. The other region is independent of the viscosity effects. The region close to the wall where the wall is stationary or subjected to a velocity different to that of the fluid gives rise to a boundary layer. The formation of boundary layer is due to the dominant viscous effects which poses a resistance to the flow. The boundary layer exists till the inertial forces equal the viscous forces and velocity gradient vanishes. This theory was first proposed by Ludwig Prandtl [75] in 1904. In the same manner the thermal and the velocity boundary layers can be defined [76]. If the thermal conductivity of a fluid is lower then the velocity boundary layer is thicker than the thermal boundary layer and vice versa.

2.14 Entropy

Thermal energy per unit temperature which is unavailable for doing useful work is known as entropy [77] of a system. Every system has the energy to do useful work. But during this useful work some energy is lost in the form of heat due to friction and other factors. This loss of energy is known as the entropy of system. If efficiency of a system is 100% then its entropy is zero. Hence the entropy of

an ideal system is zero. The concept was introduced by Clausius in 1850. If Q is the amount of heat flow and T is the temperature above absolute zero, the entropy is given by $\delta S = \frac{Q}{T}$. In the problems that are considered in the present work, entropy is produced due to three important factors: the heat transfer, fluid friction and diffusive irreversibilities.

$$S''' = (S'''_{gen})_{HT} + (S'''_{gen})_{FF} + (S'''_{gen})_{DI}. \quad (2.42)$$

2.15 Physical Quantities

2.15.1 Hartmann Number

“The ratio of electromagnetic to the viscous force is called the Hartmann number”. Hartmann number is the dimensionless form of conservation equations where magnetic field is used as a body force or when the induced magnetic field effects are made a part of the study. Mathematically it is given as:

$$M = \sqrt{\frac{\delta_{el} B^2 L^2}{\mu}}, \quad (2.43)$$

where B , L , δ_{el} and μ are the intensity of magnetic field, characteristics length, electrical conductivity and the dynamic viscosity of the fluid respectively.

2.15.2 Rotational Viscosity Parameter

“Rotational viscosity is a property of a fluid which determines the rate at which the local angular momentum differences are equilibrated. It is only appreciable if there are rotational degrees of freedom for the fluid particles.” Mathematically it is given by [53]

$$K = \frac{k_0}{\mu_0}. \quad (2.44)$$

2.15.3 Reynolds Number

“The Reynolds number is the ratio of the inertial forces to the viscous forces within a fluid.” For a smaller value of the Reynolds number, the boundary layer is thicker and for a high Reynolds number boundary layer becomes thinner in the fluid. Mathematically it is given by the equation [78]

$$Re = \frac{uL}{\nu}, \quad (2.45)$$

2.15.4 Prandtl Number

“A dimensionless number given by the ratio of momentum to the thermal diffusivity”. Mathematically, it is given by [78]

$$Pr = \frac{\nu}{\alpha}, \quad (2.46)$$

The value of the Prandtl number for liquid metals ranges from 0.001 to 0.1 and for gases it is around 0.7 and for liquids its value is greater than 1.

2.15.5 Eckert Number

“The relationship between a flow’s kinetic energy and the boundary layer enthalpy difference is known as the Eckert number [78].” It is a dimensionless number and given in the mathematical form as

$$Ec = \frac{u^2}{c_p \delta T}. \quad (2.47)$$

2.15.6 Thermophoresis Parameter

The force generated by the Temperature gradient produces a force which drag the nanoparticle in the fluid from higher temperature region to the colder region is called thermophoresis. The thermophoresis coefficient is denoted by D_T and is

given by [79]

$$D_T = 0.26 \frac{k_{nf}}{2k_{nf} + k_p} \frac{\mu_{nf}}{\rho_{nf}} \phi. \quad (2.48)$$

2.15.7 Brownian Motion Parameter

The microscopic random motion of a particle in water was first observed by Robert Brown in 1827. This random motion of particles was due to the motion of the molecules of water and is known as Brownian motion.

In heat transfer process, the nanoparticles are observed to increase the temperature of the fluid very rapidly. This happens due to the random motion of the nanoparticles. The Brownian coefficient is denoted by D_B and is defined as [79]

$$D_B = \frac{k_B T}{3\pi\mu d_p}, \quad (2.49)$$

where k_B , T , μ and d_p Boltzmann constant, temperature of fluid, viscosity of fluid and radius of the nanoparticle respectively.

2.15.8 Bejan Number

The ratio of heat transfer irreversibility to the total entropy (that is heat transfer irreversibility, fluid friction irreversibility and diffusion irreversibility) of the system is called the Bejan number. It is represented by Be and is given by [80]

$$Be = \frac{(S'''_{gen})_{HTI}}{(S'''_{gen})_{HTI} + (S'''_{gen})_{FFI} + (S'''_{gen})_{DI}}. \quad (2.50)$$

The value of Bejan number always lies between 0 and 1. If the value of the heat transfer irreversibility is much greater than the other irreversibilities that is fluid friction and diffusion irreversibilities in entropy, then value of Bejan number is near to 1, otherwise near to zero. Also it is the ratio between two similar quantities, hence it is a number without any unit.

2.15.9 Skin Friction Coefficient

It is the friction between the fluid surface and wall of the container. It is a dimensionless number denoted by C_f and is given by [78]

$$C_f = \frac{2\tau_w}{\rho_f u_w^2}, \quad (2.51)$$

where τ_w , ρ_f and u_w is the shear stress at the surface, fluid density and the characteristics velocity of the flow respectively.

2.15.10 Nusselt Number

“It is a dimensionless number defined as the ratio of heat transferred by convection to the heat transferred by conduction”. It gives a relative measure of the heat transfer by conduction and convection. It is denoted by Nu and mathematically written as [78]

$$Nu = \frac{k_{nf} \nabla T}{k_f}. \quad (2.52)$$

2.15.11 Sherwood Number

It is ratio of the convective mass transfer to the rate of diffusive mass transport, and is named in honor of Thomas Kilgore Sherwood. It is a dimensionless number denoted by Sh and is defined as [78]

$$Sh = \frac{x D_m \nabla C}{D_m (C_w - C_\infty)}. \quad (2.53)$$

2.16 Keller Box Method

It is a special variant of the finite difference scheme presented by H. B. Keller [81] in 1971. The details, accuracy and stability criteria of the scheme can be found in [76]. The Keller–Box method is highly stable numerical technique. It uses central

difference approximations for derivatives and function values which makes It a second order convergent method. It can compute the solution of highly coupled nonlinear equations.

The nonlinear equations are linearized and then solved by standard numerical techniques like LU factorization technique. To explain the procedural details of Keller box method the following example may be very helpful.

Example: Consider the following boundary value problem

$$f'''' - f''' = 0, \quad (2.54)$$

with boundary conditions $f(0) = 1$, $f'(0) = 1$, $f''(1) = 3e$ & $f'''(1) = e$.

Convert Eq. (2.54) into four ordinary differential equations as

$$f' = Y_1, \quad (2.55)$$

$$f'' = Y_1' = Y_2, \quad (2.56)$$

$$f''' = Y_2' = Y_3, \quad (2.57)$$

$$Y_3' - Y_3 = 0, \quad (2.58)$$

and the above boundary conditions (2.16) are changed as

$$f(0) = 1, Y_1(0) = 1, Y_2(1) = 3e \text{ and } Y_3(1) = e. \quad (2.59)$$

Now replace the functions with the averages and the derivatives with the central differences, the system (2.56–2.58) becomes

$$\frac{(f)_j - (f)_{j-1}}{h} = \frac{(Y_1)_j + (Y_1)_{j-1}}{2}, \quad (2.60)$$

$$\frac{(Y_1)_j - (Y_1)_{j-1}}{h} = \frac{(Y_2)_j + (Y_2)_{j-1}}{2}, \quad (2.61)$$

$$\frac{(Y_2)_j - (Y_2)_{j-1}}{h} = \frac{(Y_3)_j + (Y_3)_{j-1}}{2}, \quad (2.62)$$

$$\frac{(Y_3)_j - (Y_3)_{j-1}}{h} - \frac{(Y_3)_j + (Y_3)_{j-1}}{2} = 0, \quad (2.63)$$

After linearization Eqs. (2.60)–(2.63) takes the form

$$\delta(f)_j - \delta(f)_{j-1} - \frac{h}{2} [\delta(Y_1)_j + \delta(Y_1)_{j-1}] = (r_1)_{j-\frac{1}{2}}, \quad (2.64)$$

$$\delta(Y_1)_j - \delta(Y_1)_{j-1} - \frac{h}{2} [\delta(Y_2)_j + \delta(Y_2)_{j-1}] = (r_2)_{j-\frac{1}{2}}, \quad (2.65)$$

$$\delta(Y_2)_j - \delta(Y_2)_{j-1} - \frac{h}{2} [\delta(Y_3)_j + \delta(Y_3)_{j-1}] = (r_3)_{j-\frac{1}{2}}, \quad (2.66)$$

$$\begin{aligned} & (Z_1)_j \delta(f)_j + (Z_2)_j \delta(f)_{j-1} + (Z_3)_j \delta(Y_1)_j + (Z_4)_j \delta(Y_1)_{j-1} \\ & + (Z_5)_j \delta(Y_2)_j + (Z_6)_j \delta(Y_2)_{j-1} + (Z_7)_j \delta(Y_3)_j + (Z_8)_j \delta(Y_3)_{j-1} = (r_4)_{j-\frac{1}{2}}, \end{aligned} \quad (2.67)$$

where,

$$(Z_1)_j = (Z_2)_j = 0, \quad (2.68)$$

$$(Z_3)_j = (Z_4)_j = 0, \quad (2.69)$$

$$(Z_5)_j = (Z_6)_j = -1, \quad (2.70)$$

$$(Z_7)_j = 1, \quad (2.71)$$

$$(Z_8)_j = 0, \quad (2.72)$$

$$(r_1)_{j-\frac{1}{2}} = -(f)_j + (f)_{j-1} + \frac{h}{2} [(Y_1)_j + (Y_1)_{j-1}], \quad (2.73)$$

$$(r_2)_{j-\frac{1}{2}} = -(Y_1)_j + (Y_1)_{j-1} + \frac{h}{2} [(Y_2)_j + (Y_2)_{j-1}], \quad (2.74)$$

$$(r_3)_{j-\frac{1}{2}} = -(Y_2)_j + (Y_2)_{j-1} + \frac{h}{2} [(Y_3)_j + (Y_3)_{j-1}], \quad (2.75)$$

$$(r_4)_{j-\frac{1}{2}} = -\frac{(Y_3)_j - (Y_3)_{j-1}}{h} - \frac{(Y_3)_j + (Y_3)_{j-1}}{2}. \quad (2.76)$$

The boundary conditions (2.59) when solved give rise the following constraints

$$\delta(f)_0 = \delta(Y_1)_0 = \delta(Y_2)_J = \delta(Y_3)_J = 0. \quad (2.77)$$

On the basis of these constraints, the vector of unknowns is defined as:

$$\delta = \left[\delta(Y_{23})_{j-1} \quad \delta(Y_{34})_{j-1} \quad \delta(f)_j \quad \delta(Y_{12})_j \right]^T, \quad j = 1, 2, \dots, J \quad (2.78)$$

The system is written in matrix form consists of a tridiagonal matrix, a column vector and also a column vector as given below

$$M\delta = r, \quad (2.79)$$

where,

$$M = \begin{bmatrix} A_1 & C_1 & & & & & & & & & \\ B_2 & A_2 & C_2 & & & & & & & & \\ & \dots & \dots & \dots & & & & & & & \\ & & \dots & \dots & \dots & & & & & & \\ & & & \dots & \dots & \dots & & & & & \\ & & & & \dots & \dots & \dots & & & & \\ & & & & & B_{J-1} & A_{J-1} & C_{J-1} & & & \\ & & & & & & B_J & A_J & & & \end{bmatrix}, \quad (2.80)$$

$$A_j = \begin{bmatrix} 0 & 0 & 1 & -\frac{h}{2} \\ -\frac{h}{2} & 0 & 0 & 1 \\ -1 & -\frac{h}{2} & 0 & 0 \\ (Z_6)_j & (Z_8)_j & (Z_1)_j & (Z_3)_j \end{bmatrix}, \quad j = 1, 2, 3, \dots, J, \quad (2.81)$$

$$B_j = \begin{bmatrix} 0 & 0 & -1 & -\frac{h}{2} \\ 0 & 0 & 0 & -1 \\ 0 & 0 & 0 & 0 \\ 0 & 0 & (Z_2)_j & (Z_4)_j \end{bmatrix}, \quad j = 2, 3, 4, \dots, J, \quad (2.82)$$

$$C_j = \begin{bmatrix} 0 & 0 & 0 & 0 \\ -\frac{h}{2} & 0 & 0 & 0 \\ 1 & -\frac{h}{2} & 0 & 0 \\ (Z_5)_j & (Z_7)_j & 0 & 0 \end{bmatrix}, \quad j = 1, 2, 3, \dots, J-1, \quad (2.83)$$

The system defined in Eq. (2.79) is solved using LU-block factorization method. The vector of unknowns is updated till required accuracy is achieved. The numerical results obtained by Keller box method for the present problem are demonstrated in Figure 2.5.

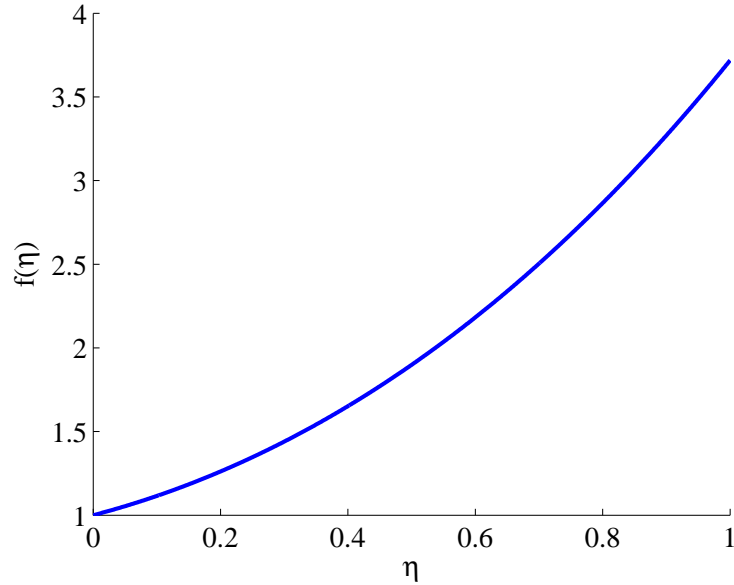


FIGURE 2.5: Flow model of the problem

The algorithm form of the scheme can be presented as:

1. Reduce the higher order boundary value problems to first order ordinary differential equations.
2. The resulting system is discretized by using central differences for the derivatives and average values for the functions as,

$$\left(\frac{df_*}{df}\right)_{j-\frac{1}{2}} = \frac{(f_*)_j - (f_*)_{j-1}}{h}, \quad (2.84)$$

$$(f_*)_{j-\frac{1}{2}} = \frac{(f_*)_j + (f_*)_{j-1}}{2}. \quad (2.85)$$

3. The nonlinear difference equations are linearized by the Newton's method in the following sense,

$$(f_*)_j^{i+1} = (f_*)_j^i + \delta (f_*)_j^i. \quad (2.86)$$

4. The resulting linear system is written in the matrix form $M\delta = \mathbf{r}$.
5. The vector of unknowns δ is obtained by solving the system $M\delta = \mathbf{r}$ by using *LU*-decomposition method.
6. Updation is made to the solution vector and the process is continued until a required accuracy is achieved.

The obtained numerical values are strongly depend on the step size interval. The step size values are taken to fulfill the boundary condition asymptotically.

Chapter 3

MHD Squeezing Flow of a Nanofluid Model Using Cattaneo–Christov Theory

3.1 Introduction

This chapter gives an account of the heat transfer characteristics of the squeezing flow of a nanofluid between two flat plates with upper plate moving vertically (up and down) and the lower in the horizontal direction. Tiwari and Das nanofluid model has been utilized to give a comparative analysis of the heat transfer in the Cu–water and Al₂O₃–water nanofluids with entropy generation. The modeling is carried out with the consideration of Lorentz forces to observe the effect of magnetic field on the flow. The Joule heating effect is included to discuss the heat dissipation in the fluid and its effect on the entropy of the system. The nondimensional ordinary differential equations are solved using the Keller box method to assess the numerical results which are presented by the graphs and tables. An interesting observation is that the entropy is generated more near the lower plate as compared with that at the upper plate. Also, the heat transfer rate is found to be higher for the Cu nanoparticles in comparison with the Al₂O₃

nanoparticles.

3.2 Mathematical Formulation

An unsteady squeezing flow of the Newtonian nanofluid between two parallel flat plates with the Cattaneo–Christov heat flux model has been considered. The lower plate has a stretching velocity $U_w = Sx/(1 - \sigma t)$ along the x -axis and is located at $y = 0$. The upper plate placed at $y = h(t)$, where $h(t) = \sqrt{\nu_f(1 - \sigma t)/S}$, moves towards and away from the lower plate with the velocity $V_h = dh/dt$. The dimension of parameter σ is $(\text{time})^{-1}$ and $\sigma t < 1$. Here T_w and T_h signify the wall and ambient temperatures given by $T_w = T_0 + d_1x$ and $T_h = T_0 + d_2x$, respectively as shown in Figure 3.1.

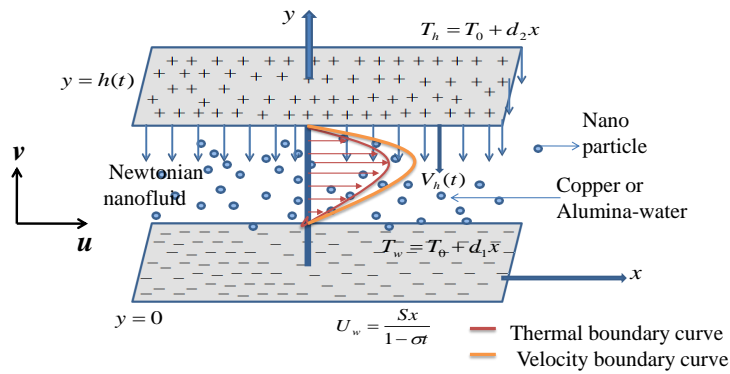


FIGURE 3.1: Schematic diagram of flow model

The following equation describes the heat flux \mathbf{q} in terms of Cattaneo–Christov theory.

$$\mathbf{q} + \delta_E \left[\frac{\partial \mathbf{q}}{\partial t} + \mathbf{V} \cdot \nabla \mathbf{q} + (\nabla \cdot \mathbf{V}) \mathbf{q} - \mathbf{q} \cdot (\nabla \mathbf{V}) \right] = k \nabla T. \quad (3.1)$$

The classical Fourier's law can be obtained from equation (3.1) by putting $\delta_E = 0$. Using the Tiwari–Das model [71] and the incompressibility of the fluid, Equation (3.1) becomes:

$$\mathbf{q} + \delta_E \left[\frac{\partial \mathbf{q}}{\partial t} + \mathbf{V} \cdot \nabla \mathbf{q} - \mathbf{q} \cdot (\nabla \mathbf{V}) \right] = k_{nf} \nabla T. \quad (3.2)$$

The viscous dissipation effect, the MHD and Joule heating effects have been taken into account. After applying the boundary layer approximation and scale analysis, the resulting constitutive equations are [82, 83]:

$$\frac{\partial u}{\partial x} + \frac{\partial v}{\partial y} = 0, \quad (3.3)$$

$$\frac{\partial u}{\partial t} + u \frac{\partial u}{\partial x} + v \frac{\partial u}{\partial y} = -\frac{1}{\rho_{nf}} \frac{\partial p}{\partial x} + \frac{\mu_{nf}}{\rho_{nf}} \left(\frac{\partial^2 u}{\partial x^2} + \frac{\partial^2 u}{\partial y^2} \right) - B_0^2 \frac{(\delta_{el})_{nf}}{\rho_{nf}} u, \quad (3.4)$$

$$\begin{aligned} \frac{\partial T}{\partial t} + u \frac{\partial T}{\partial x} + v \frac{\partial T}{\partial y} + \alpha \Omega_E &= \frac{\kappa_{nf}}{(\rho c_p)_{nf}} \left(\frac{\partial^2 T}{\partial x^2} + \frac{\partial^2 T}{\partial y^2} \right) + B_0^2 \frac{(\delta_{el})_{nf}}{(\rho c_p)_{nf}} u^2 \\ &+ \frac{\mu_{nf}}{(\rho c_p)_{nf}} \left[2 \left\{ \left(\frac{\partial u}{\partial x} \right)^2 + \left(\frac{\partial v}{\partial y} \right)^2 \right\} + \left(\frac{\partial u}{\partial y} + \frac{\partial v}{\partial x} \right)^2 \right], \end{aligned} \quad (3.5)$$

where the physical properties of the nanofluids have been expressed in terms of the following relations [84]

$$\rho_{nf} = \phi_1 \rho_p + (1 - \phi_1) \rho_f, \quad (3.6)$$

$$(\rho c_p)_{nf} = \phi_1 (\rho c_p)_p + (1 - \phi_1) (\rho c_p)_f, \quad (3.7)$$

$$\mu_{nf} = \frac{\mu_f}{(1 - \phi_1)^{2.5}}, \quad (3.8)$$

$$k_{nf} = k_f \left[\frac{(k_p + 2k_f) - 2\phi_1 (k_f - k_p)}{(k_p + 2k_f) + \phi_1 (k_f - k_p)} \right], \quad (3.9)$$

$$(\delta_{el})_{nf} = \left[1 + \frac{3 \{ (\delta_{el})_p - (\delta_{el})_f \} \phi_1}{\{ (\delta_{el})_p + 2(\delta_{el})_f \} - \{ (\delta_{el})_p - (\delta_{el})_f \} \phi_1} \right] (\delta_{el})_f, \quad (3.10)$$

$$\begin{aligned} \Omega_E &= \frac{\partial^2 T}{\partial t^2} + u \frac{\partial u}{\partial x} \frac{\partial T}{\partial x} + v \frac{\partial v}{\partial y} \frac{\partial T}{\partial y} + u^2 \frac{\partial^2 T}{\partial x^2} + v^2 \frac{\partial^2 T}{\partial y^2} + \frac{\partial u}{\partial t} \frac{\partial T}{\partial x} + 2uv \frac{\partial^2 T}{\partial x \partial y} \\ &+ 2u \frac{\partial^2 T}{\partial x \partial t} + u \frac{\partial v}{\partial x} \frac{\partial T}{\partial y} + \frac{\partial v}{\partial t} \frac{\partial T}{\partial y} + v \frac{\partial u}{\partial y} \frac{\partial T}{\partial x} + 2v \frac{\partial^2 T}{\partial y \partial t}. \end{aligned} \quad (3.11)$$

The boundary conditions for the above stated unsteady squeezing plates are

$$\begin{aligned} u|_{y=0} &= U_w(x, t) = \frac{Sx}{1 - \sigma t}, \quad v|_{y=0} = 0, \quad T|_{y=0} = T_w = T_0 + d_1 x, \\ u_{y \rightarrow h(t)} &\rightarrow 0, \quad v_{y \rightarrow h(t)} = V_h = \frac{dh}{dt} = -\frac{\sigma}{2} \sqrt{\frac{\nu_f}{S(1 - \sigma t)}}, \\ T|_{y \rightarrow h(t)} &\rightarrow T_h = T_0 + d_2 x. \end{aligned} \quad (3.12)$$

In the above equations, $S > 0$ is a dimensional constant and represents the stretching velocity of the lower plate. The similarity transform [82] for the above problem

is

$$\left. \begin{aligned} \Psi &= x \sqrt{\frac{S\nu_f}{1-\sigma t}} f(\eta), & \eta &= \sqrt{\frac{S}{\nu_f(1-\sigma t)}} y, & u &= \frac{Sx}{1-\sigma t} f', \\ v &= -\sqrt{\frac{S\nu_f}{1-\sigma t}} f, & \theta &= \frac{T-T_h}{T_w-T_0}. \end{aligned} \right\} \quad (3.13)$$

Applying these similarity transformation to the governing equations of the problem, the PDEs (3.3)–(3.5) are converted to the nondimensional ODEs as are written below.

$$f'''' - f' f'' + f f''' - \frac{sq}{2} (3f'' + \eta f''') - \frac{A_5}{A_1} M^2 f'' = 0, \quad (3.14)$$

$$\begin{aligned} & \frac{A_1 A_4}{A_2 A_3} \theta'' + \frac{Pr}{2} (2f \theta' - sq \eta \theta') - Pr \beta e (f^2 \theta'' + f f' \theta' - sq \eta f \theta'') \\ & - \frac{Pr}{4} \eta \beta e sq^2 (3 \theta' + \eta \theta'') + \frac{Pr}{2} \beta e sq (3f \theta' + \eta f' \theta') \\ & - \frac{A_5}{A_2} M^2 Pr Ec_x f'^2 + 4 \frac{A_3}{A_2} Pr Ec f'^2 + \frac{A_1}{A_2} Pr Ec_x f''^2 = 0, \end{aligned} \quad (3.15)$$

$$\begin{aligned} \text{where, } sq &= \frac{\sigma}{S}, & M^2 &= \frac{1-\sigma t}{S} \frac{(\delta_{el})_f}{\rho_f} B_0^2, & Pr &= \frac{\mu_f c_p}{k_f}, & \beta e &= \frac{S\alpha}{(1-\sigma t)}, \\ Ec_x &= \frac{S^2 x^2}{(1-\sigma t)^2 (T_w - T_0) c_p}, & Ec &= \frac{\mu_f S}{\rho_f (T_w - T_0) (1-\sigma t) c_p}, & A_1 &= \frac{\rho_{nf}}{\rho_f}, \\ A_2 &= \frac{(\rho c_p)_{nf}}{(\rho c_p)_f}, & A_3 &= \frac{\mu_{nf}}{\mu_f}, & A_4 &= \frac{k_{nf}}{k_f} \text{ and } A_5 = \frac{(\delta_{el})_{nf}}{(\delta_{el})_f}. \end{aligned}$$

Since pressure is the function of the variable x only so differentiating Eq (3.4) with respect to y will eliminate the pressure term but it is transformed into f' , hence we can say that pressures is present in terms of velocity.

The similarity transformation converts the boundary conditions (3.12) to the following form:

$$\left. \begin{aligned} f(\eta) &= 0, & f'(\eta) &= 1, & \theta(\eta) &= 1 - S_1 \text{ at } \eta = 0, \\ f(\eta) &= \frac{sq}{2}, & f'(\eta) &= 0, & \theta(\eta) &= 0 \text{ when } \eta = 1. \end{aligned} \right\} \quad (3.16)$$

To judge how efficient a system is, its entropy analysis is of crucial importance. The entropy in the present scenario is produced due to two important factors: the heat transfer and the fluid friction irreversibilities. The case for $\beta e = 0$ is discussed

here and the entropy equation is given as:

$$S''' = \frac{k_{nf}}{T_0^2} \left[\left(\frac{\partial T}{\partial x} \right)^2 + \left(\frac{\partial T}{\partial y} \right)^2 \right] + \frac{\mu_{nf}}{T_0} \left[2 \left\{ \left(\frac{\partial u}{\partial x} \right)^2 + \left(\frac{\partial v}{\partial y} \right)^2 \right\} + \left(\frac{\partial u}{\partial y} + \frac{\partial v}{\partial x} \right)^2 \right] + \frac{(\delta_{el})_{nf}}{T_0} B_0^2 u^2. \tag{3.17}$$

The characteristics entropy generated in the system is given by

$$S_0''' = \frac{k_{nf} S (T_w - T_0)^2}{\nu_{nf} T_0^2 (1 - \sigma t)}.$$

Dividing Equation (3.17) with the characteristics function and using the similarity transform, we get the non-dimensional form of entropy, given as:

$$Ng = \theta'^2 + \frac{A_3^2}{A_1 A_4} \left(\frac{Pr Ec_x}{\Omega} f'^2 + 4 \frac{Ec Pr}{\Omega} f'^2 \right) + \frac{A_3 A_5 M^2 Ec_x Pr}{A_1 A_4 \Omega} f'^2. \tag{3.18}$$

The Bejan number is a very important quantity which gives the ratio of the entropy produced by the heat transfer irreversibility to the total entropy of the system, given as under:

$$\text{Bejan Number} = \frac{Nh}{Ng} = \frac{\theta'^2}{Ng}. \tag{3.19}$$

The other physical quantities which are of great interest are the skin friction coefficient and the Nusselt number. The skin friction [82] is given by:

$$C_{fx} = \frac{\tau_w}{\rho_{nf} U_w^2}, \tag{3.20}$$

where τ_w is given by:

$$\tau_w = \mu_{nf} \left(\frac{\partial u}{\partial y} \right)_{y=h(t)} = \mu_{nf} \frac{Sx}{1 - \sigma t} \sqrt{\frac{S}{\nu_f (1 - \sigma t)}}. \tag{3.21}$$

Substituting the values of U_w and τ_w in Equation (3.20) we get,

$$\frac{A_1}{A_3} \sqrt{Re_x} C_{fx} = f''(1), \tag{3.22}$$

$$C_f = |f''(1)|, \tag{3.23}$$

where $Re_x = \frac{U_w x}{\nu_f}$ and $C_f = \frac{A_1}{A_3} \sqrt{Re_x} C_{fx}$. The Nusselt number [85–90] is given by

$$Nu_x = \frac{q_w x}{k_{nf} (T_w - T_h)}, \quad (3.24)$$

where q_w is given as,

$$q_w = -k_{nf} \left(\frac{\partial T}{\partial y} \right)_{y=h(t)}, \quad (3.25)$$

$$= -k_{nf} (T_w - T_h) \sqrt{\frac{S}{\nu_f (1 - \sigma t)}} \theta'(1). \quad (3.26)$$

Putting the above form of q_w in Equation (3.24), we obtain the Nusselt number that is:

$$\sqrt{\frac{\nu_f (1 - \sigma t)}{S}} \frac{1}{x} Nu_x = -\theta'(1), \quad (3.27)$$

$$Nu = -\theta'(1), \quad (3.28)$$

where $Nu = \sqrt{\frac{\nu_f (1 - \sigma t)}{S}} \frac{1}{x} Nu_x$.

3.3 Solution Methodology

In order to find the solution of the problem under discussion, a finite different scheme namely the Keller box method, has been implemented [81]. The algorithmic form of this method is presented on page 38 and 39.

The thermophysical properties of base fluid and nanoparticles with their units are given in the Table 3.1 (see Hussain *et al.* [91])

	ρ Kg m^{-3}	c_p $\text{JKg}^{-1}\text{K}^{-1}$	k $\text{Wm}^{-1}\text{K}^{-1}$	δ_{el} $(\Omega\text{m})^{-1}$
Pure water (H ₂ O)	997.1	4179	0.6130	0.05
Copper (Cu)	8933	385.0	401.00	5.96×10^7
Alumina (Al ₂ O ₃)	3970	765.0	40.000	1×10^{-10}

TABLE 3.1: Thermophysical properties of the base fluid and nanoparticles.

In order to validate our code, the numerical value of the Nusselt number and skin friction coefficient presented by Dogonchi *et al.* [83] and Mustafa *et al.* [92] are successfully reproduced. The comparison of the values of the Nusselt number and skin friction coefficient has been shown in the Table 3.2 which shows an excellent agreement.

S	Dogonchi [83]		Mustafa [92]		Present	
	$-f''(1)$	$-\theta'(1)$	$-f''(1)$	$-\theta'(1)$	$-f''(1)$	$-\theta'(1)$
-1	2.170091	3.319888	2.170090	3.319899	2.170075	3.319851
-0.5	2.617403	3.129491	2.614038	3.129491	2.617395	3.129470
0.01	3.007133	3.047091	3.007134	3.047092	3.007134	3.047092
0.5	3.336449	3.026323	3.336449	3.026324	3.336459	3.026342
2	4.167041	3.113386	4.167389	3.118551	4.167431	3.118617

TABLE 3.2: For different values of S and for fixed values of $Pr = Ec = 1$ and $\delta = 0.1$.

3.4 Discussion on Results

In this section, the numerical solution of the system of nondimensional boundary value problem (3.14)–(3.16) has been presented. A discussion on the physical significance of these results has also been included. Table 3.3 explains the effect of different physical parameters on the Nusselt number and the skin friction coefficient of copper–water and alumina–water. As the value of the squeezing parameter sq is increased, the upper plate moves in the downward direction and pressure is applied on the nanofluid present between the two plates which increases its temperature and Nusselt number is enhanced for both the copper–water and the alumina–water. As the upper plate moves in the downward direction, the fluid friction at the plate increases. As a result, the skin friction coefficient increases as evident from the Table 3.3. The same behaviour is observed for the negative values of the squeezing parameter. From the table, it can be seen that the Nusselt number increases as the upper plate moves in the upward direction. Initially, the temperature of the nanofluid decreases so the fluid absorbs the heat energy from the upper plate as its temperature is higher than that of the fluid. Enhancement in the relaxation time parameter, results in the decline in the heat transfer rate in

both cases of Cu/Al₂O₃–water.

Thermal relaxation parameter, Eckert number and the local Eckert number have a negligible effect on the skin friction coefficient of the nanofluid. As the values of the Eckert and local Eckert numbers increase, the value of the Nusselt number increases. For greater values of the Eckert number means the rise in temperature of fluid with its motion. The increasing values of the magnetic parameter M causes an increase in heat transfer rate of the fluid as well as the skin friction. Due to the increasing values of the volumetric fraction of the nanoparticles, there is a small decrease in the skin friction coefficient also the values of the Nusselt number decreases. Heat transfer rate reduces for greater values of the thermal stratification.

sq	β_e	Ec_x	Ec	M	ϕ_1	S_1	Cu–water		Al ₂ O ₃ –water	
							C_f	Nu	C_f	Nu
1.0	0.5	0.5	0.5	3	0.04	0.2	1.3440	1.4074	1.3413	1.6378
0.5							0.2886	1.5470	0.2905	1.5951
2.0							4.7311	12.2607	4.7267	21.6778
-0.5							3.4274	6.0599	3.4275	6.3360
-1.0							4.9317	13.8014	4.9309	17.0857
-2.0							7.8046	1.9047	7.8020	14.1391
	0.0						1.3440	1.4020	1.3413	1.6042
	0.9						1.3440	1.4036	1.3413	1.6463
		0.3					1.3440	1.6388	1.3413	1.8679
		0.9					1.3440	0.9447	1.3413	1.1778
			0.3				1.3440	1.0356	1.3413	1.1941
			0.9				1.3440	2.1511	1.3413	2.5253
				1			1.2177	3.2587	1.2168	3.4825
				5			1.4644	-2.3432	1.4601	-2.1035
					0.02		1.3574	1.3580	1.3575	1.4733
					0.06		1.3338	1.4447	1.3268	1.7880
						0.0	1.3440	1.6715	1.3413	1.9137
						0.4	1.3440	1.1434	1.3413	1.3620

TABLE 3.3: Reduced Nusselt number and skin friction coefficient for copper–water and alumina–water when $Pr = 6.2$

Figures 3.2-3.3 reflect the effect of the squeezing parameter on the velocity profile. Figure 3.2 is plotted for the positive values of the squeezing parameter sq which physically means that the upper plate is moving towards the lower plate. The

graph indicates that the velocity is at a rise with the growing values of sq . The opposite happens in the case when the upper plate moves away from the lower plate, as it can be seen in Figure 3.3 that velocity decreases for the decreasing negative values of sq .

The behavior of temperature profile for the increasing positive values of the squeezing parameter is observed in Figure 3.4. The Figure demonstrates that the temperature rises as the values of sq increases. The behavior suggests that the intermolecular distances shrink between the atoms of the fluid causing more collisions between the atoms as the fluid flows between the plates giving a rise in the temperature of the fluid. The rise in temperature is more pronounced when the Cu nanoparticles are used in comparison with the Al_2O_3 nanoparticles.

Figures 3.5 and 3.6 show a discussion on the entropy variation in the system with the variation in the squeezing parameter. Looking at the graphs, we conclude that in both the cases i.e., the negative values of the squeezing parameter or the positive values of the squeezing parameter, the entropy at the lower plate is very high as compare with the entropy at the upper plate. This is due to the fact that both the contributing factors of the entropy i.e., the fluid friction and the heat transfer factor have higher values at the lower plate. The variation of the entropy is more pronounced in the case of negative squeezing parameter.

Figure 3.7 give the variation in the Bejan number for increasing values of the squeezing parameter. There is a gradual increase in the Bejan number at the lower plate suggesting as the two plates come closer the entropy generation at the lower plate is dominated by the fluid friction factor and the opposite happens at the upper plate. In Figure 3.8 the value of the Bejan number increases near both the plates as the negative values of the squeezing parameter increases which is an indication of the domination of the heat transfer irreversibility factor in entropy generation.

Figure 3.9 gives an account of the behavior of the temperature profile for the variation of the relaxation time parameter. It is observed in the figure that as we move away from the lower plate towards the upper, the temperature falls for

the rising values of βe . Physically, the growing values of the relaxation time parameter lead to a delay in the thermal change in the system, which results in lower temperature of the system.

Eckert number gives an idea about the heat dissipation that is caused in the system. Greater value of Eckert number shows that the advective transport has a greater role to play in the heat transfer as compared with the enthalpy difference of the system. The effects of Eckert number on the temperature profile, entropy and the Bejan number are discussed in Figures 3.10-3.12. Figure 3.10 shows an increase in the temperature profile as we increase the value of the Eckert number which is obvious for its contribution in the heat dissipation. The entropy of the system increases with an increase in the Eckert number as seen in figure 3.11. At the lower plate, the increasing values of the Eckert number have a greater effect due to the advective transport factor.

The Bejan number is plotted for growing values of Eckert number in Figure 3.12. The impact of increasing the Eckert number can be seen in the form of a increase in the Bejan number which is a suggestion that an increase in the Eckert number leads to a greater entropy due to the heat transfer irreversibility.

Figure 3.13 reveals the effect of magnetic parameter on the velocity profile. The greater values of Hartmann number result in a decline in the velocity of the fluid near the lower plate but opposite behaviour is seen near the upper plate. This is because an increase in the Lorentz forces halts the flow of the fluid at the lower plate. The resistance to the flow gives rise to the temperature of the fluid as evident from Figure 3.14.

The entropy of the system seems to be greater at the lower plate for the growing values of the magnetic parameter but as we move towards the upper plate, the entropy is reduced which can be observed from Figure 3.15. The Bejan number's plot in Figure 3.16 for varying the magnetic parameter reveals that at both the plates the entropy is dominated by heat transfer irreversibility. Figure 3.17 discusses the effect of the volume fraction of the nanoparticles on the temperature profile. It is observed that the increasing the volume fraction of both the alumina

or Cu nanoparticle leads to a decrease in the temperature. This is an indication that the nanoparticles take the heat away from the boundary layer as the fluid flows.

It is interesting to note that the entropy of the system is lower for greater volume fraction ϕ_1 for either of the nanoparticles. The entropy in case of the alumina nanoparticles is greater than that for the Cu nanoparticles for a given value of ϕ_1 (see Figure 3.18).

The Bejan number is examined for changing values of ϕ_1 in Figure 3.19. Similar to the previous observations for the Bejan number, the entropy at the lower plate is mainly because of the fluid friction effect. This behavior is due to the fact that the lower plate is in motion along the horizontal direction, so the inertial effects lead to a rise in the fluid friction near the plate. The entropy due to the fluid friction becomes maximum when η is around 0.3. But as we move away from the lower plate, the effect of entropy due to heat transfer irreversibility becomes dominant at around $\eta = 0.85$.

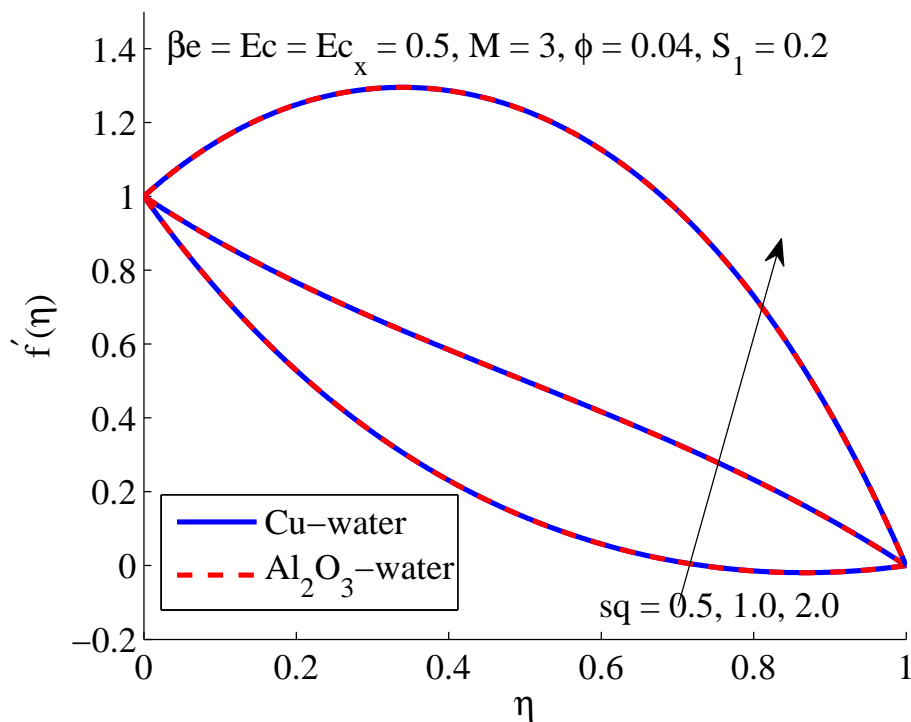


FIGURE 3.2: Impact of sq on f' .

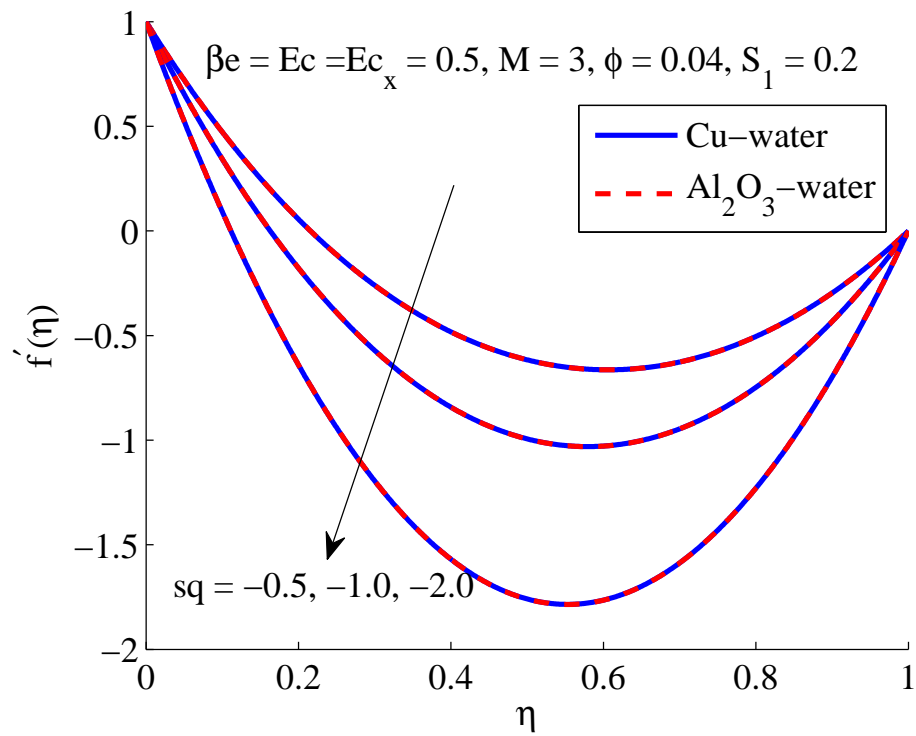


FIGURE 3.3: Impact of $-sq$ on f' .

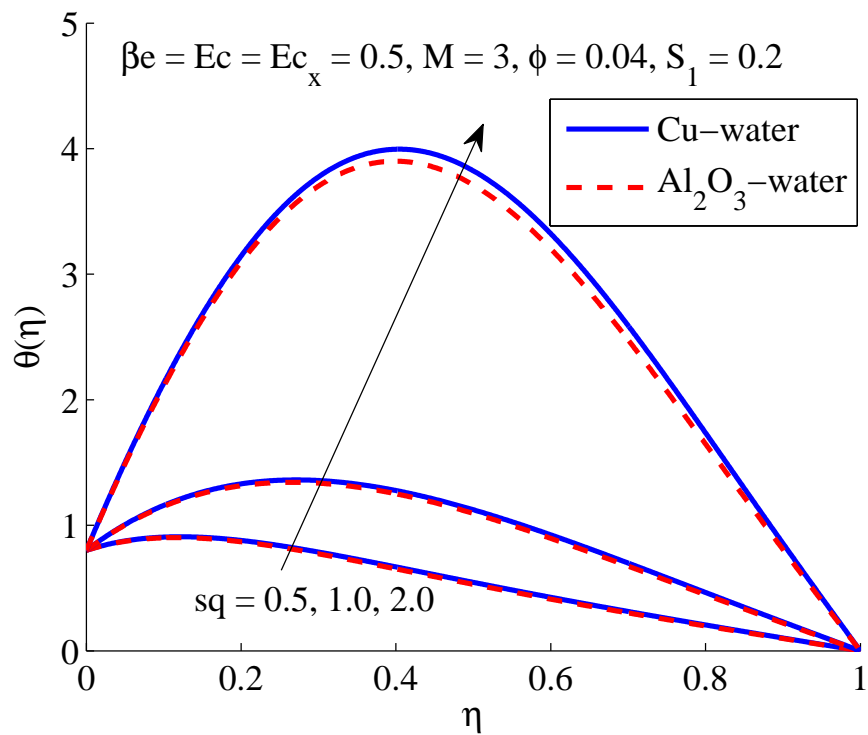


FIGURE 3.4: Impact of sq on θ .

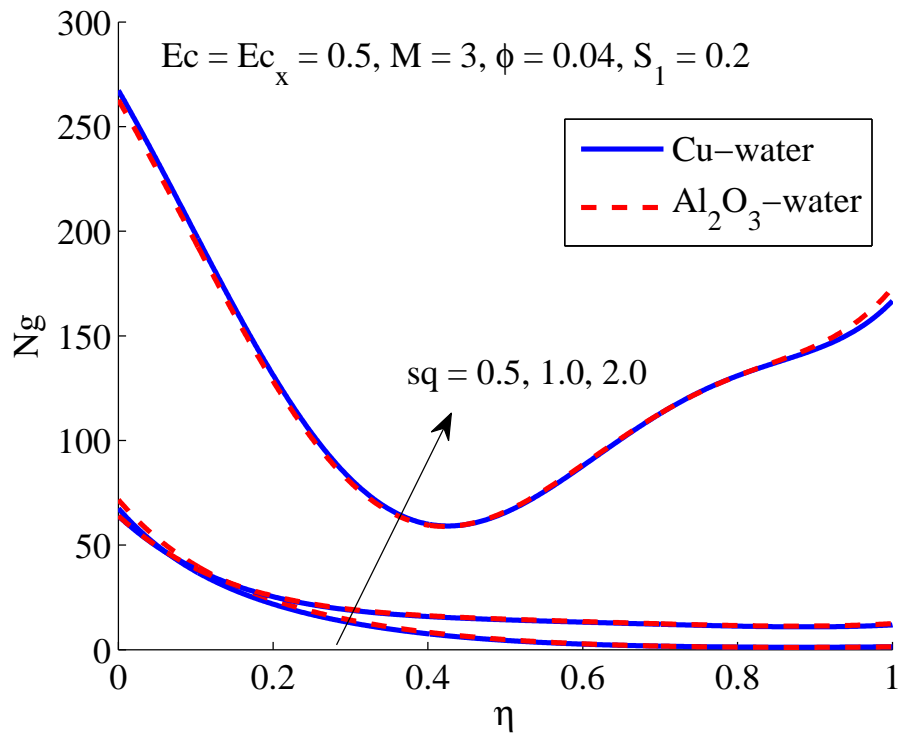


FIGURE 3.5: Impact of sq on N_g .

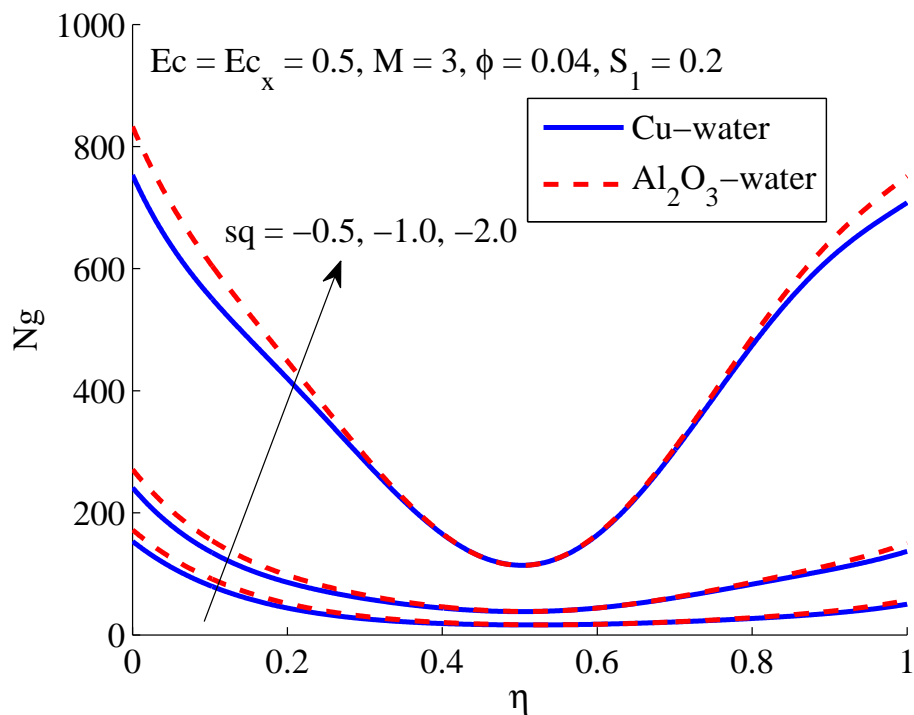


FIGURE 3.6: Impact of $-sq$ on N_g .

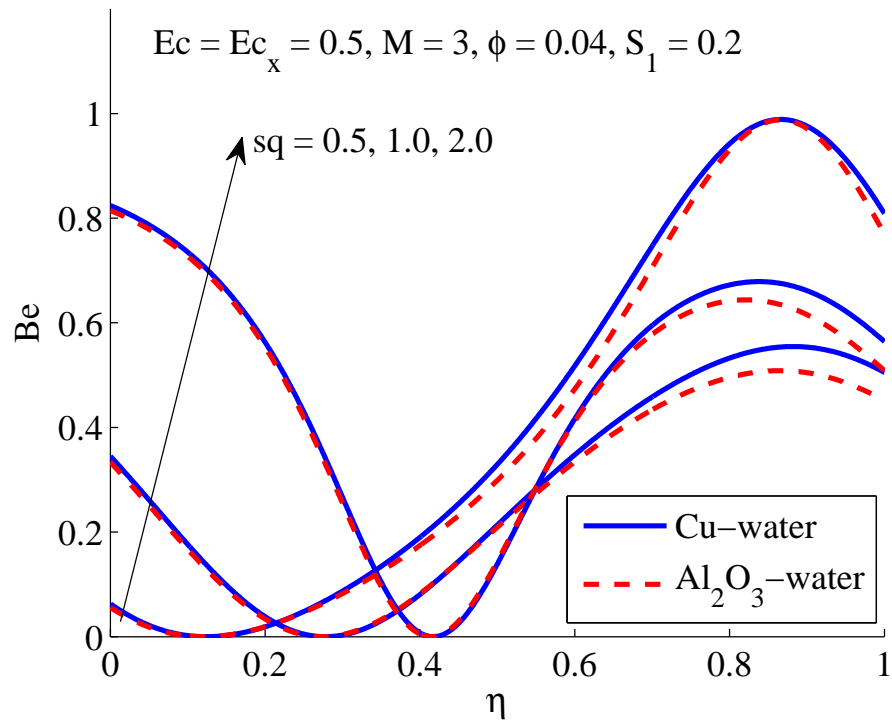


FIGURE 3.7: Impact of sq on Be .

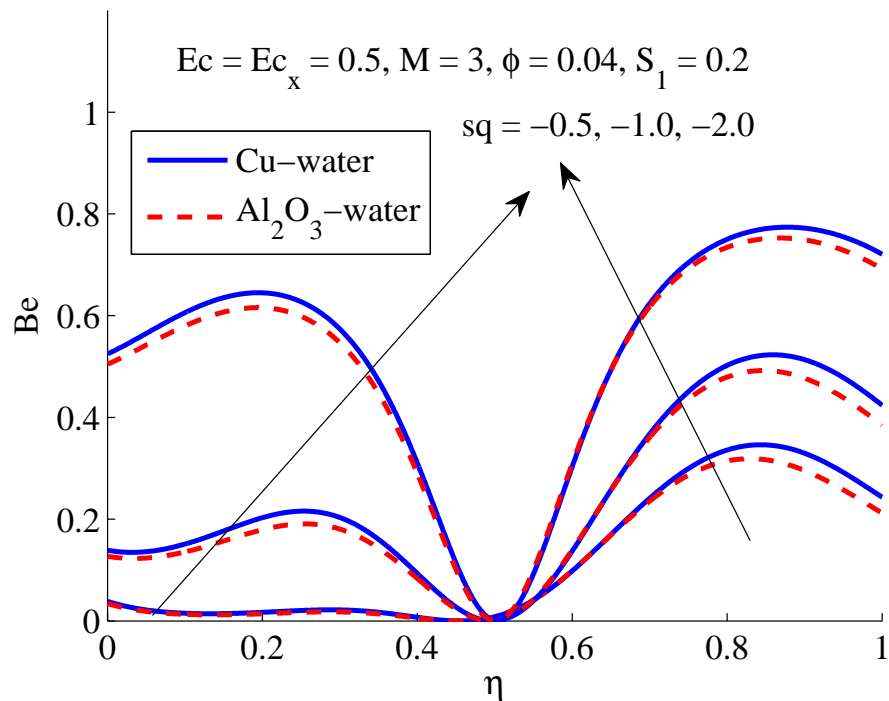


FIGURE 3.8: Impact of $-sq$ on Be .

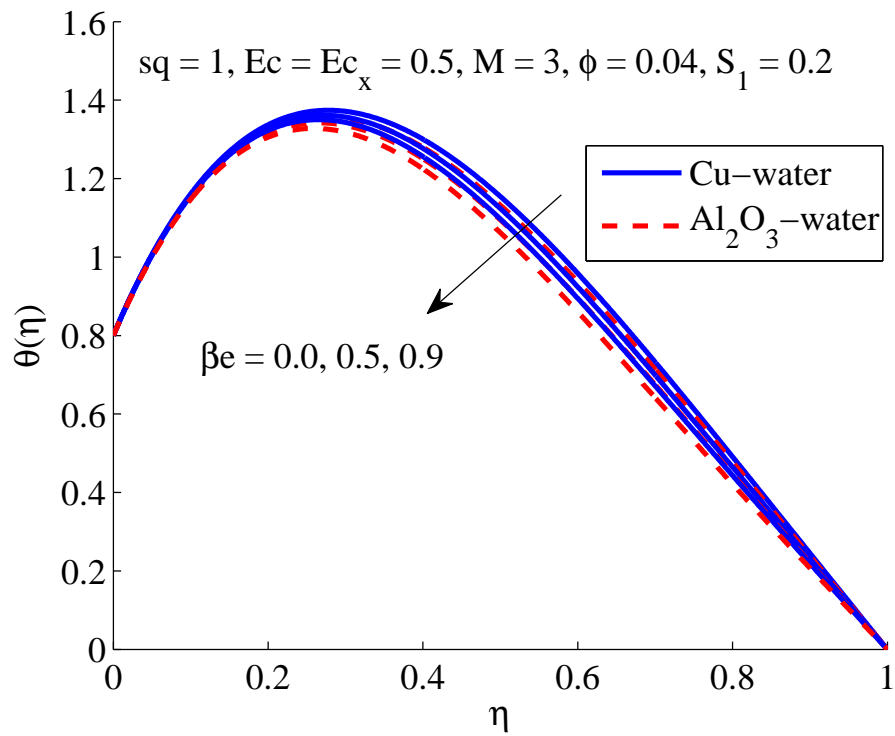


FIGURE 3.9: Impact of β_e on θ .

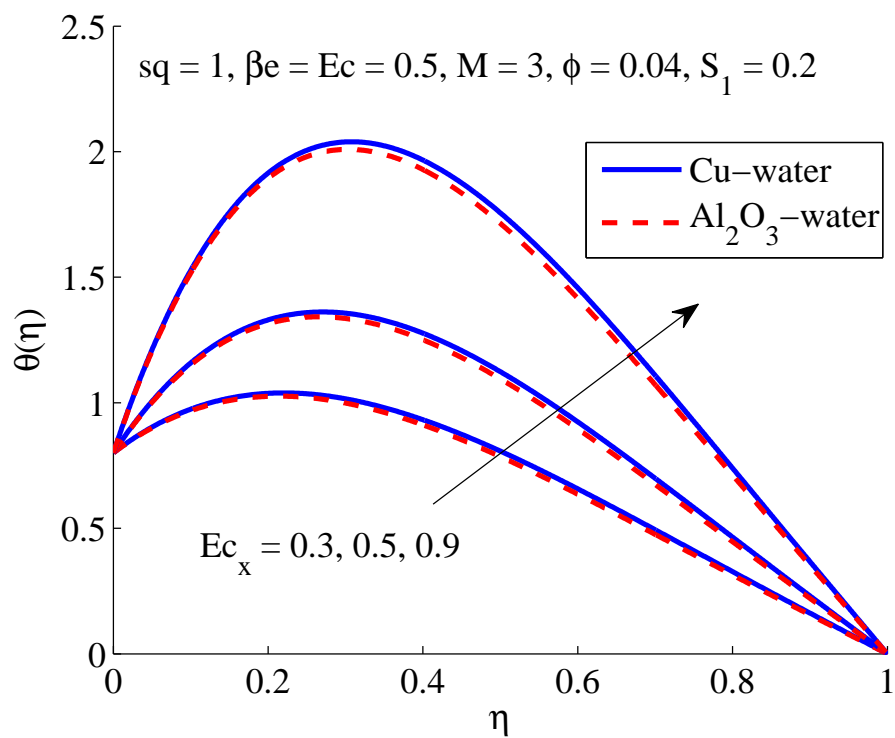


FIGURE 3.10: Impact of Ec_x on θ .

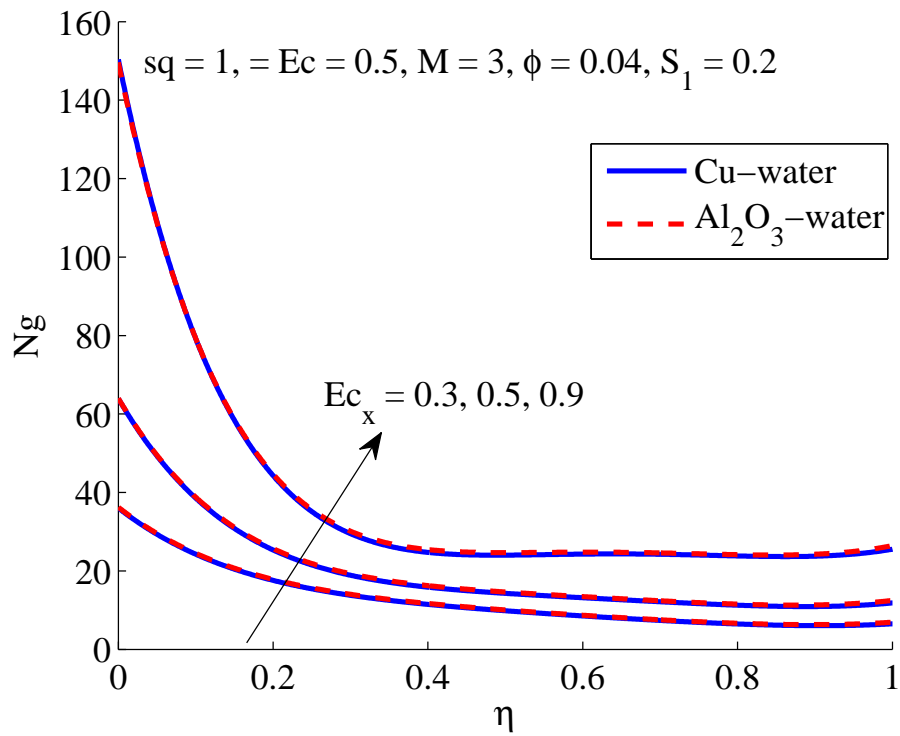


FIGURE 3.11: Impact of Ec_x on Ng .

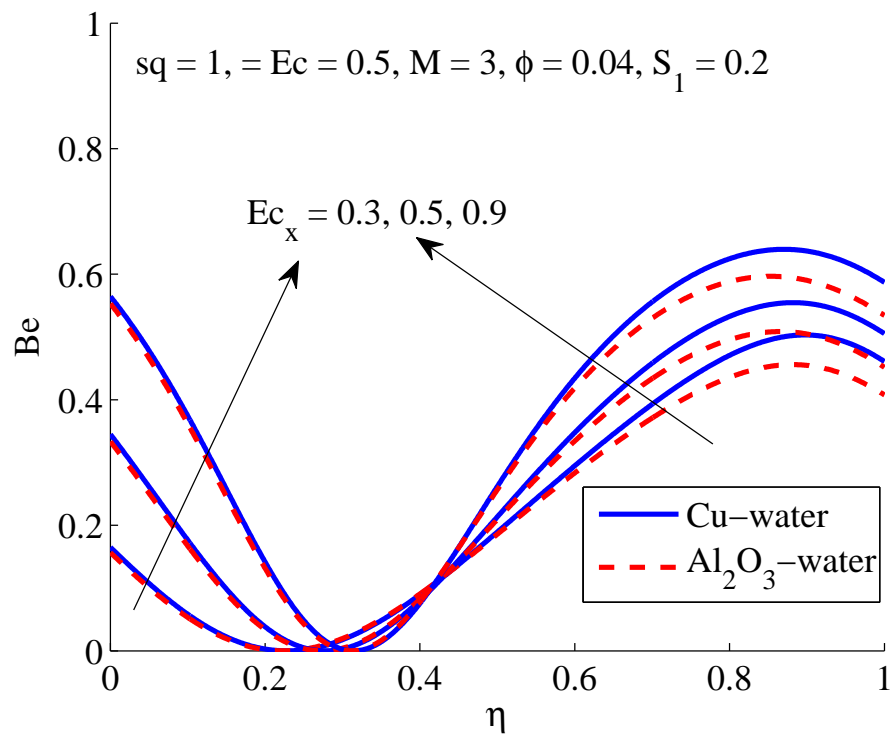
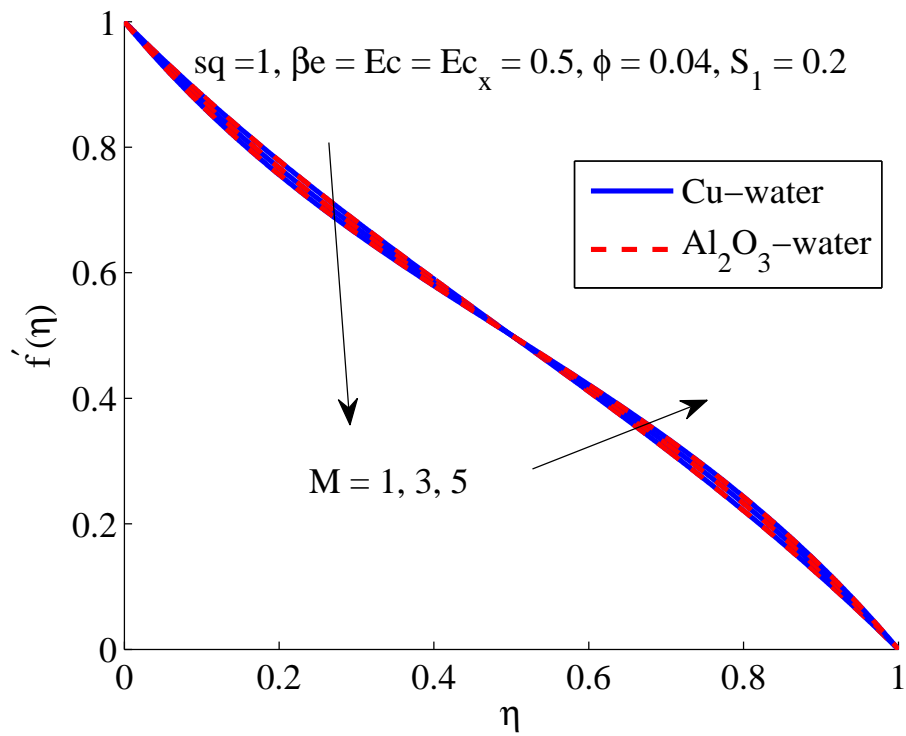
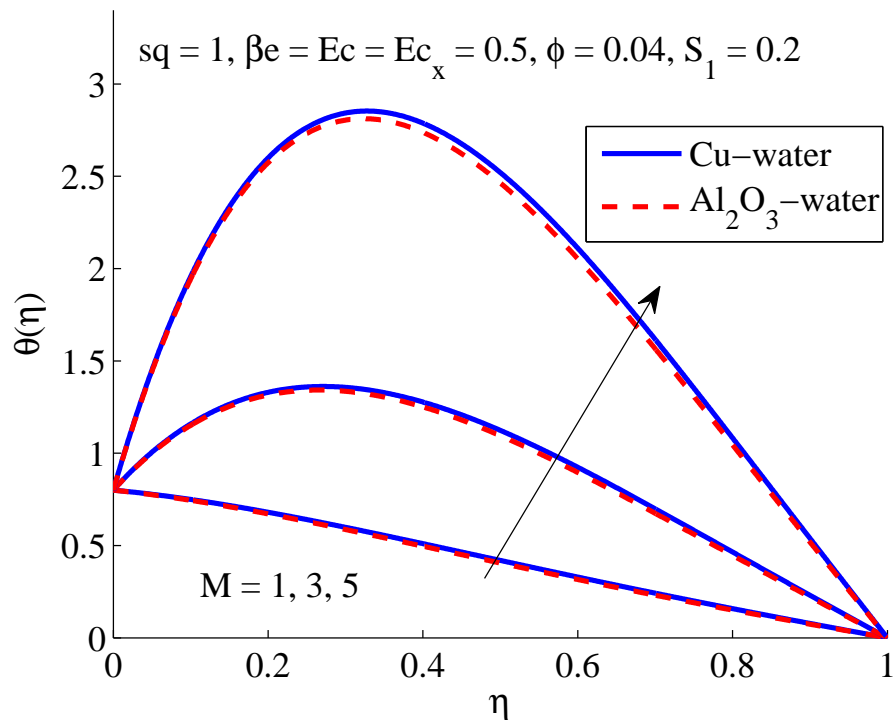


FIGURE 3.12: Impact of Ec_x on Be .

FIGURE 3.13: Impact of M on f' .FIGURE 3.14: Impact of M on θ .

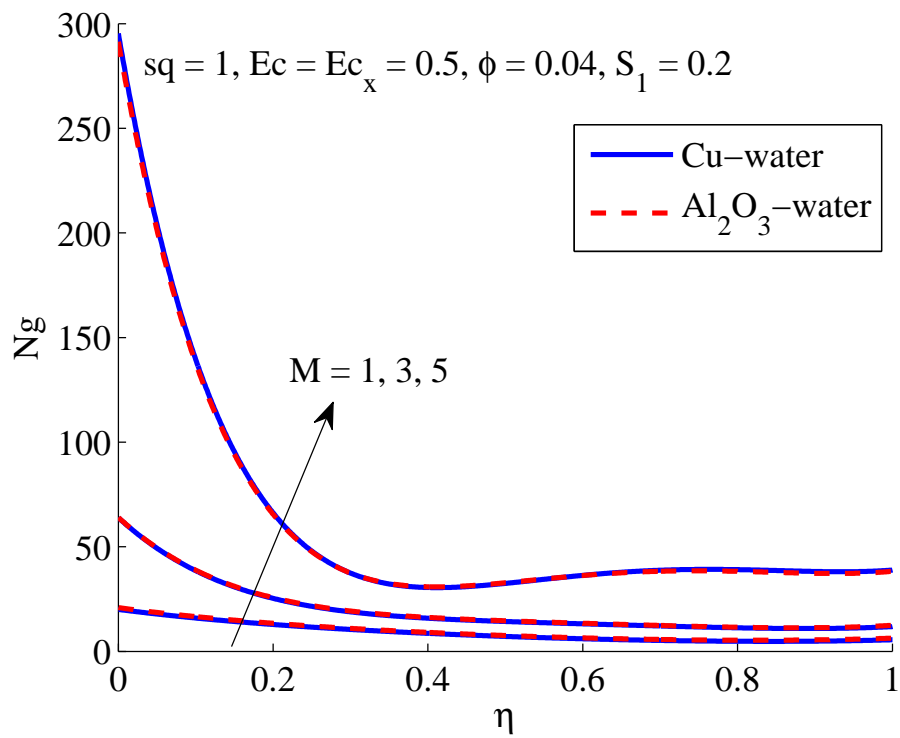


FIGURE 3.15: Impact of M on Ng.

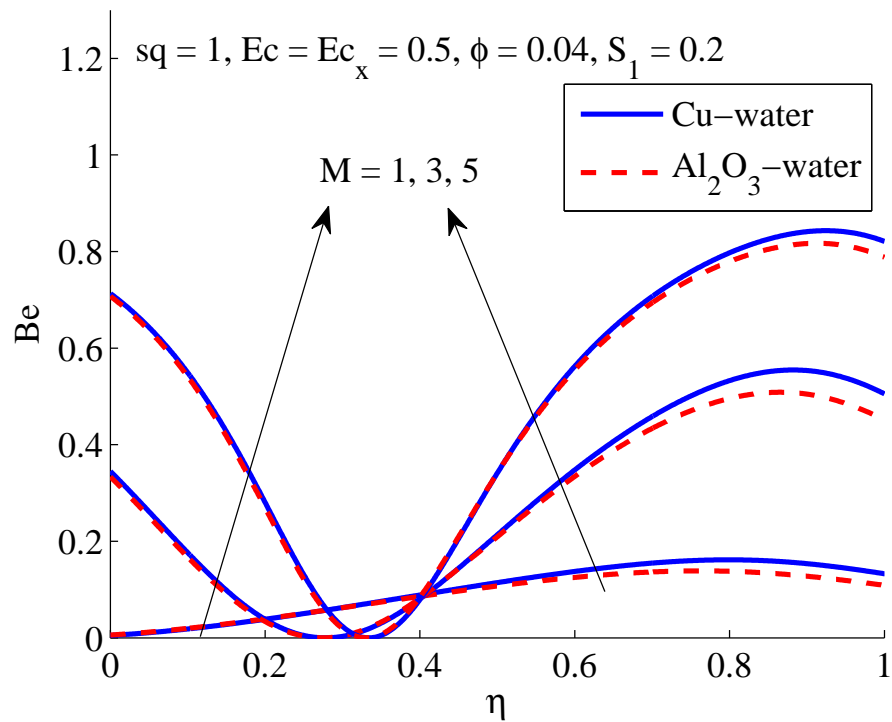


FIGURE 3.16: Impact of M on Be.

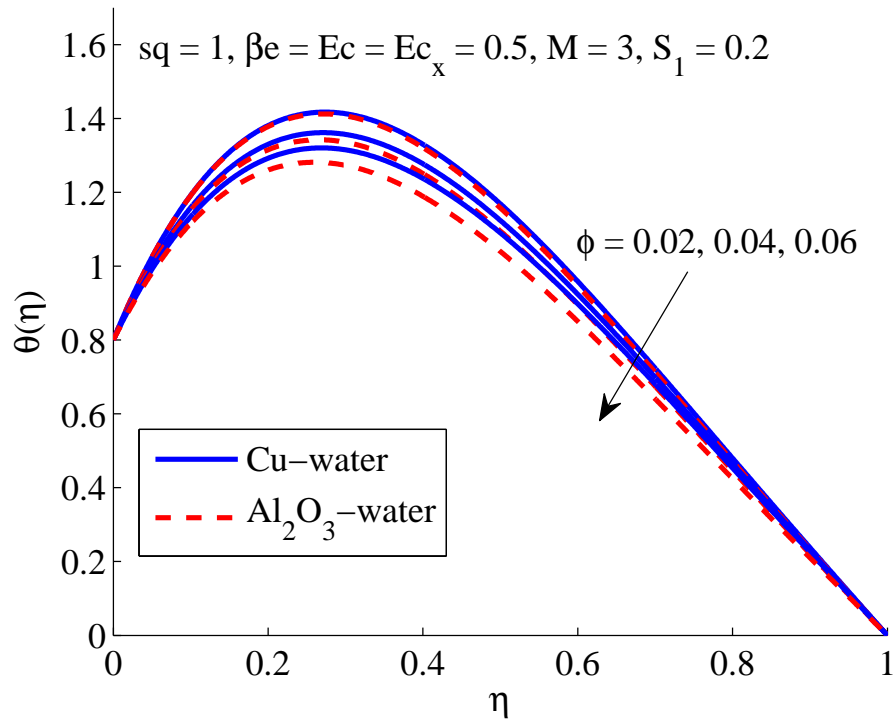


FIGURE 3.17: Impact of ϕ_1 on θ .

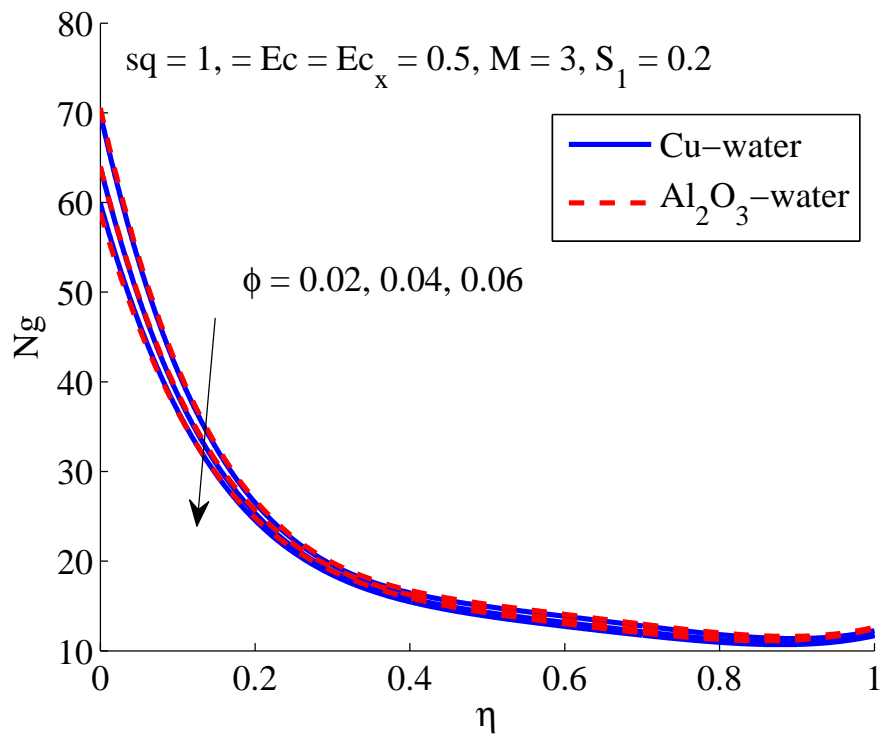
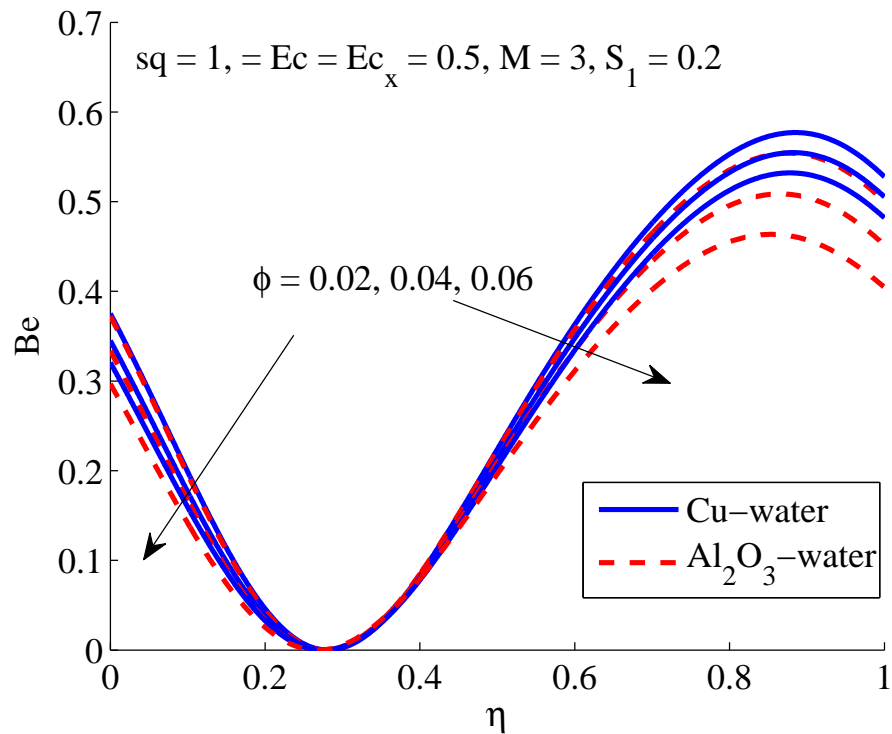


FIGURE 3.18: Impact of ϕ_1 on Ng .

FIGURE 3.19: Impact of ϕ_1 on Be.

3.5 Conclusion

The numerical results obtained by making use of the Keller box method revealed the following observations:

- The increasing values of the magnetic parameter M reduce the velocity but increase the temperature in the boundary layer as well as the entropy of the system.
- Higher positive squeezing parameter values result in an increase in the velocity of the fluid due to the added pressure exerted by the plate while negative growth of sq results in a decrease in the velocity of the fluid. The temperature of the fluid rises for the rise in sq . The entropy of the system is inclined for the increasing values of sq .
- The temperature of the system seems to be decreasing for the increasing values of the volume fraction ϕ_1 as well as the entropy of the system increases.

- The growing local Eckert numbers Ec_x enhance the temperature and the entropy of the system.
- A rise in the relaxation time parameter β_e results in the fall of the temperature of the fluid.

Chapter 4

Study of Micropolar Nanofluids with Power-law Spin Gradient Viscosity Model

4.1 Introduction

The spin gradient viscosity with power-law model and its effects on the heat transfer capabilities of the nanofluids have been examined. The theoretical analysis provides an insight into the heat conduction properties of the shear thinning and the shear thickening fluids. Boundary layer approximation based nonlinear PDEs are transformed into the nonlinear self-similar ODEs. In self-similar flows, the effect of the unbounded domain has local effect and the solution to the problem is valid in all the regions describing the fluid properties. The PDEs of fluid dynamics that describe the flow, contains dependent and independent variables that can be scaled in a manner that the problem reduces to a system of ODEs. The self-similar problem in the present chapter has been efficiently handled by a reliable finite difference scheme of Keller Box (KBM). KBM is a second order convergent unconditionally stable scheme, which is conditionally stable. The results demonstrate that the heat exchange in the nanofluids is affected substantially by the

index exponent and the modified material parameter. In addition, the physical quantities of interest from the engineering perspective, the Nusselt and the Sherwood numbers, are calculated to examine the heat and mass transport efficiency of the nanofluids. It is discovered that the temperature profile augments with an upsurge in the Brownian motion and thermophoresis parameters and decreases with an increase in the Prandtl number and power-law index. However the concentration is down-surged with a rise in the Brownian motion parameter and Schmidt number but increases with an upsurge in the thermophoresis parameter, Prandtl number and the power-law index.

4.2 Mathematical Formulation

The heat and mass transfer of micropolar nanofluid with power-law spin viscosity over the stretching surface has been considered. The flow is assumed to be steady, laminar and two-dimensional. The shear flow is produced due to large velocity gradient in the boundary layer controlled by the stretching surface moving with a velocity U_w in the horizontal direction. The large particles in fluid, as shown in Figure 4.1, represent the micropolar and small ones the nanofluid particles. The microrotation of the micropolar particles prominently affects the viscosity of the fluid and also its thermal conductivity. These microstructures have a significant impact on the flow pattern and heat transport phenomena in fluids.

Figure 4.1 shows the schematic diagram of the flow. The concentration boundary curve (CBC), temperature boundary curve (TBC) and the velocity boundary curve (VBC) are shown in the figure. The fluid, which is outside the VBC, has no rotation of micropolar particles in it. The temperature of the sheet is T_w which is greater than T_∞ the ambient temperature. The concentration of nano-particles on the sheet is C_w and C_∞ is the ambient concentration. The sheet has been pulled along the horizontal positive x -axis direction due to which the micropolar particles rotate in the anticlockwise direction. The governing equations[93] of the two-dimensional laminar flow are:

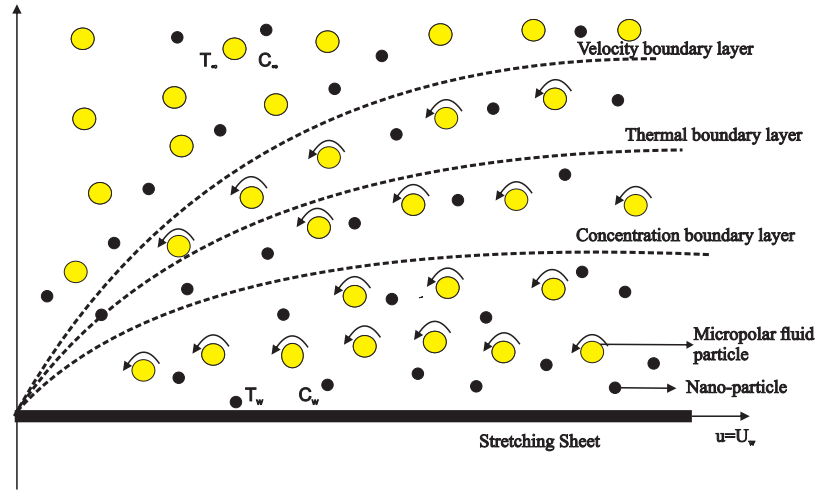


FIGURE 4.1: Flow model of the problem

$$\frac{\partial u}{\partial x} + \frac{\partial v}{\partial y} = 0, \quad (4.1)$$

$$u \frac{\partial u}{\partial x} + v \frac{\partial u}{\partial y} = \left(\frac{\mu_f + \kappa^*}{\rho} \right) \frac{\partial}{\partial y} \left(|N|^{n-1} \frac{\partial u}{\partial y} \right) + \frac{\kappa^*}{\rho} \frac{\partial}{\partial y} (|N|^{n-1} N), \quad (4.2)$$

$$\rho j \left(u \frac{\partial N}{\partial x} + v \frac{\partial N}{\partial y} \right) = \frac{\partial}{\partial y} \left(\gamma \frac{\partial N}{\partial y} \right) - \kappa^* |N|^{n-1} \left(2N + \frac{\partial u}{\partial y} \right), \quad (4.3)$$

$$u \frac{\partial T}{\partial x} + v \frac{\partial T}{\partial y} = \frac{\kappa}{\rho c_p} \frac{\partial}{\partial y} \left(|N|^{n-1} \frac{\partial T}{\partial y} \right) + \tau_1 D_B \frac{\partial T}{\partial y} \frac{\partial C}{\partial y} + \frac{\tau_1 D_T}{T_\infty} \left(\frac{\partial T}{\partial y} \right)^2 + \left(\frac{\mu_f + \kappa^*}{\rho c_p} \right) \left(|N|^{n-1} \frac{\partial u}{\partial y} \right)^2, \quad (4.4)$$

$$u \frac{\partial C}{\partial x} + v \frac{\partial C}{\partial y} = \frac{D_T}{T_\infty} \frac{\partial^2 T}{\partial y^2} + D_B \frac{\partial^2 C}{\partial y^2}. \quad (4.5)$$

The shear stress of the micropolar fluid is given as $\tau = -(\mu_f + \kappa^*) |N|^{n-1} \frac{\partial u}{\partial y} - \kappa^* |N|^{n-1} N$ [93]. The exponent n typically lies in the range $0 < n < 1$ and for $n = 1$, it represents the Newtonian fluid. The spin gradient viscosity is defined as [93]

$$\gamma = \left(\mu_f + \frac{\kappa^*}{2} \right) |N|^{n-1} j = \mu_f |N|^{n-1} \left(1 + \frac{K}{2} \right) j, \quad (4.6)$$

where K is the material parameter representing the dimensionless viscosity ratio and the inertia per unit mass $j = \left(\frac{U_w^{n-2} \mu_f x}{\rho} \right)^{\frac{2}{n+1}}$ has dimension L^2 and it represents the local reference length for $n = 1$. The boundary conditions for the

problem Eqs. (4.1)–(4.5), are as under [93]

$$u = U_w, \quad v = 0, \quad N = -m \frac{\partial u}{\partial y}, \quad T = T_w, \quad C = C_w, \quad \text{at } y = 0, \quad (4.7)$$

$$u \rightarrow 0, \quad v \rightarrow 0, \quad N \rightarrow 0, \quad T \rightarrow T_\infty, \quad C \rightarrow C_\infty \quad \text{as } y \rightarrow \infty, \quad (4.8)$$

where U_w shows the constant velocity of the sheet independent of its size and m is a constant which ranges from 0 to 1. For $m = 0$, there is no angular spin in the fluid rather it just has a very small spin near the sheet. On the other hand for $m = 1$, there is maximum spin in the fluid which represents the turbulent flow of the fluid. Here, we are using $m = \frac{1}{2}$ so that the concentration of the fluid remains mediator, which means that the antisymmetrical part of the stress tensor is deleted.

To convert the constitutive Eqs. (4.1)–(4.5) into the nondimensional form, the following similarity transforms [93] have been used.

$$\left. \begin{aligned} \psi &= \left(\frac{U_w^{2n-1} x \mu_f}{\rho} \right)^{\frac{1}{n+1}} f(\eta), & N &= \left(\frac{U_w^3 \rho}{\mu_f x} \right)^{\frac{1}{n+1}} R(\eta), \\ \eta &= \left(\frac{U_w^{2-n} \rho}{\mu_f x} \right)^{\frac{1}{n+1}} y, & \theta &= \frac{T - T_\infty}{T_w - T_\infty}, & \phi &= \frac{C - C_\infty}{C_w - C_\infty}. \end{aligned} \right\} \quad (4.9)$$

Using the above similarity transforms in Eqs. (4.1)–(4.5), the following non-dimensional ordinary differential equations can be achieved.

$$(1 + K) |R|^{n-1} \left(f''' + (n-1) \frac{R'}{R} f'' \right) + Kn |R|^{n-1} R' + \frac{1}{n+1} f f'' = 0, \quad (4.10)$$

$$\begin{aligned} &\left(1 + \frac{K}{2} \right) |R|^{n-1} \left((n-1) \frac{R'^2}{R} + R'' \right) - K |R|^{n-1} (2R + f'') \\ &+ \frac{1}{n+1} (f'R + fR') = 0, \end{aligned} \quad (4.11)$$

$$\begin{aligned} &|R|^{n-1} \left(\theta'' + (n-1) \frac{R'}{R} \theta' \right) + Pr \left(\frac{1}{n+1} f \theta' + Nb \theta' \phi' + Nt \theta'^2 \right) \\ &+ (1 + K) Ec |R|^{2(n-1)} f'^2 = 0, \end{aligned} \quad (4.12)$$

$$\phi'' + \frac{1}{n+1} Sc f \phi' + \frac{Nt}{Nb} \theta'' = 0. \quad (4.13)$$

The dimensionless boundary conditions are:

$$f(\eta) = 0, \quad f'(\eta) = 1, \quad R(\eta) = -\frac{1}{m}f''(\eta), \quad \theta(\eta) = 1, \quad \phi(\eta) = 1, \quad \text{at } \eta = 0, \quad (4.14)$$

$$f'(\eta) = 0, \quad R(\eta) = 0, \quad \theta(\eta) = 0, \quad \phi(\eta) = 0, \quad \text{as } \eta \rightarrow \infty. \quad (4.15)$$

The formulae of different parameters used in the above dimensionless model are:

$$Nb = \tau_1 D_B (C_w - C_\infty) \left(\frac{\rho^2 x^{n-1}}{U_w^{3n-3} \mu_f^2} \right)^{\frac{1}{n+1}}, \quad Nt = \tau_1 D_T \frac{T_w - T_\infty}{T_\infty} \left(\frac{\rho^2 x^{n-1}}{U_w^{3n-3} \mu_f^2} \right)^{\frac{1}{n+1}}$$

$$Pr = \frac{c_p \mu_f}{\kappa}, \quad Ec = \frac{1}{c_p} \left(\frac{U_w^{12n} \rho^{3n-1}}{x \mu_f^{3n-1}} \right)^{\frac{1}{n+1}} \quad \text{and} \quad Sc = \left(\frac{U_w^{3n-3} \mu_f^2}{D_B \rho^2 x^{n-1}} \right)^{\frac{1}{n+1}}.$$

Regarding their applications in the engineering industry, Nusselt and Sherwood numbers are given significant importance in the heat and mass transfer analysis. Nusselt number that is the heat transfer rate whereas Sherwood number is the mass transfer rate for the shear flow. These two are respectively formulated as shown below:

$$Nu_x = \frac{x q_w}{k_{nf} (T_w - T_\infty)}, \quad Sh_x = \frac{x q_m}{D_B (C_w - C_\infty)},$$

where $k_{nf} = \kappa |N|^{n-1}$, $q_m = -D_B \frac{\partial C}{\partial y} \Big|_{y=0}$ and $q_w = -\kappa \left(|N|^{n-1} \frac{\partial T}{\partial y} \right)_{y=0}$.

Using these expressions for q_w , k_{nf} and q_m and after some necessary simplifications, one can easily get

$$Nu = \frac{Nu_x}{Re_x^{\frac{1}{n+1}}} = -\theta'(0) \quad \text{and} \quad Sh = \frac{Sh_x}{Re_x^{\frac{1}{n+1}}} = -\phi'(0),$$

where $Re_x = \frac{\rho x^n U_w^{2-n}}{\mu_f}$ is the local Reynolds number.

4.3 Solution Methodology

Grid test was conducted to ensure that the solution of the problem is independent of the mesh grid. Different values of the step size and different values at

boundary are considered corresponding to the fixed values of the parameters $Nb = Nt = 0.1, Le = K = n = 1, Ec = 0.5$ and $Pr = 2$ and values of reduced Nusselt number and reduced Sherwood number has been calculated. It is clear from the values of Nusselt and Sherwood numbers for .002 and 0.001 that values are independent mesh size and η_∞ .

Keller box method, which is an unconditionally stable finite difference scheme

Step Size h	Nu			Sh		
	$\eta_\infty = 5$	$\eta_\infty = 10$	$\eta_\infty = 12$	$\eta_\infty = 5$	$\eta_\infty = 10$	$\eta_\infty = 12$
0.2	0.585364	0.595767	0.595915	0.111289	0.086616	0.086753
0.1	0.582010	0.592523	0.595915	0.114520	0.086615	0.086753
0.05	0.580378	0.590986	0.591132	0.116047	0.090816	0.090954
0.02	0.579395	0.590091	0.590237	0.116959	0.091575	0.091712
0.01	0.579057	0.589797	0.589943	0.117275	0.091822	0.091959
0.008	0.578987	0.589739	0.589884	0.117342	0.091971	0.092008
0.005	0.578879	0.589711	0.589796	0.117445	0.092018	0.092012
0.002	0.578762	0.589709	0.589708	0.117561	0.092018	0.092019
0.001	0.578762	0.589708	0.589708	0.117561	0.092017	0.092018

TABLE 4.1: Values of Nusselt and Sherwood numbers for different values of h and η_∞

with a second order convergence [81] has been used to solve the system of non-linear ODEs (4.10)-(4.13) along with the boundary conditions (4.14) and (4.15) numerically. The present section includes the detailed procedural description of this method. A flow chart summarizing the computational procedure of the Keller box method is shown in Figure 4.2.

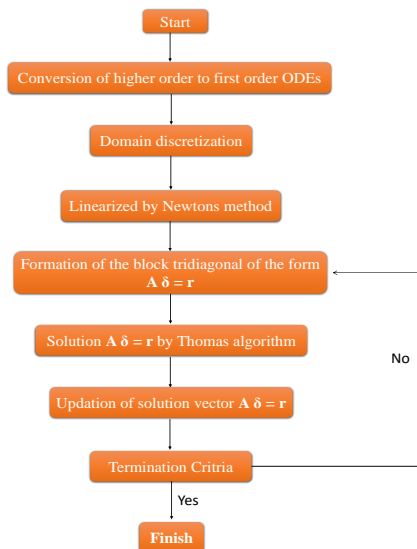


FIGURE 4.2: Flow Chart: Keller box method

To have a more insight of the Keller box method applied to a problem of similar nature, [94] can also be consulted. The first step of this procedure is to write the equations (4.10)-(4.13) as defined under.

$$f''' = g(\eta, f, f'', R, R'), \tag{4.16}$$

$$R'' = h(\eta, f'', R, R'), \tag{4.17}$$

$$\theta'' = k(\eta, f, R, R', \theta', \phi'), \tag{4.18}$$

$$\phi'' = l(\eta, f, \theta'', \phi'). \tag{4.19}$$

In the second step, convert the equations (4.16)-(4.19) to a system of first order ODEs as

$$f' = u, \tag{4.20}$$

$$u' = v, \tag{4.21}$$

$$R' = G, \tag{4.22}$$

$$\theta' = t, \tag{4.23}$$

$$\phi' = p, \tag{4.24}$$

$$v' = g(\eta, f, v, R, G), \tag{4.25}$$

$$G' = R(\eta, v, R, G), \tag{4.26}$$

$$t' = k(\eta, f, R, G, t, p), \tag{4.27}$$

$$p' = l(\eta, f, t', p). \tag{4.28}$$

With the newly introduced variables, the boundary conditions become:

$$f(\eta) = 0, \quad u(\eta) = 1, \quad R(\eta) = -\frac{1}{m}v(\eta), \quad \theta(\eta) = 1, \quad \phi(\eta) = 1, \quad \text{at } \eta = 0, \tag{4.29}$$

$$u(\eta) = 0, \quad R(\eta) = 0, \quad \theta(\eta) = 0, \quad \phi(\eta) = 0, \quad \text{as } \eta \rightarrow \infty. \tag{4.30}$$

Now, the system of ODEs (4.20)-(4.28) will be discretized as the third step in the following sense:

$$(f')_{j-\frac{1}{2}}^{i+1} = (u)_{j-\frac{1}{2}}^{i+1}, \tag{4.31}$$

$$(u')_{j-\frac{1}{2}}^{i+1} = (v)_{j-\frac{1}{2}}^{i+1}, \tag{4.32}$$

$$(R')_{j-\frac{1}{2}}^{i+1} = (G)_{j-\frac{1}{2}}^{i+1}, \tag{4.33}$$

$$\delta = \left[\delta_1 \quad \delta_2 \quad - \quad - \quad \delta_{J-1} \quad \delta_J \right]^T, \tag{4.43}$$

and

$$r = \left[(r_1)_{j-\frac{1}{2}} \quad (r_2)_{j-\frac{1}{2}} \quad (r_3)_{j-\frac{1}{2}} \quad (r_4)_{j-\frac{1}{2}} \quad (r_5)_{j-\frac{1}{2}} \quad (r_6)_{j-\frac{1}{2}} \quad (r_7)_{j-\frac{1}{2}} \quad (r_8)_{j-\frac{1}{2}} \quad (r_9)_{j-\frac{1}{2}} \right]^T, \tag{4.44}$$

where $[]^T$ denotes the transpose of $[]$.

Also the matrices A_1 and A_j are defined as:

$$A_1 = \begin{bmatrix} 0 & 0 & 0 & 0 & 1 & 0 & 0 & 0 & 0 \\ 0 & 0 & 0 & 0 & 0 & \frac{-h}{2} & 0 & 0 & 0 \\ -1 & \frac{-h}{2} & 0 & 0 & 0 & 0 & \frac{-h}{2} & 0 & 0 \\ 0 & 0 & \frac{-h}{2} & 0 & 0 & 0 & 0 & \frac{-h}{2} & 0 \\ 0 & 0 & 0 & \frac{-h}{2} & 0 & 0 & 0 & 0 & \frac{-h}{2} \\ (a_8)_1 & (a_{10})_1 & (a_{14})_1 & (a_{18})_1 & (a_1)_1 & (a_5)_1 & (a_9)_1 & (a_{13})_1 & (a_{17})_1 \\ (b_8)_1 & (b_{10})_1 & (b_{14})_1 & (b_{18})_1 & (b_1)_1 & (b_5)_1 & (b_9)_1 & (b_{13})_1 & (b_{17})_1 \\ (c_8)_1 & (c_{10})_1 & (c_{14})_1 & (c_{18})_1 & (c_1)_1 & (c_5)_1 & (c_9)_1 & (c_{13})_1 & (c_{17})_1 \\ (d_8)_1 & (d_{10})_1 & (d_{14})_1 & (d_{18})_1 & (d_1)_1 & (d_5)_1 & (d_9)_1 & (d_{13})_1 & (d_{17})_1 \end{bmatrix}, \tag{4.45}$$

$$A_j = \begin{bmatrix} \frac{-h}{2} & 0 & 0 & 0 & 1 & 0 & 0 & 0 & 0 \\ -1 & 0 & 0 & 0 & 0 & \frac{-h}{2} & 0 & 0 & 0 \\ 0 & -1 & 0 & 0 & 0 & 0 & \frac{-h}{2} & 0 & 0 \\ 0 & 0 & -1 & 0 & 0 & 0 & 0 & \frac{-h}{2} & 0 \\ 0 & 0 & 0 & -1 & 0 & 0 & 0 & 0 & \frac{-h}{2} \\ (a_4)_j & (a_8)_j & (a_{12})_j & (a_{16})_j & (a_1)_j & (a_5)_j & (a_9)_j & (a_{13})_j & (a_{17})_j \\ (b_4)_j & (b_8)_j & (b_{12})_j & (b_{16})_j & (b_1)_j & (b_5)_j & (b_9)_j & (b_{13})_j & (b_{17})_j \\ (c_4)_j & (c_8)_j & (c_{12})_j & (c_{16})_j & (c_1)_j & (c_5)_j & (c_9)_j & (c_{13})_j & (c_{17})_j \\ (d_4)_j & (d_8)_j & (d_{12})_j & (d_{16})_j & (d_1)_j & (d_5)_j & (d_9)_j & (d_{13})_j & (d_{17})_j \end{bmatrix}; 2 \leq j \leq J, \tag{4.46}$$

The matrix B_j is given by

$$B_j = \begin{bmatrix} 0 & 0 & 0 & 0 & -1 & 0 & 0 & 0 & 0 & 0 \\ 0 & 0 & 0 & 0 & 0 & \frac{-h}{2} & 0 & 0 & 0 & 0 \\ 0 & 0 & 0 & 0 & 0 & 0 & \frac{-h}{2} & 0 & 0 & 0 \\ 0 & 0 & 0 & 0 & 0 & 0 & 0 & \frac{-h}{2} & 0 & 0 \\ 0 & 0 & 0 & 0 & 0 & 0 & 0 & 0 & \frac{-h}{2} & 0 \\ 0 & 0 & 0 & 0 & (a_2)_j & (a_6)_j & (a_{10})_j & (a_{14})_j & (a_{16})_j & 0 \\ 0 & 0 & 0 & 0 & (b_2)_j & (b_6)_j & (b_{10})_j & (b_{14})_j & (b_{16})_j & 0 \\ 0 & 0 & 0 & 0 & (c_2)_j & (c_6)_j & (c_{10})_j & (c_{14})_j & (c_{16})_j & 0 \\ 0 & 0 & 0 & 0 & (d_2)_j & (d_6)_j & (d_{10})_j & (d_{14})_j & (d_{16})_j & 0 \end{bmatrix}, \quad (4.47)$$

where $3 \leq j \leq J$,

The matrix C_j is defined as:

$$C_j = \begin{bmatrix} \frac{-h}{2} & 0 & 0 & 0 & 0 & 0 & 0 & 0 & 0 & 0 \\ 1 & 0 & 0 & 0 & 0 & 0 & 0 & 0 & 0 & 0 \\ 0 & 1 & 0 & 0 & 0 & 0 & 0 & 0 & 0 & 0 \\ 0 & 0 & 1 & 0 & 0 & 0 & 0 & 0 & 0 & 0 \\ 0 & 0 & 0 & 1 & 0 & 0 & 0 & 0 & 0 & 0 \\ (a_3)_j & (a_7)_j & (a_{11})_j & (a_{15})_j & 0 & 0 & 0 & 0 & 0 & 0 \\ (b_3)_j & (b_7)_j & (b_{11})_j & (b_{15})_j & 0 & 0 & 0 & 0 & 0 & 0 \\ (c_3)_j & (c_7)_j & (c_{11})_j & (c_{15})_j & 0 & 0 & 0 & 0 & 0 & 0 \\ (d_3)_j & (d_7)_j & (d_{11})_j & (d_{15})_j & 0 & 0 & 0 & 0 & 0 & 0 \end{bmatrix}, \quad (4.48)$$

where $2 \leq j \leq J - 1$.

Then, the LU factorization is applied to the system (4.41) to determine the vector of unknowns δ . The solution vector is updated by the expression given in (4.40). In order to verify our Matlab code, the numerical values of the Nusselt number are calculated by using Keller box method code and presented in Table 4.2 which are matched with the values of Nusselt number reported by Mustafa [95]. Mustafa used a collocation based MATLAB routine for finding the solution of the governing model.

Nt	M	α	Pr	Mustafa [95]	Present	
					Keller box	bvp4c
0.1	0.5	0.25	7	0.407717	0.407717	0.407717
0.3	0.5	0.25	7	0.347439	0.347441	0.347439
0.5	0.5	0.25	7	0.289524	0.289522	0.289522
0.7	0.5	0.25	7	0.180515	0.238632	0.238638
0.5	0.2	0.25	7	0.399324	0.399324	0.399324
0.5	0.4	0.25	7	0.323281	0.323281	0.323280
0.5	0.8	0.25	7	0.206541	0.206513	0.206516
0.5	0.5	0.0	10	0.339731	0.339731	0.339725
0.5	0.5	0.2	10	0.330622	0.330620	0.330619
0.5	0.5	0.5	10	0.315646	0.315647	0.315646
0.5	0.5	1.0	10	0.288854	0.288855	0.288855
0.5	0.5	0.25	5	0.254657	0.254656	0.254654
0.5	0.5	0.25	6.2	0.276789	0.276788	0.276787
0.5	0.5	0.25	8	0.303769	0.303772	0.303769
0.5	0.5	0.25	13	0.358263	0.358265	0.358263

TABLE 4.2: Nusselt number for different values of Nt , M , α and Pr and for the fixed values of parameters $\gamma = 0.25$, $Nb = 0.5$ and $Sc = 10$.

4.4 Discussion on Results

In this section the solution of the system of nondimensional boundary value problem (4.10)–(4.15) has been presented in the form of tables and graphs with a brief description on the physical significance of the pertinent physical parameters. The Nusselt and the Sherwood numbers corresponding to different physical parameters are included in Table 4.3. By increasing the Brownian motion parameter Nb , the value of the Nusselt number starts decreasing but an opposite trend is seen in the Sherwood number. Due to an increase in the Brownian motion of nano-particles in the fluid, the heat transfer rate is increased which is reason of the decrease in the Nusselt number and on the other hand the concentration of the fluid increases. A decrement in the heat and mass transfer rates is witnessed when the thermophoresis parameter is increased. An enhancement in the Prandtl number leads to an increment in the Nusselt number but an opposite trend is seen for Sherwood number. As the value of the Schmidt number increases, the value of the Nusselt number decreases but the Sherwood number shows an opposite trend. The values of the Nusselt as well as the Sherwood numbers increase, with an

increase in the spin viscosity number K . The power index number n increases the Nusselt number but causes a decrement in the Sherwood number. CPU time is calculated on the laptop with the specification are Core i3 2.00GHz with RAM 4GB.

Figures 4.3 and 4.4 elaborate the Brownian motion effect on the temperature and

Nb	Nt	Pr	Sc	K	n	Ec	Nu	Sh	CPU time(seconds)
0.1	0.1	2.0	1.0	1.0	0.9	0.5	0.43010	0.25649	8.063635
	0.3						0.36000	0.43217	8.070924
	0.5						0.29708	0.46589	7.911895
	0.7						0.24122	0.47937	8.870895
		0.3					0.38668	-0.10372	8.077485
		0.5					0.34722	-0.34064	8.005270
		0.7					0.31144	-0.47501	8.126491
			0.7				0.13119	0.46761	8.035622
			5.0				0.77909	-0.022962	8.086052
			6.2				0.8715	-0.10101	7.879745
				0.5			0.44594	0.018951	7.966110
				1.5			0.4213	0.4267	8.248886
				2.0			0.41559	0.5636	8.444462
					0.5		0.45006	0.22214	7.975184
					1.5		0.41296	0.28392	8.617824
					2.0		0.39782	0.30662	9.371674
						0.75	0.33261	0.37314	11.077164
						0.85	0.4007	0.29371	8.915333
						0.95	0.45712	0.220	7.430111
						1.00	0.48219	0.18552	6.806964
						1.05	0.50568	0.15133	6.515914
						0.1	0.56191	0.14634	7.913128
						0.7	0.36401	0.31174	7.940444
						0.9	0.29778	0.3671	7.714811

TABLE 4.3: Nusselt number and Sherwood number corresponding to different values of parameters.

concentration profiles. Figure 4.3 reveals that a greater Brownian motion parameter increases the temperature in boundary layer. This happens because a greater Brownian motion increases the kinetic energy of the fluid which in return makes the temperature of the fluid high in the boundary layer.

In Figure 4.4, it is witnessed that the concentration of the nanofluid in the boundary layer decreases with an increase in the Brownian motion parameter. The

reason for this is a high concentration difference of the nano-particles with greater values of the Brownian motion parameter, which decreases the mass transfer rate. Figure 4.5 discusses the impact of the thermophoresis on the temperature profile. The temperature in the boundary layer is observed to rise with an increment in the thermophoresis parameter Nt . A thermophoretic force is produced due to the influence of the thermophoresis parameter, which moves the nanoparticles from the hotter region to the colder region, thus the concentration of the nanoparticles is increased in the colder region that is near the lower plate. Greater the value of the thermophoresis parameter, greater is the thermophoretic force produced. Hence the concentration of nanoparticles is greater than 1 near the lower plate which can be observed in Figure 4.6.

Figures 4.7-4.8 illuminate the changes in the temperature and concentration profiles with variation in the Prandtl number. In Figure 4.7, it can be seen that increasing values of the Prandtl number Pr decline the temperature profile but the boundary layer thickness is increased. Near the surface, the increasing values of the Prandtl number increase the concentration profile but the behavior changes as we move away from the surface as revealed in Figure 4.8. An increment in the Prandtl number is an indication that the convective transport is dominant to the diffusive transport in the nanofluid. Since the velocity is maximum at the plate surface, so the convective transport effects are dominant, hence the increasing values of Prandtl number are responsible for an increase in the concentration profile. As we move away from the surface, the convective effects are less dominant, so greater Prandtl number reduces the concentration profile.

Figure 4.9 indicates that the growing values of the Schmidt number increase the concentration boundary layer thickness because less mass is diffused from the boundary. Figures 4.10-4.11 discuss the impact of rotation viscosity parameter K on the fluid flow properties in the boundary layer. The greater K affects positively on the velocity of the nanofluid near the wall (see Figure 4.10), which in return reduces the effects of the angular velocity (see Figure 4.11). Thus a rise in K decreases the angular velocity near the wall. However, as we move away from the wall, the linear velocity tends to decrease which results in an increase in the

angular velocity of the nanofluid. Figures 4.12-4.13 illuminate the impact of the rotation viscosity on the temperature and concentration profiles. As the rotation viscosity increases, both the temperature and the concentration profiles decrease.

Figure 4.14 analyzes the effect of the power-law index on the velocity of the nanofluid. The results are produced for the case of shear thinning nanofluids. This Figure describes that a rise in the power-law index n leads to a decline in the fluid velocity but the velocity boundary layer thickness is enhanced. The physical explanation to this behavior is that an increase in the power-law index decreases the viscosity of the fluid, thus less resistance is experienced by the fluid. The angular velocity is plotted against the variation in the power-law index in Figure 4.15. This figure shows that the shear thinning effect of the nanofluid increases the linear velocity near the wall, which negatively affects the angular velocity. However, away from the wall, an opposite behavior is witnessed. Looking at the graph, we observe that the behavior of the graph changes at a certain point away from the surface. There is a point of inflection observed in the flow. Before the point of inflection, the profile is concaved down whereas after that point, the profile is concaved up.

Figures 4.16-4.17 narrate the impact of the power-law index on the temperature and concentration profiles. With an augmentation in the power-law index, the thermal profile increases but the concentration profile is found to decrease. Figure 4.18 explains the impact of Eckert number on the temperature profile. As the Eckert number is the ratio of kinetic energy to the enthalpy of the system, so with an enhancement in the value of the Eckert number the temperature profile of the fluid increases. Figures 4.19-4.21 present the stream lines for different values of the power-law index n . As the values of n are increased, the stream lines become thinner. As the viscosity of the fluid is increased, the velocity is found to decline. Figures 4.22-4.24 are plotted to portray the stream lines for different values of the spin gradient viscosity parameter K . As we increase the values of the parameter K , the stream lines become thinner, can be seen from colour blue to red which expresses that with the increasing values of K , the fluid becomes dense, hence the velocity of the fluid decreases.

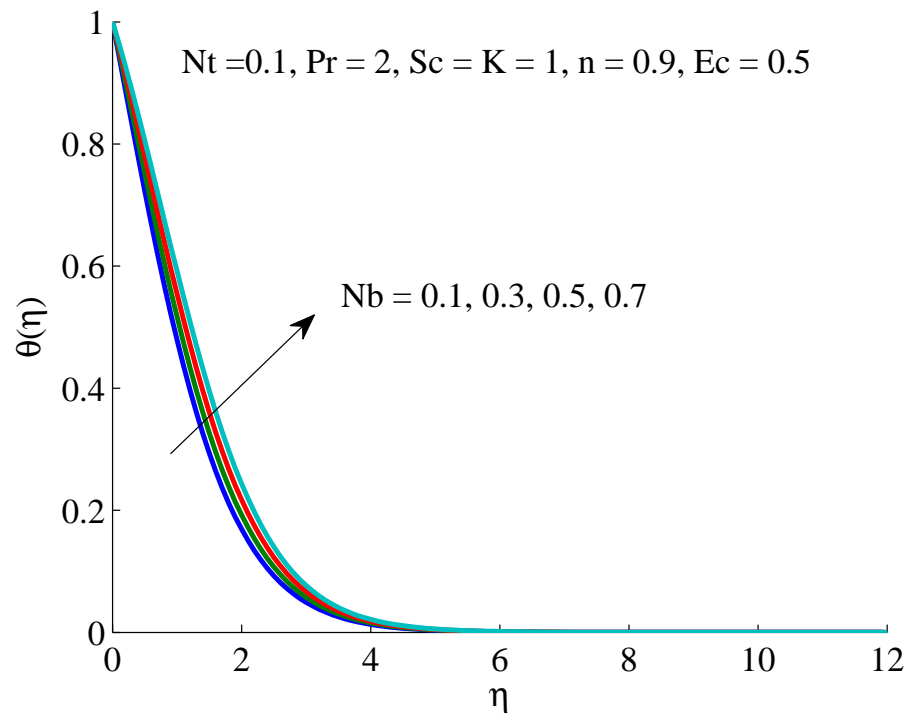


FIGURE 4.3: Variation in θ subject to Nb .

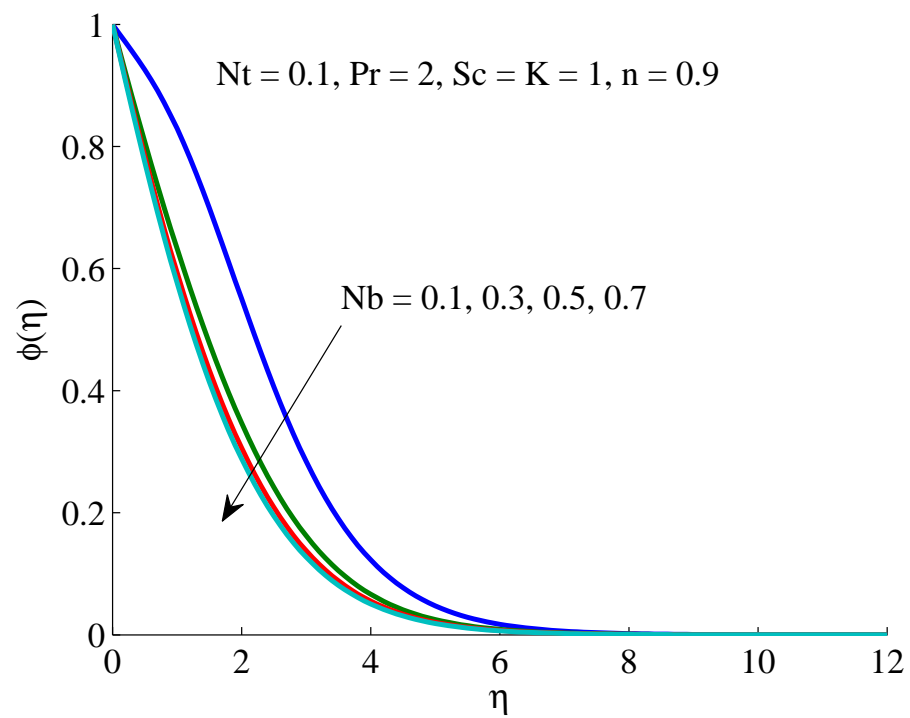


FIGURE 4.4: Variation in ϕ subject to Nb .

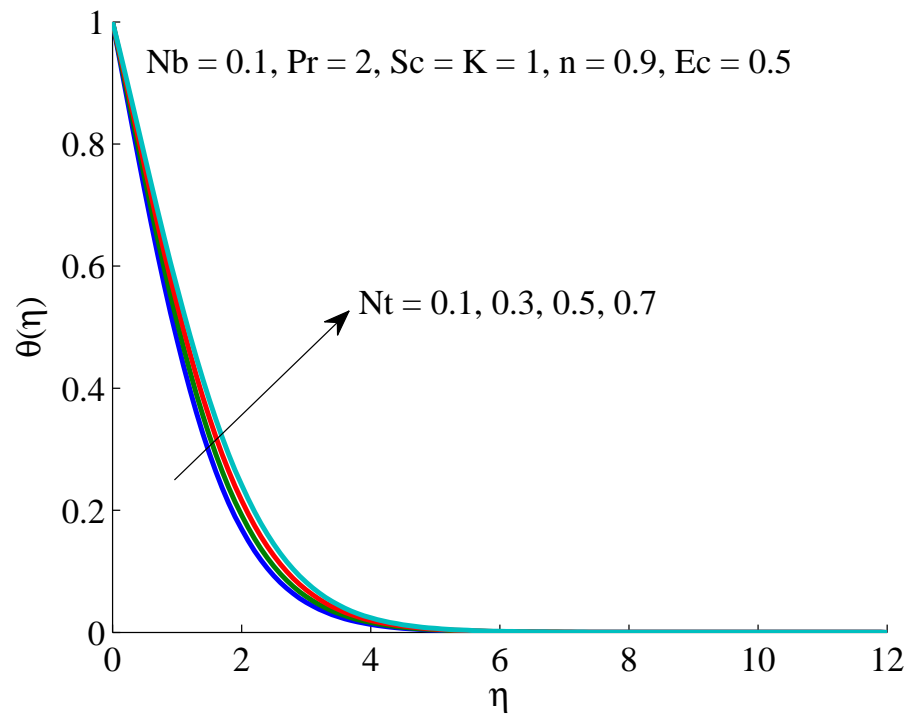


FIGURE 4.5: Variation in θ subject to Nt .

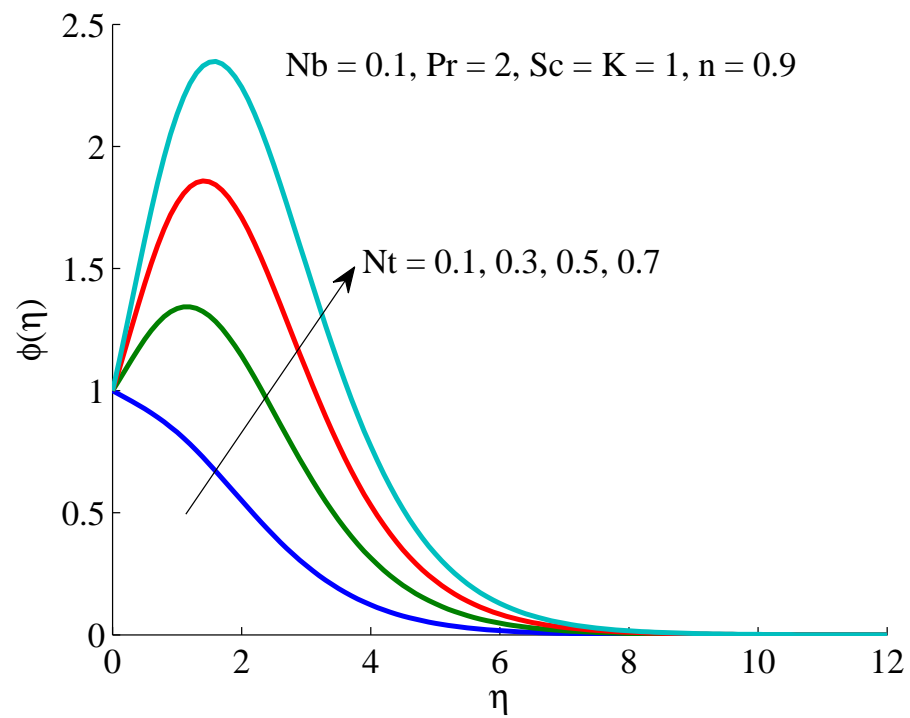


FIGURE 4.6: Variation in ϕ subject to Nt .

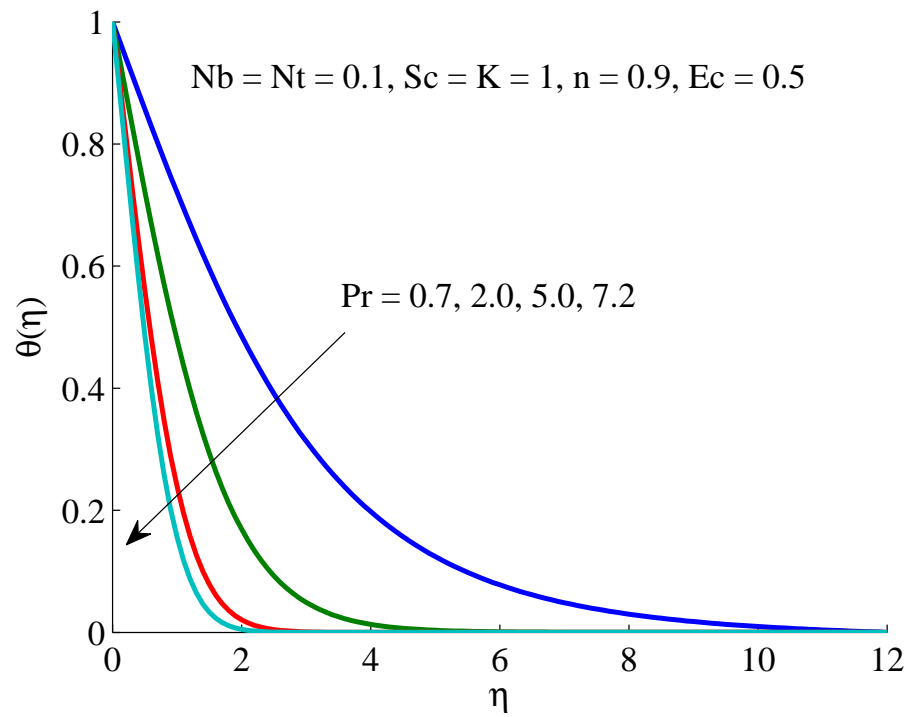


FIGURE 4.7: Variation in θ subject to Pr.

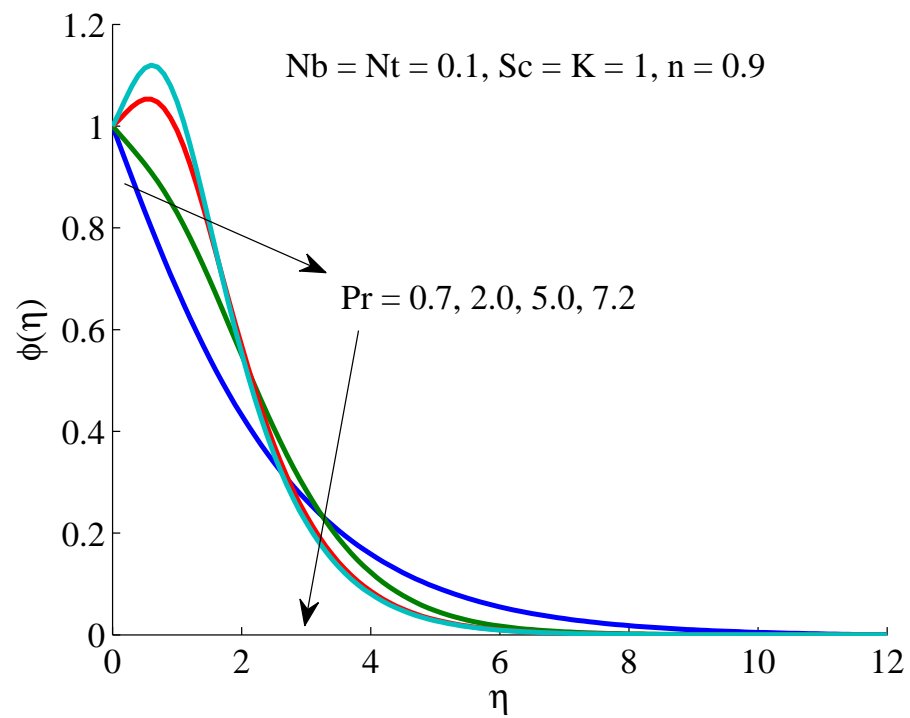


FIGURE 4.8: Variation in ϕ subject to Pr.

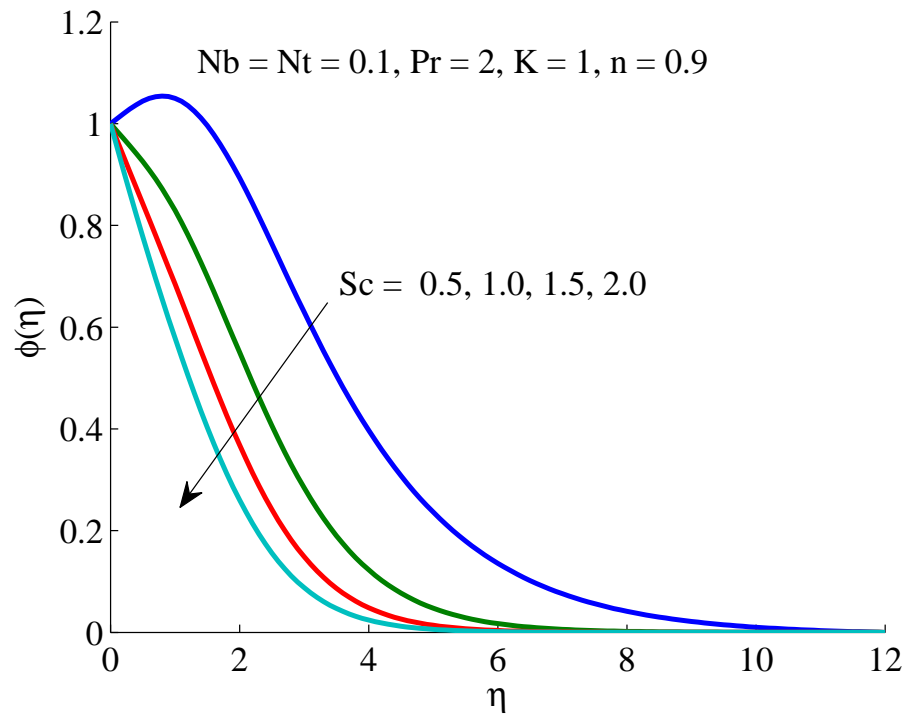


FIGURE 4.9: Variation in ϕ subject to Sc .

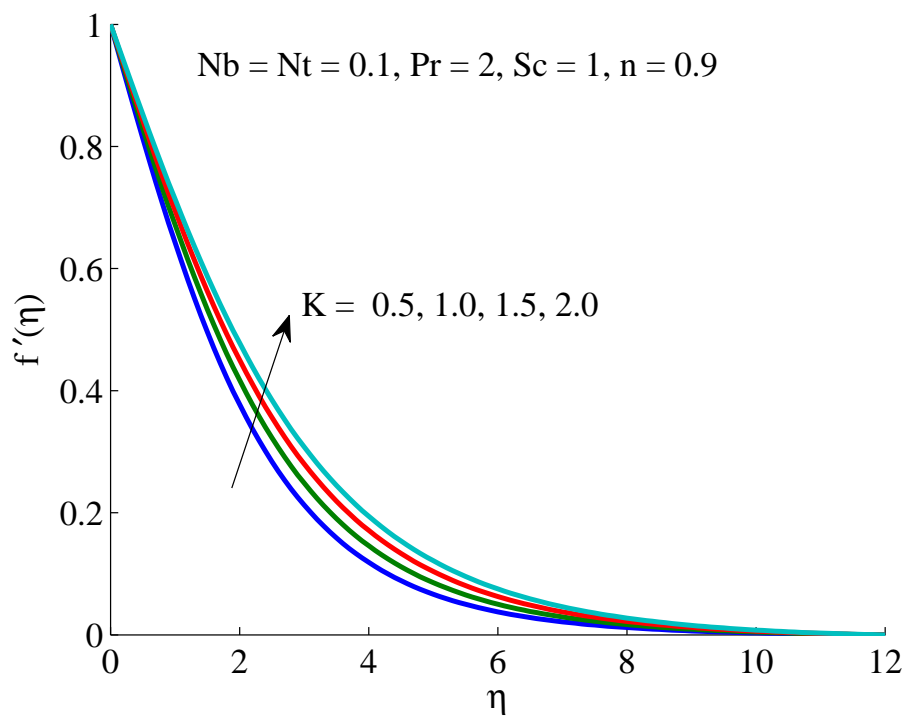


FIGURE 4.10: Variation in f' subject to K .

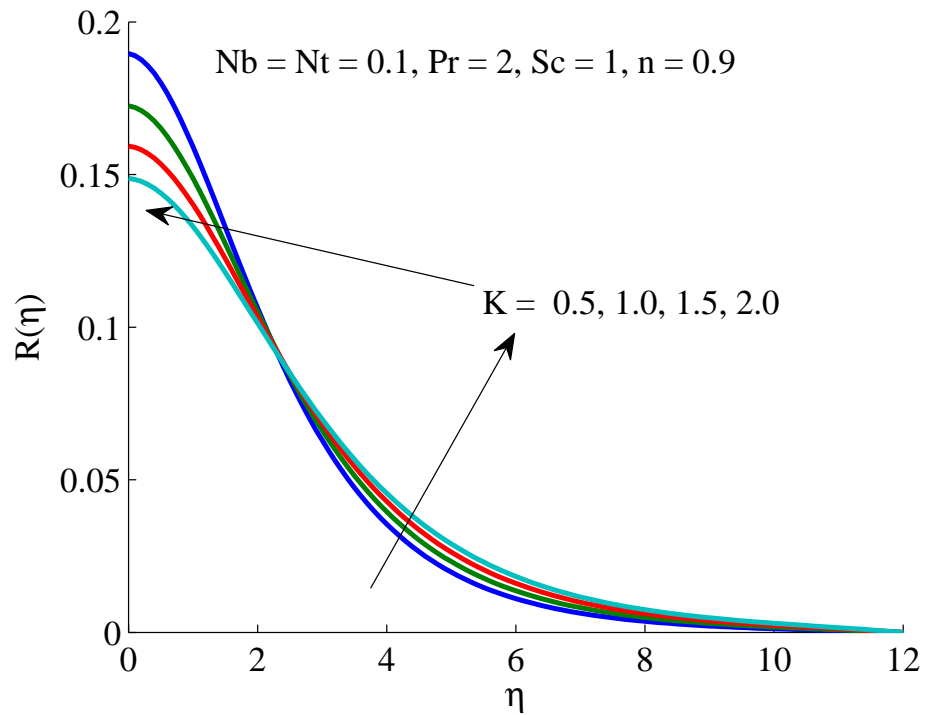


FIGURE 4.11: Variation in R subject to K .

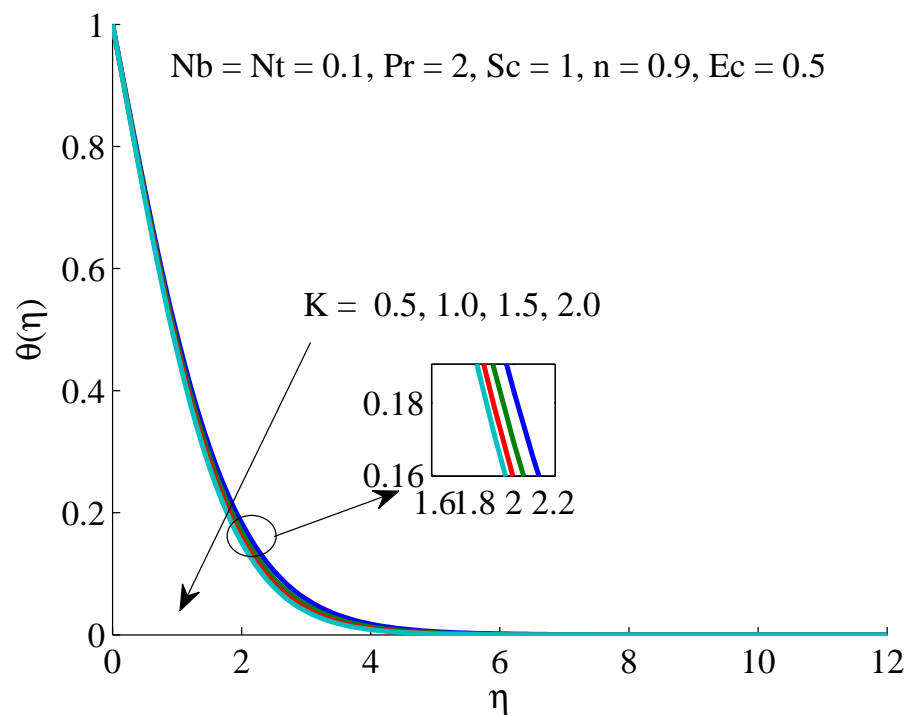


FIGURE 4.12: Variation in θ subject to K .

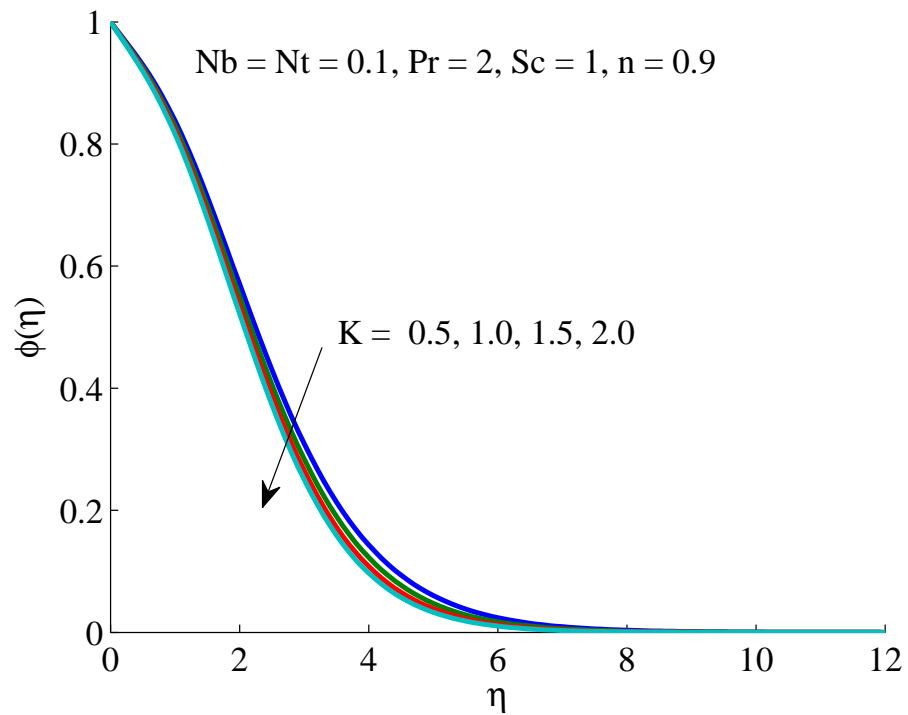


FIGURE 4.13: Variation in ϕ subject to K .

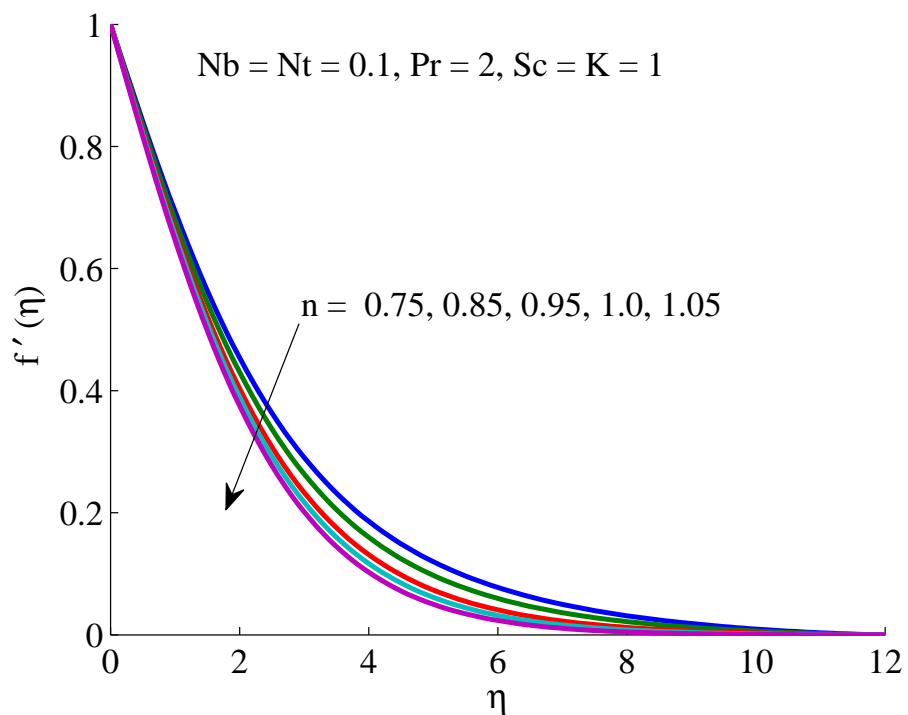


FIGURE 4.14: Variation in f' subject to n .

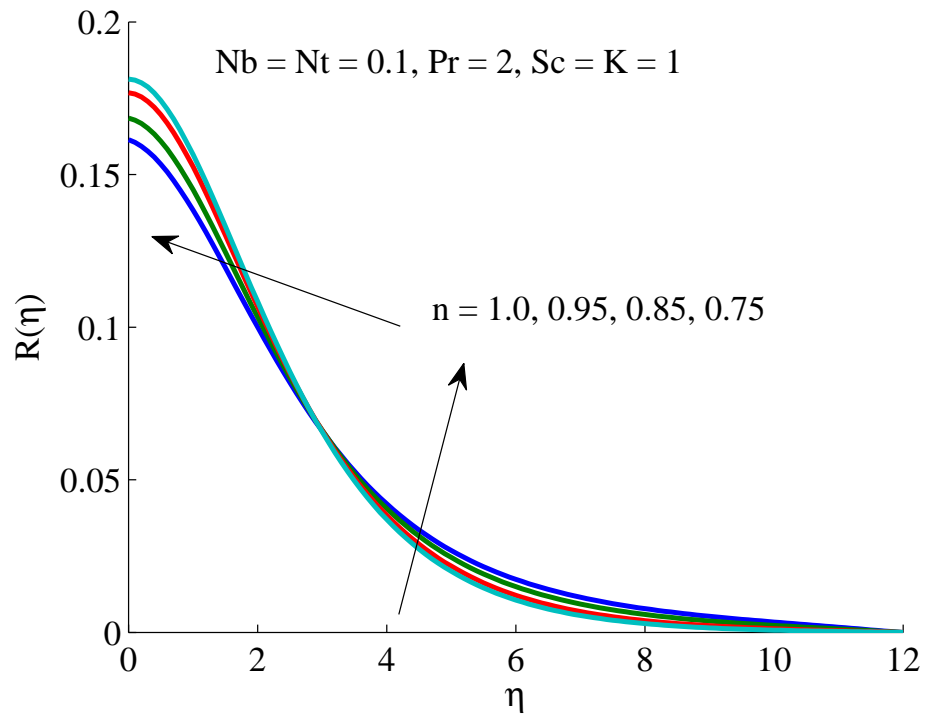


FIGURE 4.15: Variation in R subject to n .

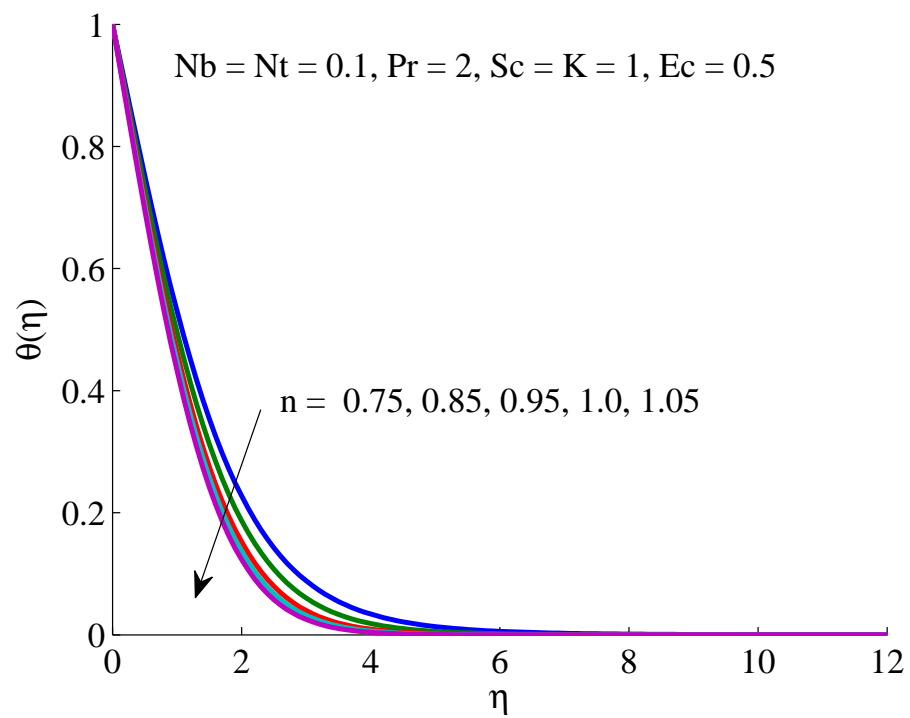


FIGURE 4.16: Variation in θ subject to n .

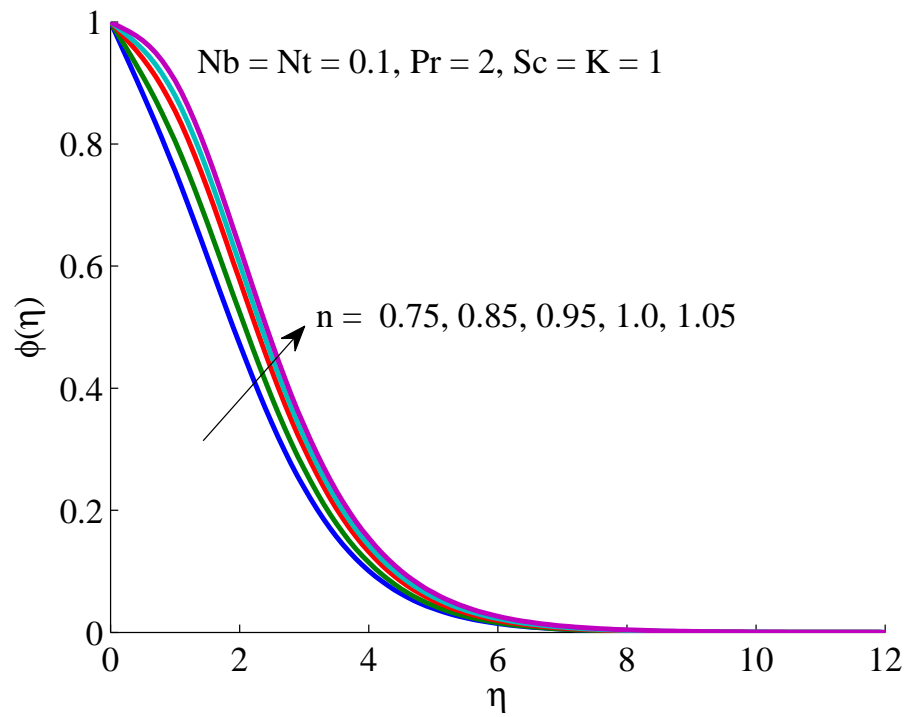


FIGURE 4.17: Variation in ϕ subject to n .

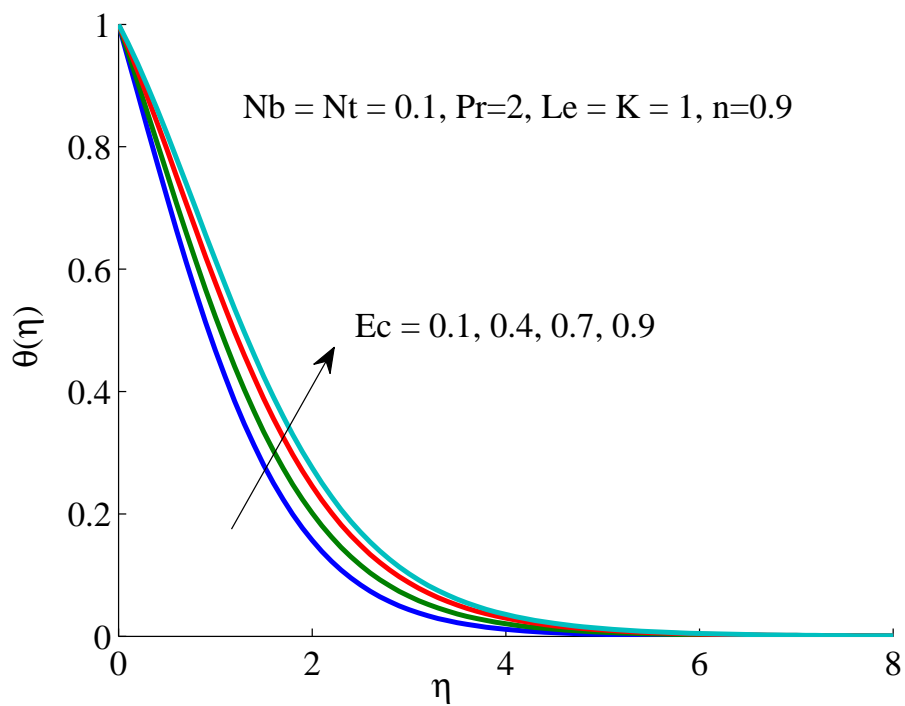


FIGURE 4.18: Variation in θ subject to Ec .

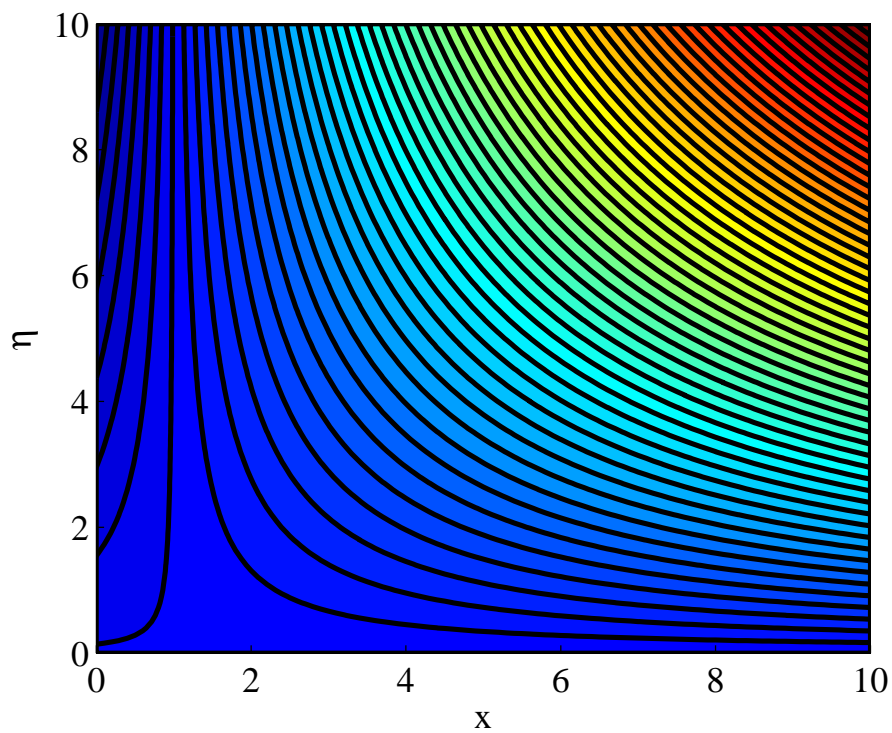


FIGURE 4.19: Stream lines for $n = 0.75$.

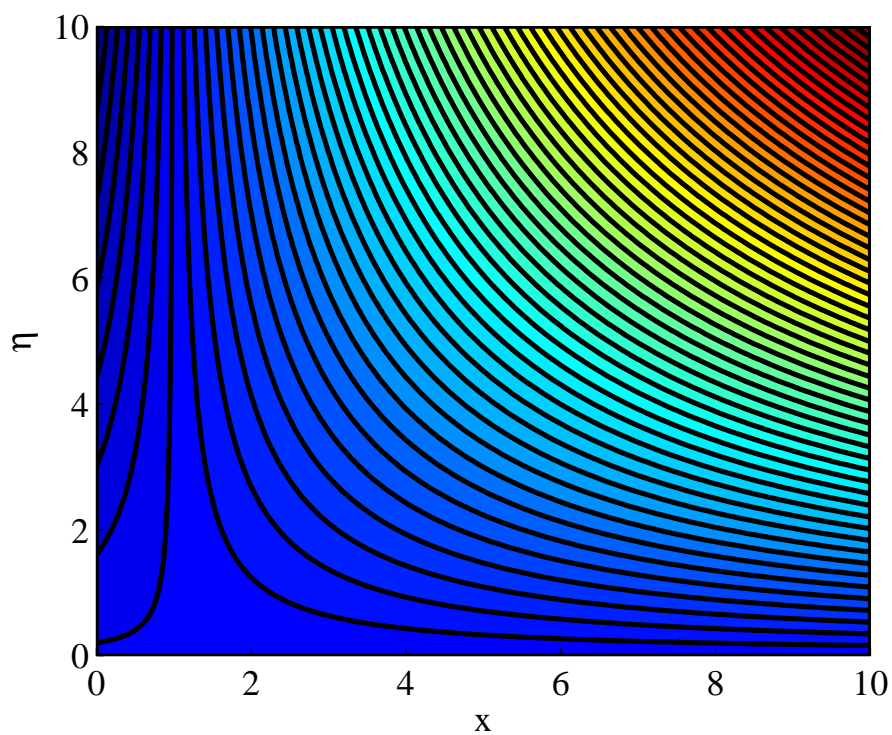


FIGURE 4.20: Stream lines for $n = 0.85$.

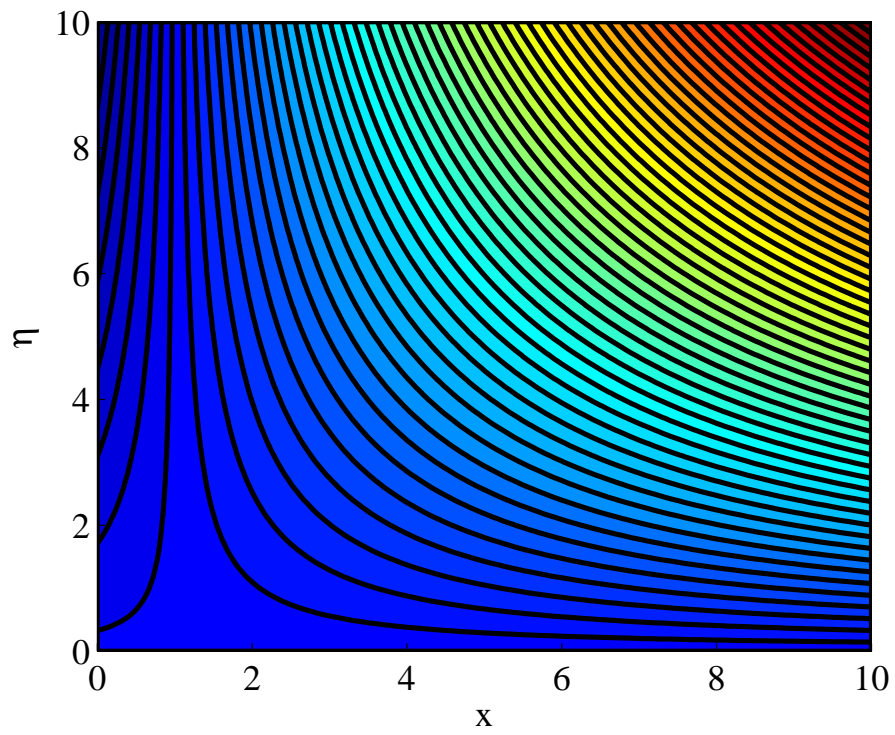


FIGURE 4.21: Stream lines for $n = 1.0$.

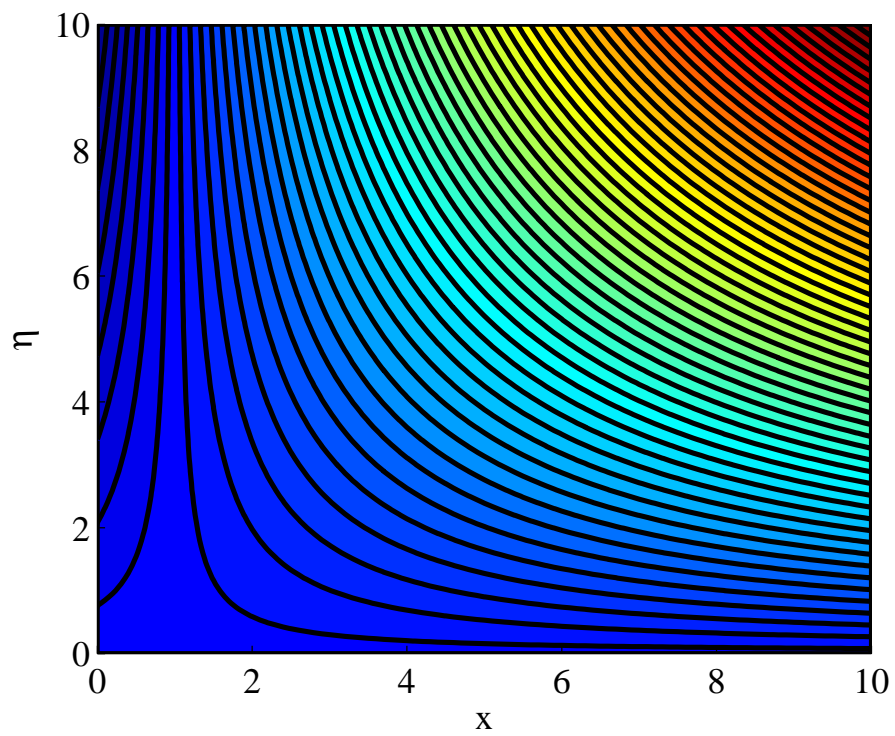


FIGURE 4.22: Stream lines for $K = 0.0$.

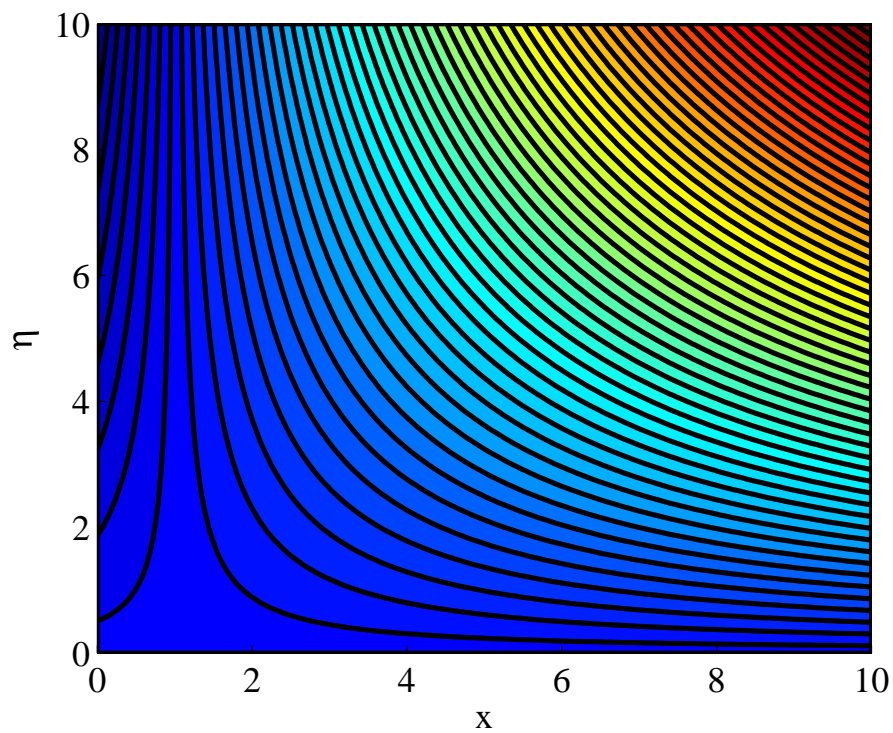


FIGURE 4.23: Stream lines for $K = 0.5$.

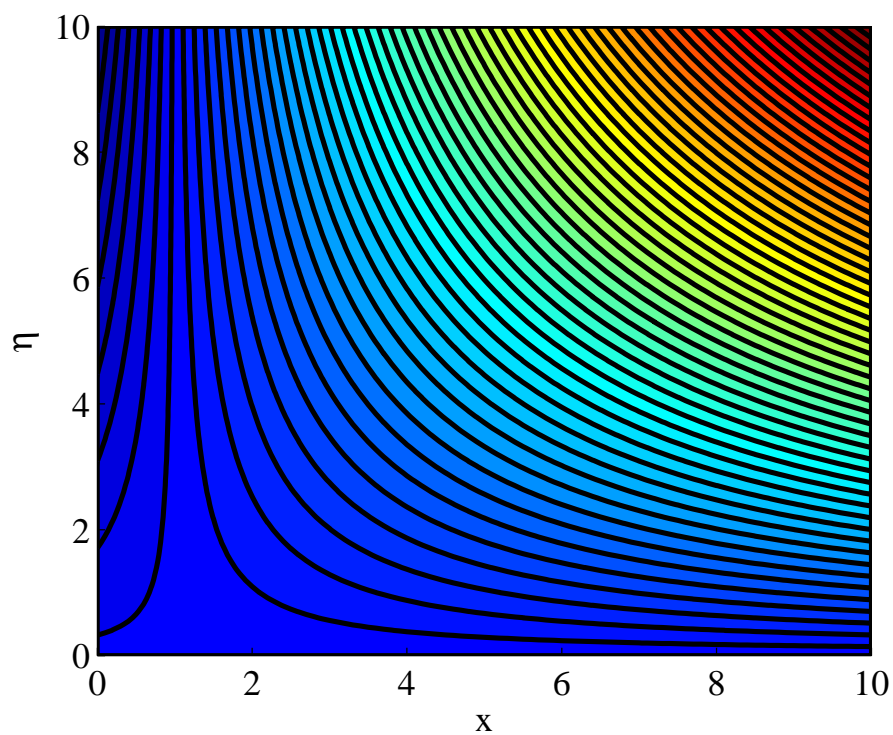


FIGURE 4.24: Stream lines for $K = 1.0$.

4.5 Conclusion

The power-law nanofluids with power-law spin gradient viscosity model are analyzed in this study. The modeling is carried via the Buongiorno nanofluid model. Keller box method is employed to obtain the numerical results. The key observations of this investigation have been listed down.

- The Brownian motion increases the temperature of the power-law nanofluids but decreases the concentration profile.
- The temperature and concentration profiles seem to rise for the increasing values of the thermophoresis parameter.
- The growing Prandtl number decreases the temperature profile but augments the concentration profile near the wall and decreases the profile towards the free stream.
- Schmidt number reduces the concentration profile as well as the concentration boundary layer thickness.
- The parameter K representing the strength of the rotation viscosity accelerates the linear flow of the nanofluid. The angular momentum near the boundary layer wall is reduced with an enhancement in K due to a greater concentration of the rotation particles but the profile is enhanced away from the wall for greater K .
- The angular momentum is augmented for the shear thinning as well as the shear thickening fluid close to the wall but away from the wall, the opposite happens.
- The temperature profile is reduced for growing power-law index whereas the concentration is increased.

Chapter 5

Investigation of Free Convection in Micropolar Nanofluid with Induced Magnetic Field

5.1 Introduction

With the advent of nanofluids, the heat transfer capabilities of conventional fluids are enhanced dramatically, resulting in the wider use of such fluids in many engineering applications as well as in the fields of physics, magnetic drug targeting, solar collector etc [2, 91, 94, 96]. It is interesting to analyze the super heated nanofluids in the presence of strong magnetic field with the consideration of the induced magnetic field. Recently, Sheikholeslami and Rokni [97] explored this aspect by considering the two phase model to look at the effect of induced magnetic field on a free convective nanofluidic flow between two vertical plates. The fluid used in the study was Newtonian and incompressible. The problem, of the hot non-Newtonian nanofluid with spin gradient viscosity has not been studied so far. In this chapter we are focused to investigate the free convection in a non-Newtonian micropolar fluid in the presence of transversal magnetic field taking the induced magnetic field into account. The modeling is carried out by using

the Buongiorno model. Nondimensional equations are solved by the Keller box method and results presented in the form of tables and graphs.

5.2 Mathematical Formulation

A steady, laminar and incompressible micropolar nanofluid flow is considered between two parallel plates. The plates are assumed to be porous with suction velocity v_0 in the y -direction. The fluid velocity vector is given as $\vec{u} = [u, v_0, 0]$. The lower plate coincides with x -axis at $y = 0$ and the upper plate is situated at $y = h$. A magnetic field b_0 is applied normal to the flow of nanofluid. Among the two plates, upper plate is considered to be electrically conducting while the lower plate is non-conductor of electricity. The fluid is supposed to have sufficient electrical conductivity of strength δ_{el} so that it induces electric current. Thus we consider the induced magnetic field effects in the x -direction of strength b_x . $\vec{B} = [b_x, b_0, 0]$ represents the magnetic field vector. The flow of the fluid between the plates is occurred due to gravity as we are considering the vertical channel. The governing equations of the model are given as:

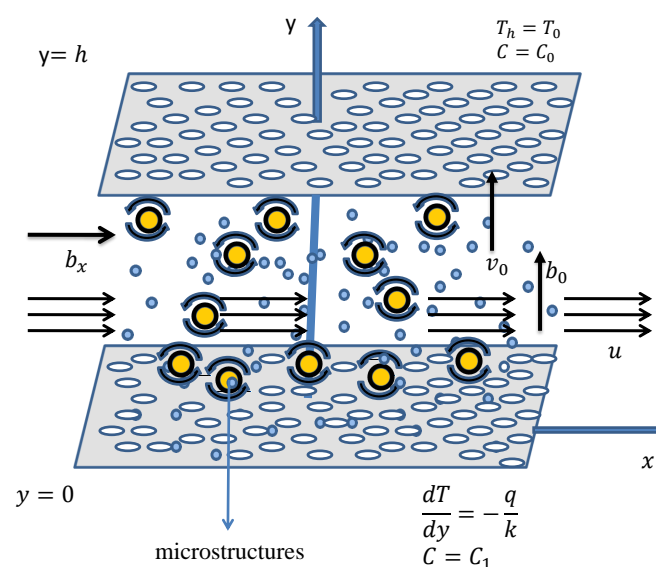


FIGURE 5.1: Schematic diagram of the flow model

$$\begin{aligned} & \left(\nu_f + \frac{\kappa^*}{\rho_f} \right) \frac{d^2 u}{dy^2} + \frac{\kappa^*}{\rho_f} \frac{dN}{dy} + v_0 \frac{du}{dy} + \frac{\mu_e b_0}{\rho_f} \frac{db_x}{dy} + g\beta(T - T_0) \\ & + g\beta_c(C - C_0) = 0, \end{aligned} \quad (5.1)$$

$$\left(\nu_f + \frac{\kappa^*}{2\rho_f} \right) j \frac{d^2 N}{dy^2} - \kappa^* \left(2N + \frac{du}{dy} \right) + jv_0 \frac{dN}{dy} = 0, \quad (5.2)$$

$$\frac{1}{\mu_e \delta_{el}} \frac{d^2 b_x}{dy^2} + b_0 \frac{du}{dy} + v_0 \frac{db_x}{dy} = 0, \quad (5.3)$$

$$\frac{\kappa}{(\rho c_p)_f} \frac{d^2 T}{dy^2} + \tau_1 D_B \frac{dT}{dy} \frac{dC}{dy} + \frac{\tau_1 D_T}{T_0} \left(\frac{dT}{dy} \right)^2 + v_0 \frac{dT}{dy} + \frac{\mu_f}{(\rho c_p)_f} \left(\frac{du}{dy} \right)^2 = 0, \quad (5.4)$$

$$\frac{D_T}{T_0} \frac{d^2 T}{dy^2} + D_B \frac{d^2 C}{dy^2} + v_0 \frac{dC}{dy} = 0. \quad (5.5)$$

Here, ratio of the effective heat capacity of nanoparticle material to the effective heat capacity of the base fluid is $\tau_1 = \frac{(\rho c_p)_s}{(\rho c_p)_f}$. The boundary conditions have been considered as follows [97, 98]:

$$u = 0, \quad N = 0, \quad b_x = 0, \quad \frac{dT}{dy} = -\frac{q}{k}, \quad C = C_1, \quad \text{at } y = 0, \quad (5.6)$$

$$u = 0, \quad N = 0, \quad \frac{db_x}{dy} = 0, \quad T = T_0, \quad C = C_0, \quad \text{at } y = h. \quad (5.7)$$

The nondimensional form of Eqs. (5.1)-(5.5) is obtained by using the following transformations:

$$\left. \begin{aligned} Y = \frac{y}{h}, \quad f' = U = \frac{\mu_f u}{\rho_f g \beta h^2 \Delta T}, \quad R = \frac{\mu_f N}{\rho_f g \beta h \Delta T}, \quad B_x = \sqrt{\frac{\mu_e}{\rho_f}} \frac{b_x \mu_f}{\rho_f g \beta h^2 \Delta T}, \\ \theta = \frac{T - T_0}{\Delta T}, \quad \phi = \frac{C - C_0}{\Delta C}, \quad \Delta T = \frac{hq}{k}, \quad \Delta C = C_1 - C_0. \end{aligned} \right\} \quad (5.8)$$

Using the above transforms, Eqs. (5.1)-(5.5) take the form:

$$(1 + K) \frac{d^2 f'}{dY^2} + V_0 \frac{df'}{dY} + M \frac{dB_x}{dY} + K \frac{dR}{dY} + \theta + Br\phi = 0, \quad (5.9)$$

$$\left(1 + \frac{K}{2} \right) \frac{d^2 R}{dY^2} + V_0 \frac{dR}{dY} - Kb \left[2R + \frac{df'}{dY} \right] = 0, \quad (5.10)$$

$$\frac{d^2 B_x}{dY^2} + V_0 Pm \frac{dB_x}{dY} + MPm \frac{df'}{dY} = 0, \quad (5.11)$$

$$\frac{d^2 \theta}{dY^2} + Nb \frac{d\theta}{dY} \frac{d\phi}{dY} + Nt \left(\frac{d\theta}{dY} \right)^2 + V_0 Pr \frac{d\theta}{dY} + Pr Ec \left(\frac{df'}{dY} \right)^2 = 0, \quad (5.12)$$

$$\frac{d^2\phi}{dY^2} + \frac{Nt}{Nb} \frac{d^2\theta}{dY^2} + V_0 Sc \frac{d\phi}{dY} = 0, \quad (5.13)$$

The dimensionless form of the boundary conditions becomes:

$$\left. \begin{aligned} f'(0) = 0, \quad R(0) = 0, \quad B_x(0) = 0, \quad \frac{d\theta}{dY} \Big|_{Y=0} = -1, \quad \phi(0) = 1, \\ f'(1) = 0, \quad R(1) = 0, \quad \theta(1) = 0, \quad \frac{dB_x}{dY} \Big|_{Y=1} = 0, \quad \phi(1) = 0. \end{aligned} \right\} \quad (5.14)$$

Here,

$$\begin{aligned} Pr &= \frac{\mu_f c_p}{k}, & Pm &= \frac{\mu_f \mu_e \delta_{el}}{\rho_f}, & M &= \frac{B_0 h}{\nu_f} \sqrt{\frac{\mu_e}{\rho_f}}, & V_0 &= \frac{v_0 h}{\nu_f}, \\ Sc &= \frac{\mu_f}{\rho_f D_B}, & Nt &= \frac{\tau D_T \Delta T}{\alpha T_0}, & Nb &= \frac{\tau_1 D_B \Delta C}{\alpha}, & K &= \frac{\kappa^*}{\mu_f}, \\ \alpha &= \frac{k}{(\rho c_p)_f}, & Ec &= \frac{\rho_f^2 g^2 \beta^2 h^4}{\mu_f^2 c_p}, & Br &= \frac{\beta_c \Delta C}{\beta \Delta T}. \end{aligned}$$

Nusselt number is the measure of the heat transfer by the process of convection to conduction. When Nusselt number is greater than 1, the convective heat transfer dominates the conductive one. In the present study, Nusselt number is calculated at the lower plate, where there exists a constant heat flux. The local Nusselt number has been formulated as:

$$Nu_x = \frac{h q_w}{(T - T_0)}.$$

Here, $q_w = -\frac{dT}{dy} \Big|_{y=0}$. Making use of the introduced nondimensional variables, we get the nondimensionalized form of Nusselt number as

$$Nu = \frac{1}{\theta(0)}.$$

The dimensional form of the skin friction is defined as

$$C_{fx} = (\mu_f + \kappa^*) \frac{du}{dy} \Big|_{y=0} + \kappa^* N \Big|_{y=0}.$$

The nondimensional form of the skin friction is given by

$$C_f = (1 + K)U'(0) + KR(0).$$

The dimensional form of the Sherwood number is defined as

$$Sh_x = \frac{hq_m}{D_B(C_1 - C_0)}.$$

Here, $q_m = -D_B \frac{dC}{dy} \Big|_{y=0}$. The nondimensional form of the Sherwood number is given by

$$Sh = -\phi(0).$$

5.3 Solution Methodology

The grid study is carried out in order to determine whether Matlab code has attained same values for a particular step size. In Table 5.1 the values of step size h are varied and the corresponding values of Nusselt number Nu , skin friction coefficient C_f and reduced Sherwood number Sh_x have been calculated. It is observed that from 0.002 the values of the above mentioned parameters does not change rather it just increases the calculation time only.

h	Nu_x	C_f	Sh_x
0.1	9.8098084	0.18970668	0.647216495
0.05	9.8098684	0.18976672	0.647851191
0.02	9.8099041	0.18978359	0.64802846
0.01	9.8099100	0.18978600	0.64805377
0.008	9.8099107	0.18978630	0.64805680
0.005	9.8099115	0.1897866	0.64806009
0.002	9.8099119	0.1897868	0.6480619
0.001	9.8099119	0.1897868	0.6480621
0.0008	9.8099119	0.1897868	0.6480621
0.0005	9.8099119	0.1897868	0.6480622
0.0002	9.8099119	0.1897868	0.6480622
0.0001	9.8099119	0.1897868	0.6480622

TABLE 5.1: Values of reduced Nusselt number, skin friction coefficient and Sherwood number corresponding to different values of step size

The nonlinear boundary value problem (5.9)-(5.14) has been solved by the Keller box method. Details of the method can be found in [76, 94]. The implicit Keller box scheme is unconditionally stable with second order accuracy [76]. The layout of the scheme is given as follows

- Equations (5.9)-(5.13) subject to the boundary conditions (5.14) are converted to the following system of ten first order ordinary differential equations.

$$\begin{aligned}
 f' &= Y_1, \\
 \frac{dY_1}{dY} &= Y_2, \\
 R &= Y_3, \\
 \frac{dY_3}{dY} &= Y_4, \\
 B_x &= Y_5, \\
 \frac{dY_5}{dY} &= Y_6, \\
 \theta &= Y_7, \\
 \frac{dY_7}{dY} &= Y_8, \\
 \phi &= Y_9, \\
 \frac{dY_9}{dY} &= Y_{10}, \\
 (1 + K) \frac{dY_2}{dY} + V_0 Y_2 + M Y_6 + K Y_4 + Y_7 + Br Y_9 &= 0, \\
 \left(1 + \frac{K}{2}\right) \frac{dY_4}{dY} + V_0 Y_4 - K [2Y_3 + Y_2] &= 0, \\
 \frac{dY_6}{dY} + V_0 Pm Y_6 + M Pm Y_2 &= 0, \\
 \frac{dY_8}{dY} + Nt (Y_8)^2 + V_0 Pr Y_8 + Nb Y_8 Y_{10} + Pr Ec Y_2 &= 0, \\
 \frac{dY_{10}}{dY} + \frac{Nt}{Nb} \frac{dY_8}{dY} + V_0 Sc Y_{10} &= 0.
 \end{aligned}$$

- The resulting system is discretized by using central differences for the average values and derivatives for the functions as,

$$(Y_*)_{j-\frac{1}{2}} = \frac{(Y_*)_j + (Y_*)_{j-1}}{2},$$

$$\left(\frac{dY_*}{dY}\right)_{j-\frac{1}{2}} = \frac{(Y_*)_j - (Y_*)_{j-1}}{h}.$$

- The nonlinear difference equations are linearized by the Newton's method in the following sense,

$$(Y_*)_j^{i+1} = (Y_*)_j^i + \delta (Y_*)_j^i.$$

- The resulting linear system is written in the matrix form $M\delta = \mathbf{r}$.
- The vector of unknowns δ is obtained by solving the system $M\delta = \mathbf{r}$ by using LU -decomposition method.
- Updation is made to the solution vector and the process is continued until a required accuracy of 10^{-5} is achieved.

The code validity is carried out by a comparison of the numerical results to those of the exact solution obtained by Sheikholeslami and Rokini [97]. An acceptable agreement is seen among the two results shown in the Table 5.2.

V_0	Nt	[97]	Present results
0.2	0.01	2.227115	2.227093
0.4		3.967202	3.967162
0.6		5.893628	5.893601
1		9.855793	9.855790
0.2	0.1	2.19512	2.19510
0.4		3.945781	3.945741
0.6		5.878403	5.878375
1		9.846286	9.846283
0.2	0.4	2.082635	2.082615
0.4		3.872812	3.872771
0.6		5.827099	5.827071
1		9.814468	9.814465

TABLE 5.2: Comparison of the present skin friction coefficient results to the previous results

5.4 Discussion on Results

Tables 5.3 and 5.4 provide a numerical discussion on the sundry parameters which affect the heat transfer rate and measure the drag force at the boundary. The analysis of heat transfer rate for the increasing values of the parameters has been presented in Table 5.3. Brownian motion parameter Nb and the thermophoresis parameter Nt have a similar effect on the Nusselt number, which decreases in both the cases. Prandtl number which is a measure of the conductive to the convective heat transfer leads to an enhancement in the heat transfer rate. Nusselt number is also seen to be augmented for the increasing values of the suction parameter while in the case of Eckert Ec and Schmidt numbers Sc , a reduction in the Nusselt number is witnessed. It is very clear from observing the Nusselt number with and without viscous dissipation that there is very small difference in the values of the Nusselt number. Which means impact of viscous dissipation is negligibly small so it can be neglected.

Nt	Nb	Pr	V_0	Sc	Ec	Nu_x	CPU time (seconds)	Nu_x without Eckert Number ($Ec = 0$)
0.1	0.1	10	1	1	0.4	9.8099	3.82324	9.8463
0.01						9.8245	3.767462	9.8558
0.2						9.7932	3.672609	9.8357
0.4						9.7582	3.866581	9.8145
	0.06					9.8631	3.758748	9.9037
	0.2					9.6699	3.873469	9.7029
	0.4					9.3866	3.895994	9.4172
		0.71				1.2779	4.349903	1.2787
		5				4.8738	3.818335	4.8843
		7				6.8348	3.928434	6.8538
			0.2			2.1743	3.021916	2.1951
			0.4			3.9196	3.224561	3.9458
			0.6			5.8474	3.394473	5.8784
				0.1		9.8385	4.145291	9.8864
				0.5		9.8268	3.986185	9.8693
				2		9.7704	3.957690	9.7965
					0.1	9.8372	3.969025	
					0.7	9.7828	3.855780	
					0.9	9.7647	4.013388	

TABLE 5.3: Impact of pertinent parameters on the Nusselt number with $M = 5$, $Pm = 0.8$, $K = 1$, $Br = 1$.

In Table 5.4, pertinent parameters' effects on the skin friction coefficient are discussed. Hartmann number M drags the fluid away from the plates thus the friction between the fluid and the plates decreases which is evident from the table. A similar impact can be seen in the case of magnetic Prandtl parameter. A rise in the buoyancy ratio leads to a greater convection flow which increases the skin friction coefficient. Coupling stress effect of the rotating particles is analyzed by the way of material parameter K and it is found that the skin friction is reduced with an increment in the values of K .

M	Pm	Br	V_0	K	C_f	CPU time(seconds)
5	0.8	1	1	1	0.1898	3.162722
10					0.1066	3.108670
15					0.0732	3.100924
20					0.0557	3.096294
	0.2				0.2926	3.488297
	0.4				0.2526	3.059966
	0.6				0.2189	3.212606
		0.1			0.0258	3.365033
		0.5			0.0987	3.335825
		2			0.3718	3.937914
			0.2		0.3046	2.182631
			0.4		0.2508	2.578329
			0.6		0.2231	2.800321
				0.5	0.1730	3.747141
				1.5	0.2029	3.128487
				2	0.2137	2.960538

TABLE 5.4: Impact of pertinent parameters on the skin friction with $Ec = 0.4$, $Nb = 0.1$, $Nt = 0.1$, $Sc = 1$, $Pr = 10$.

The graphs of Sherwood number Sh are plotted for the different values of Brownian motion parameter, thermophoresis parameter and Schmidt number in Figures 5.2 to 5.4. The impact of the magnetic parameter on the velocity, angular velocity and induced magnetic field is discussed in Figures 5.5–5.7. Hartmann number is a measure of the strength of the applied magnetic field. Greater Hartmann number means stronger Lorentz forces which affects the flow of the nanofluid negatively and increases the heat dissipation. Figure 5.5 reveals that the increasing values of the magnetic parameter has a halting effect on the fluid velocity as it is seen shrinking for the growing M . In case of the angular momentum, in Figure 5.6, the

angular velocity is found increasing near the lower plate but moving towards the upper plate, the opposite happens as the angular velocity starts decreasing with a stronger magnetic field. In Figure 5.7, the strength of the induced magnetic field is found to grow with a more stronger magnetic field which is consistent with the physics of the phenomenon.

Impact of the material parameter K is investigated through Figure 5.8–5.10. A rise in the material number increases the resistance due to the rotation viscosity. This implies that the greater rotation viscosity will affect the linear velocity negatively but the angular velocity positively. Figure 5.8 gives an account of the velocity variation due to K . The velocity profile can be observed to shrink for a stronger rotation viscosity which shows that the coupled stress affects reduces on the velocity of the fluid. The angular velocity is observed to be decreased with a rise in K near the lower plate but as we move towards the upper plate, the contrasting behavior can be seen in the profile (see Figure 5.9). In Figure 5.10, it is interesting to note that the induced magnetic field is an increasing function of the material parameter K . Buoyancy ratio effect on the velocity, angular velocity and the induced magnetic field is presented through figures 5.11–5.13. The Figure 5.11 reveals that a greater buoyancy ratio tends to increase the velocity of the fluid. In the physical sense, it means that a growth in convection increases the velocity of the fluid. The angular velocity has negative values near the lower plate and positive values near the upper plate depicting the coupled stress effects of the rotating particles. Angular boundary thickness is enhanced with an augmentation in the buoyancy ratio. Near the lower plate, a rise in the buoyancy ratio increases the angular momentum in the reverse direction while a transition is seen as we move towards the upper plate and the profile is more enhanced. In Figure 5.13, the induced magnetic field is found to be a decreasing function of Br which indicates that the induced magnetic field effects are reduced when a higher convection takes place.

Velocity profile, angular velocity and induced magnetic field are plotted against the magnetic Reynolds number in figures 5.14–5.16. It can be seen that the velocity is reduced while the angular velocity magnitude increases with an augmentation in

the magnetic Reynolds number (Figure 5.14 & Figure 5.15). The induced magnetic field is seen to decrease for the rising values of Pm (Figure 5.16). The Schmidt number's influence on the temperature and concentration profiles is discussed in figures 5.17–5.18. Figure 5.17 illustrates that the temperature profile augments with an increment in the Schmidt number which suggests that the temperature is dominately increased by the way of convection in the nanofluid and the temperature boundary layer thickness is reduced. The concentration profile is plotted for the variation in the Schmidt number in Figure 5.18. It is observed that the concentration profile is decreased for the increasing values of the Schmidt number.

An investigation of the impact of the suction parameter on the velocity, angular velocity, induced magnetic field and the temperature profiles is carried out in figures 5.19–5.22. Figure 5.19 reveals that the velocity of the fluid tends to decrease with an increment in the suction parameter. A similar behavior can be seen in the case of the angular momentum in Figure 5.20 as the angular momentum profile shrinks for high suction but the induced magnetic field (Figure 5.21) is augmented for the increasing values of suction parameter. The temperature of the nanofluid is observed to fall in Figure 5.22 as the suction velocity is increased. Figure 5.23 presents the impact of Brownian motion on the fluid properties. Figure 5.23 reflects that the temperature profile shows a rise with a growth in the random motion of the nanoparticles while the concentration profile of the nanofluid tends to decline as can be seen in Figure 5.24. The thermophoresis parameter impact is analyzed through figures 5.25–5.28. In Figure 5.25, we find that the velocity of the fluid is enhanced with the growing values of the thermophoresis parameter but the angular momentum has a contrasting behavior as it is shortened for the increasing thermophoresis parameter as evident from Figure 5.26. The induced magnetic field is declined with an inclination in the values of Nt (see Figure 5.27) and similarly the concentration profile also increases with a rise in Nt (see Figure 5.28). Figures 5.29 and 5.30 show that the coupled effect of significant parameters on the skin friction of the nanofluid. There is an exponential growth in the heat transfer rate with a gradual increase in both the Prandtl number and the suction velocity simultaneously as evident from Figure 5.31.

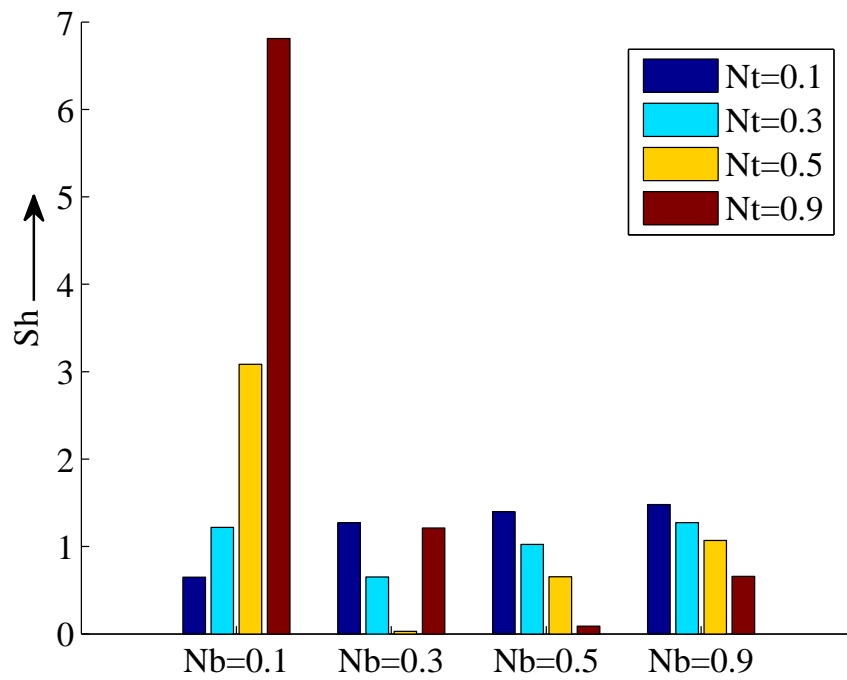


FIGURE 5.2: Impact of Brownian motion parameter Nb on Sherwood number

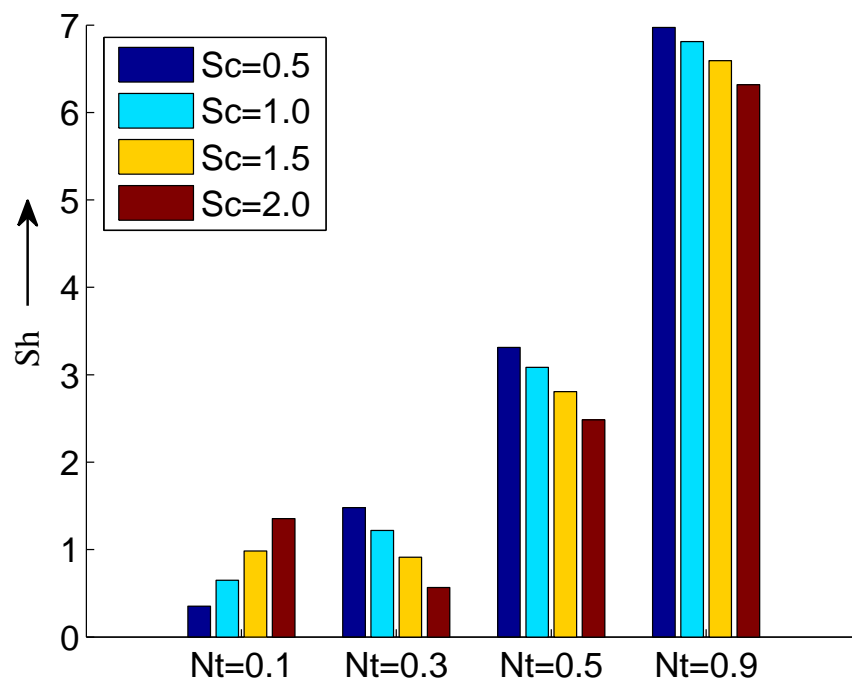


FIGURE 5.3: Impact of Thermophoresis parameter Nt on Sherwood number

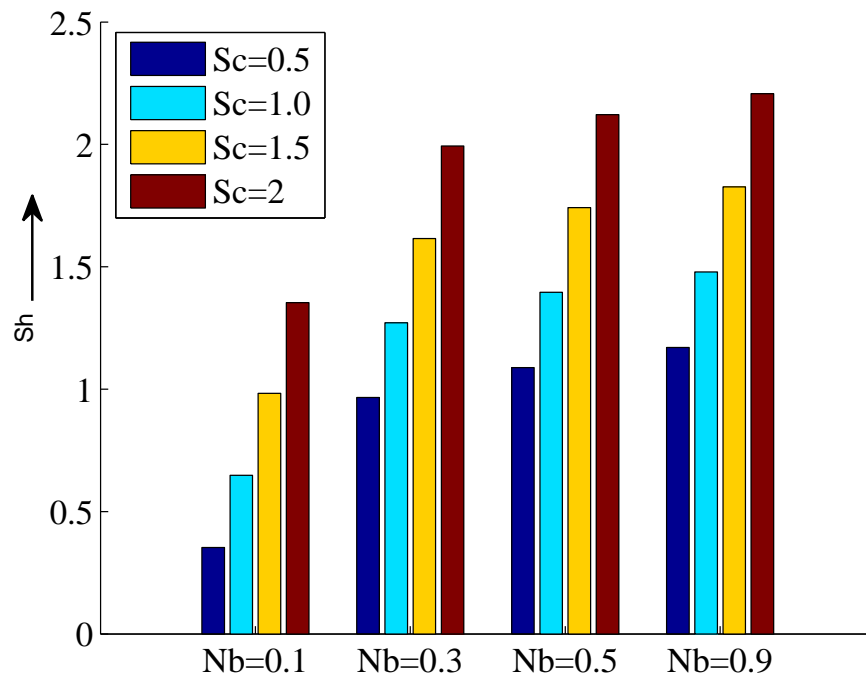


FIGURE 5.4: Impact of Schmidt number Sc on Sherwood number

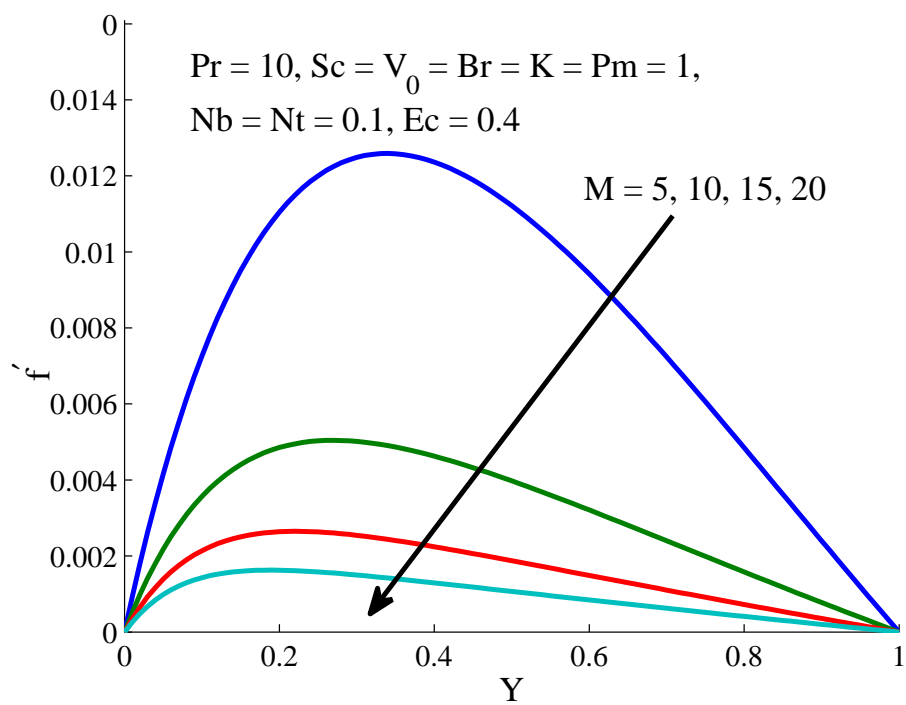
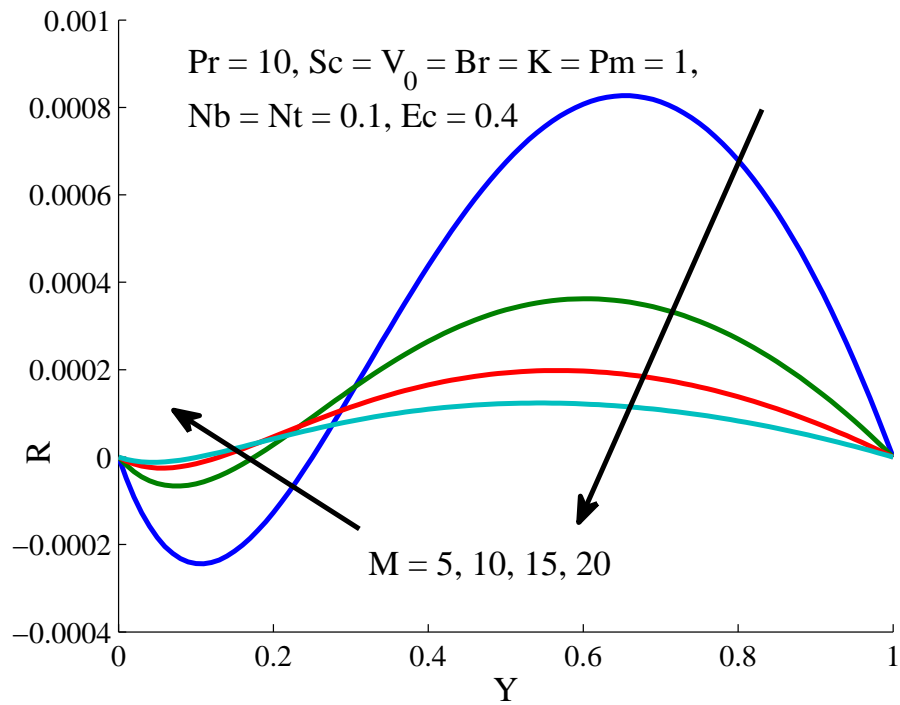
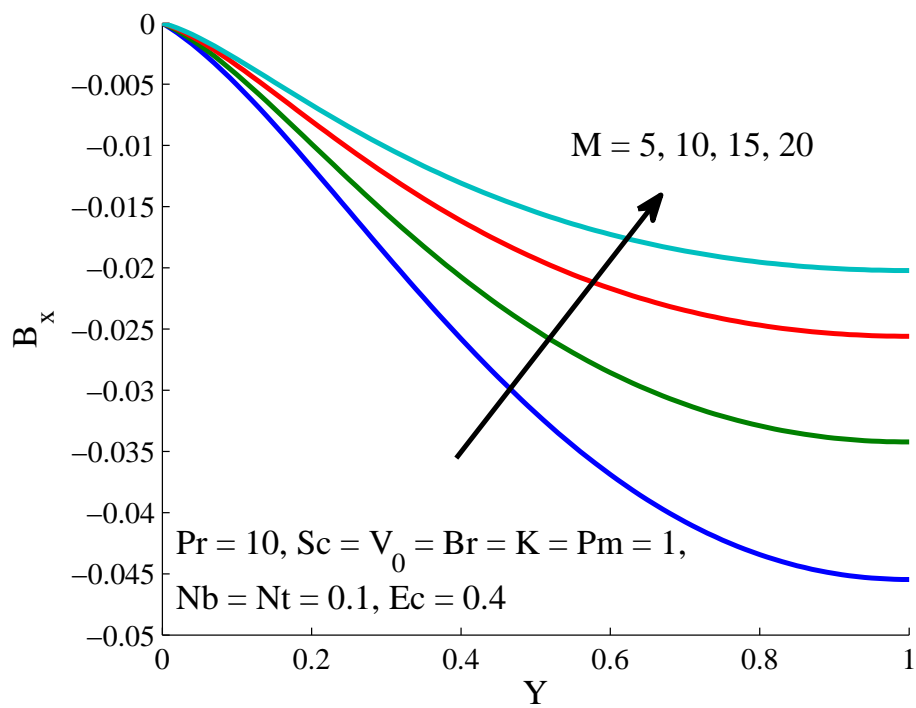
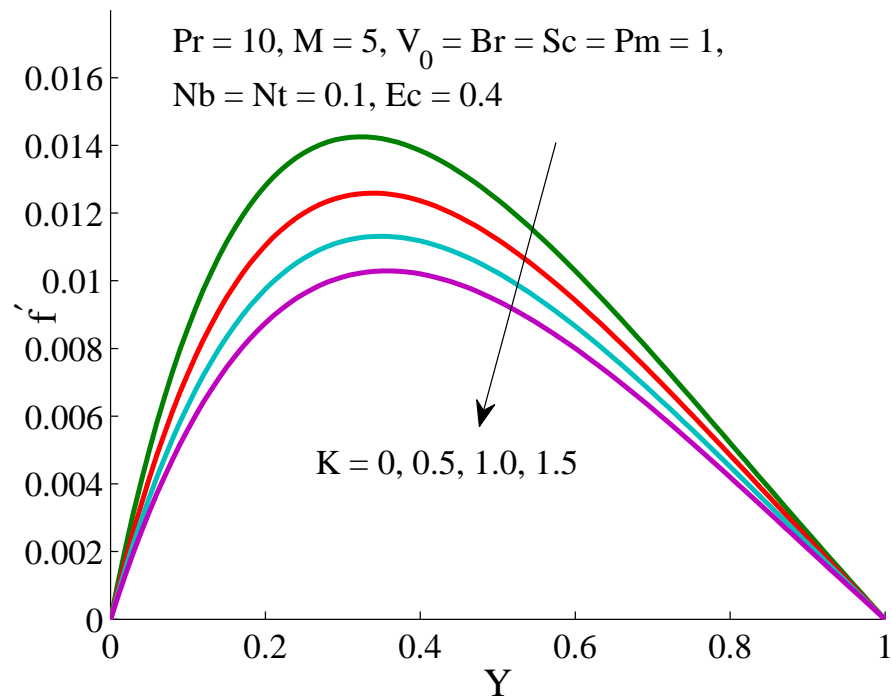
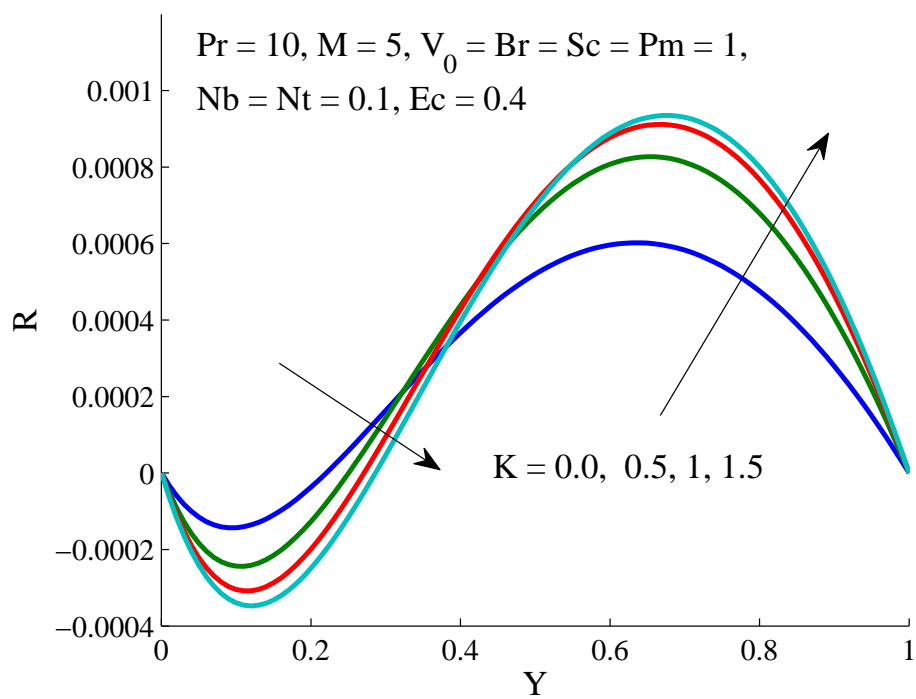
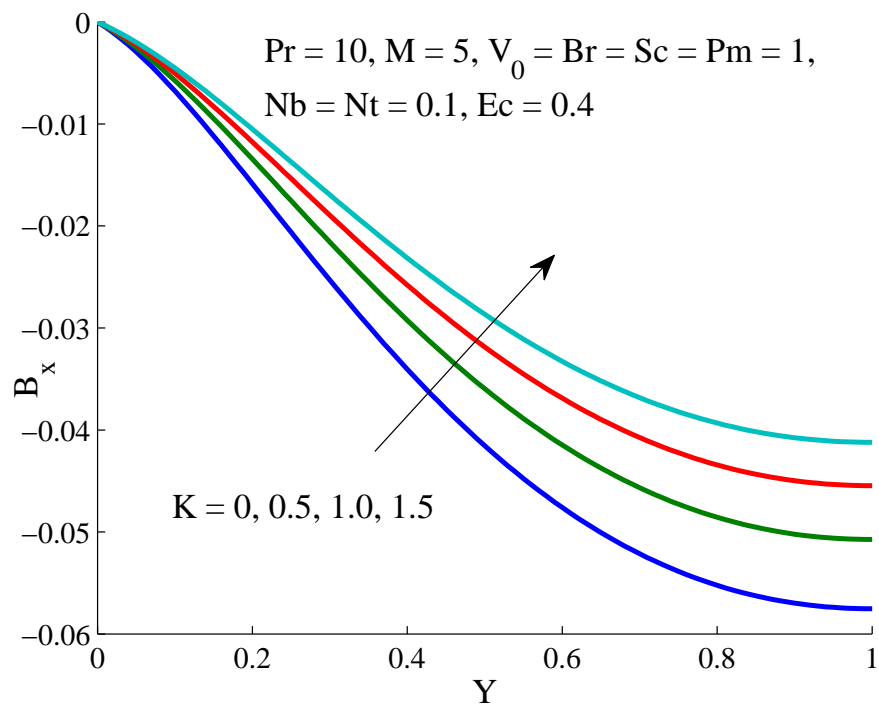
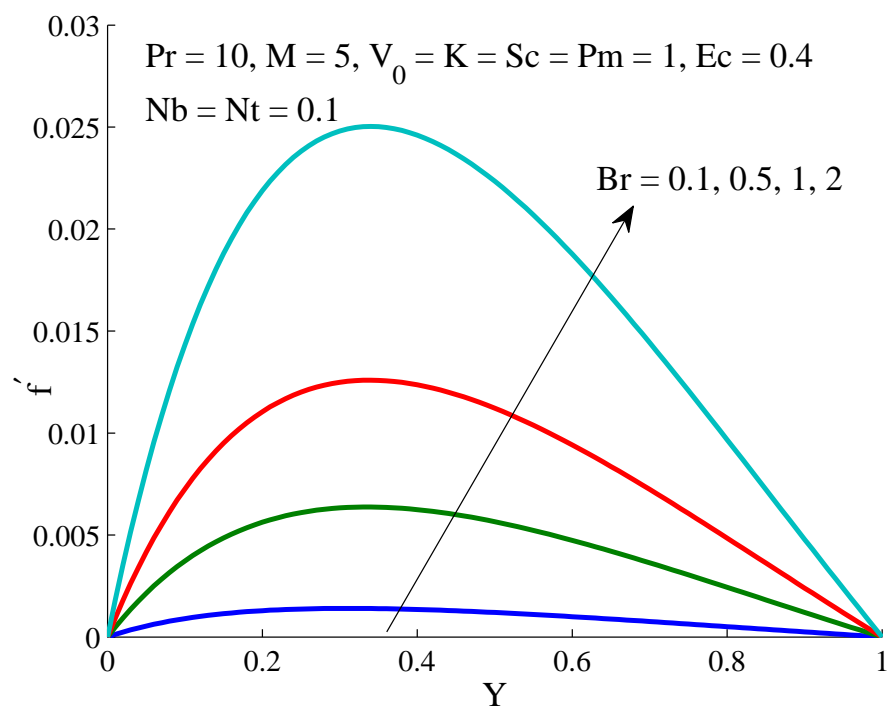
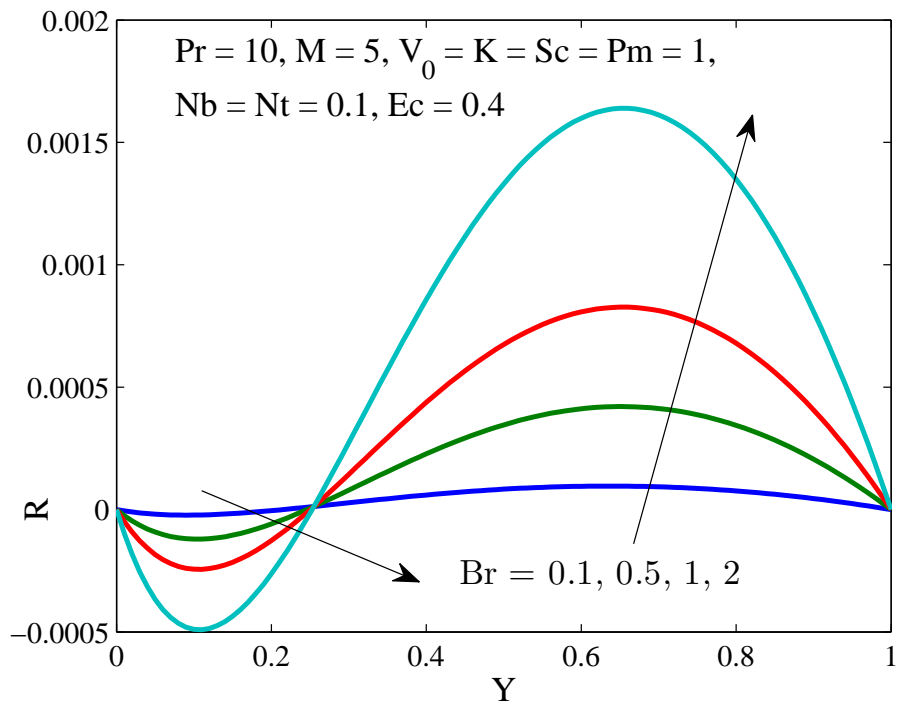
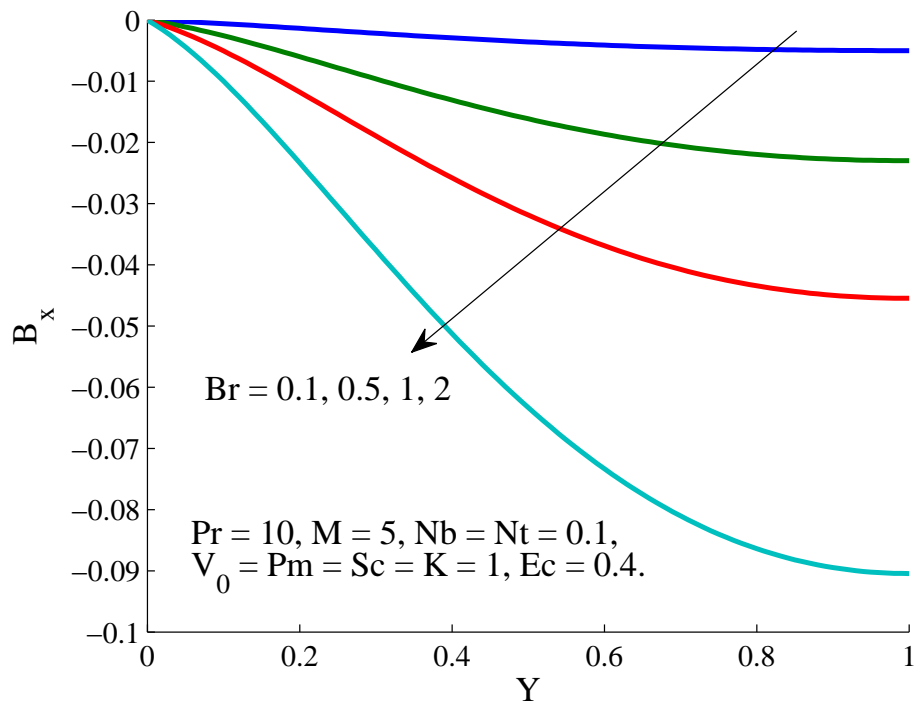


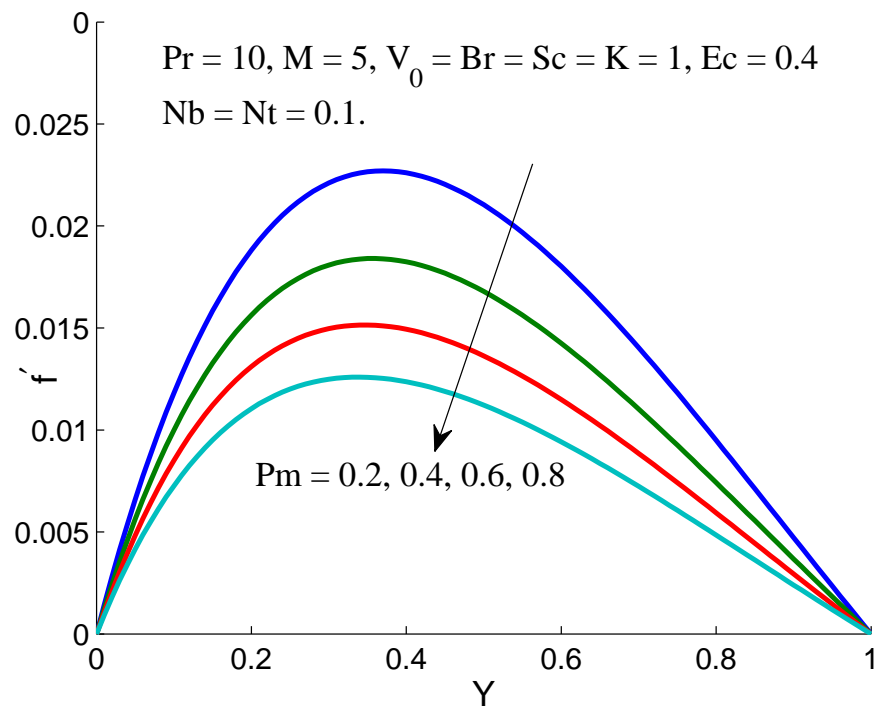
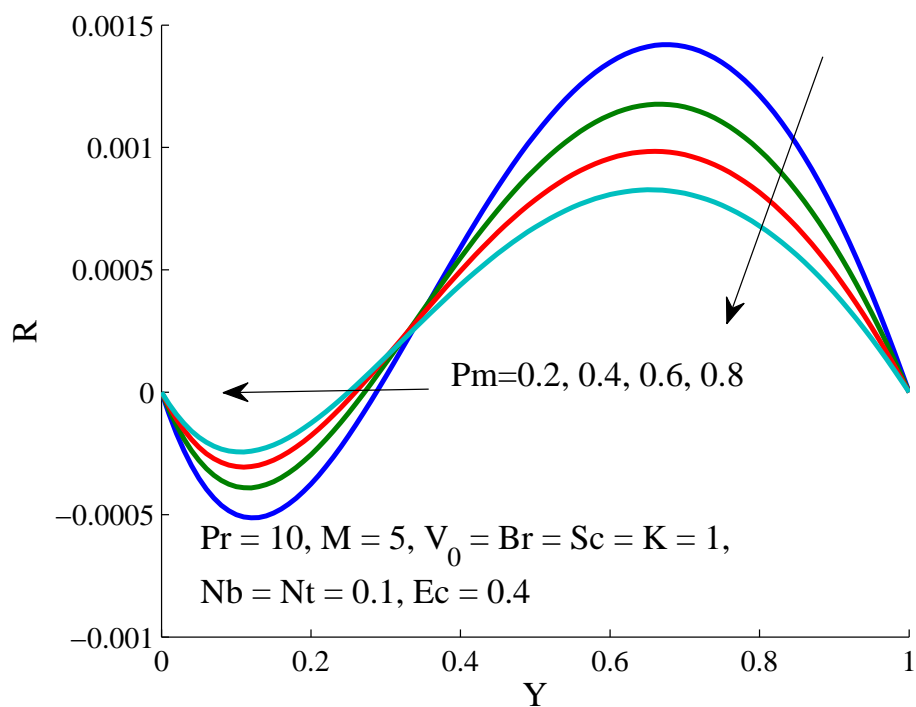
FIGURE 5.5: Impact of Hartmann number M on the velocity.

FIGURE 5.6: Impact of Hartmann number M on the angular momentum.FIGURE 5.7: Impact of Hartmann number M on the induced magnetic field.

FIGURE 5.8: Impact of rotation parameter K on the velocity.FIGURE 5.9: Impact of rotation parameter K on the angular momentum.

FIGURE 5.10: Impact of rotation parameter K on the induced magnetic field.FIGURE 5.11: Impact of buoyancy ratio Br on the velocity.

FIGURE 5.12: Impact of buoyancy ratio Br on the angular momentum.FIGURE 5.13: Impact of buoyancy ratio Br on the induced magnetic field.

FIGURE 5.14: Impact of magnetic Prandtl number Pm on the velocity.FIGURE 5.15: Impact of magnetic Prandtl number Pm on the momentum.

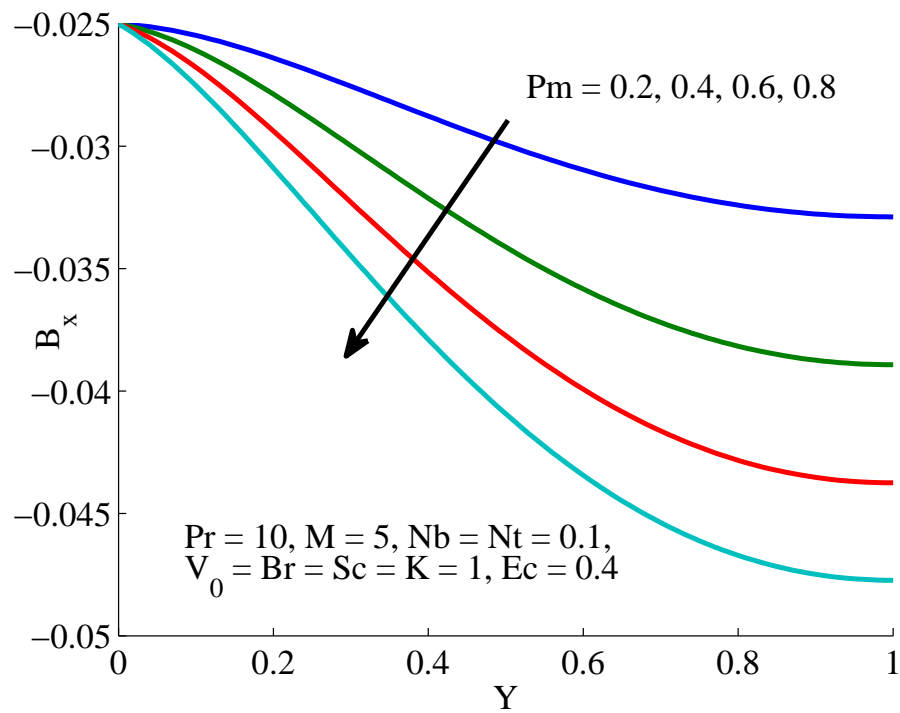


FIGURE 5.16: Impact of magnetic Prandtl number Pm on the induced magnetic field.

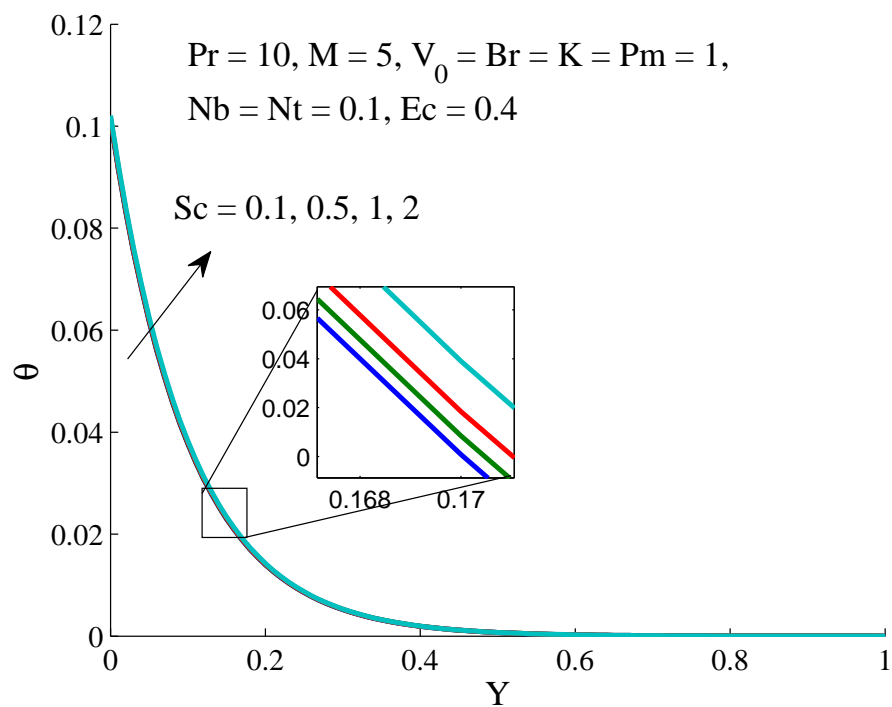
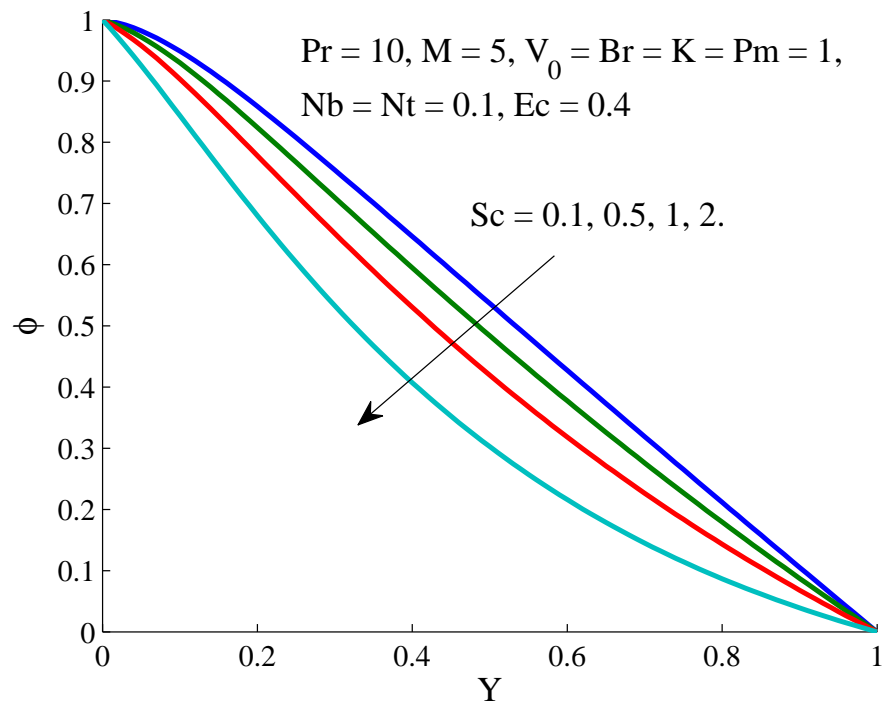
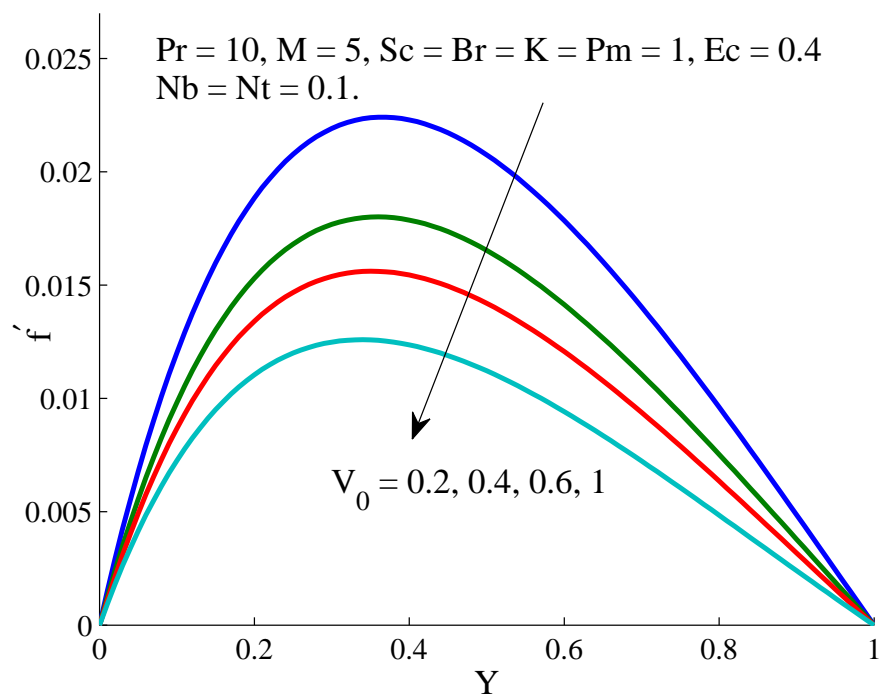
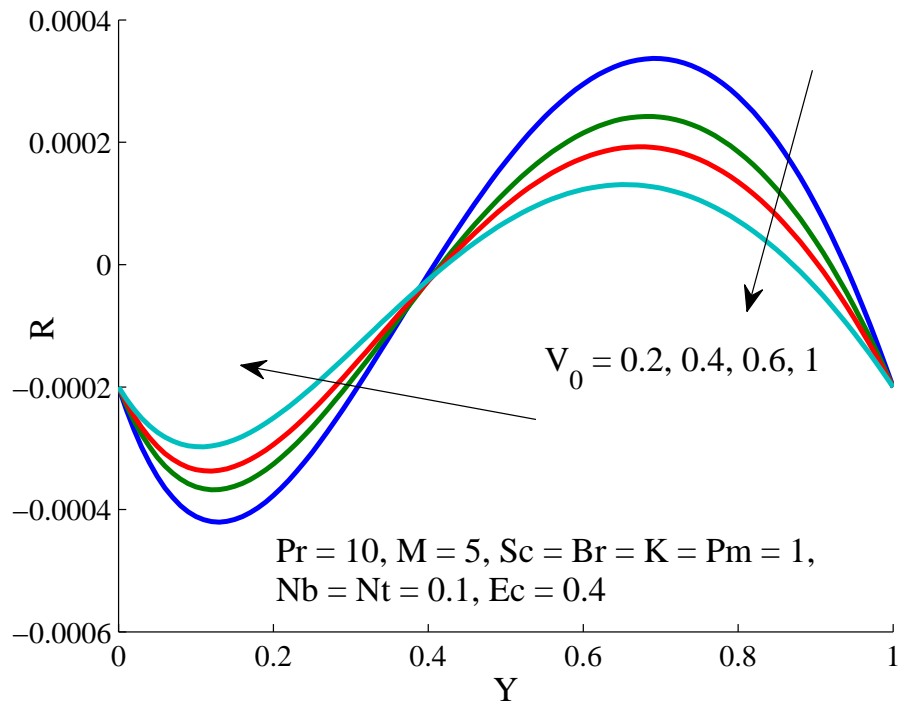
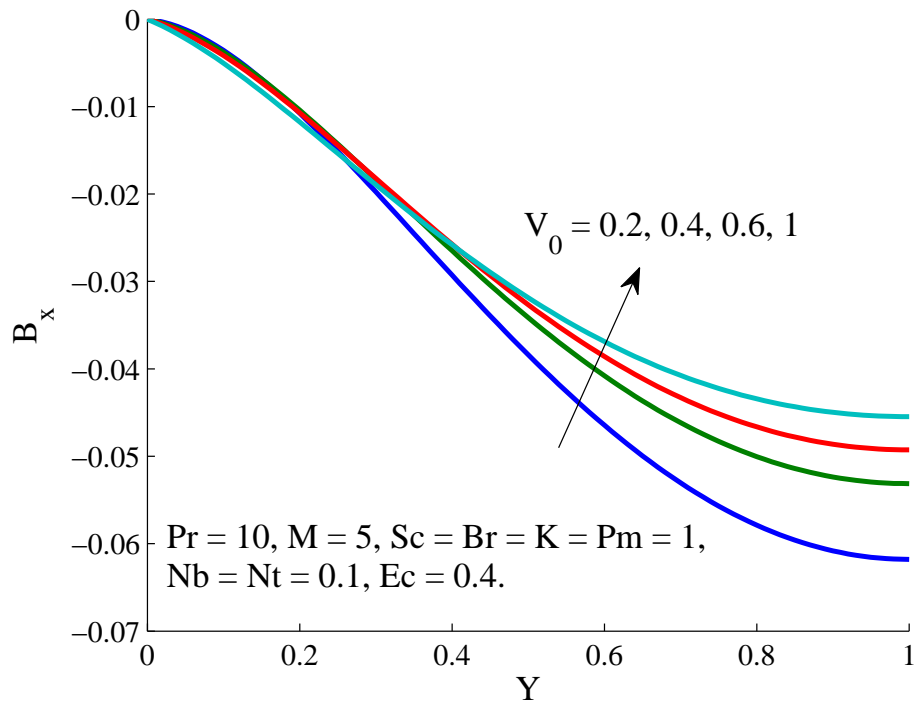
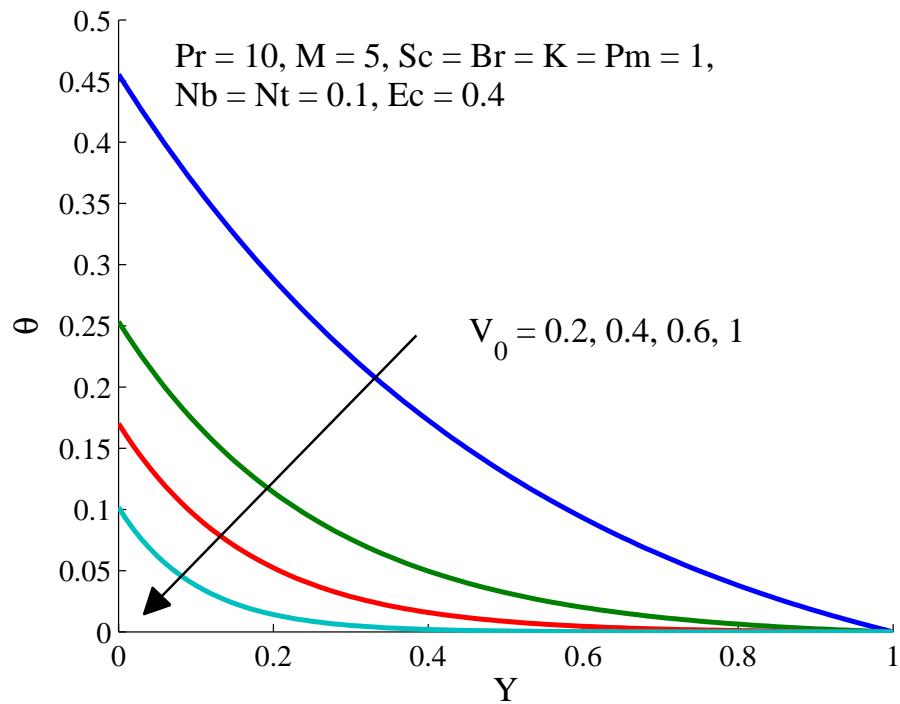
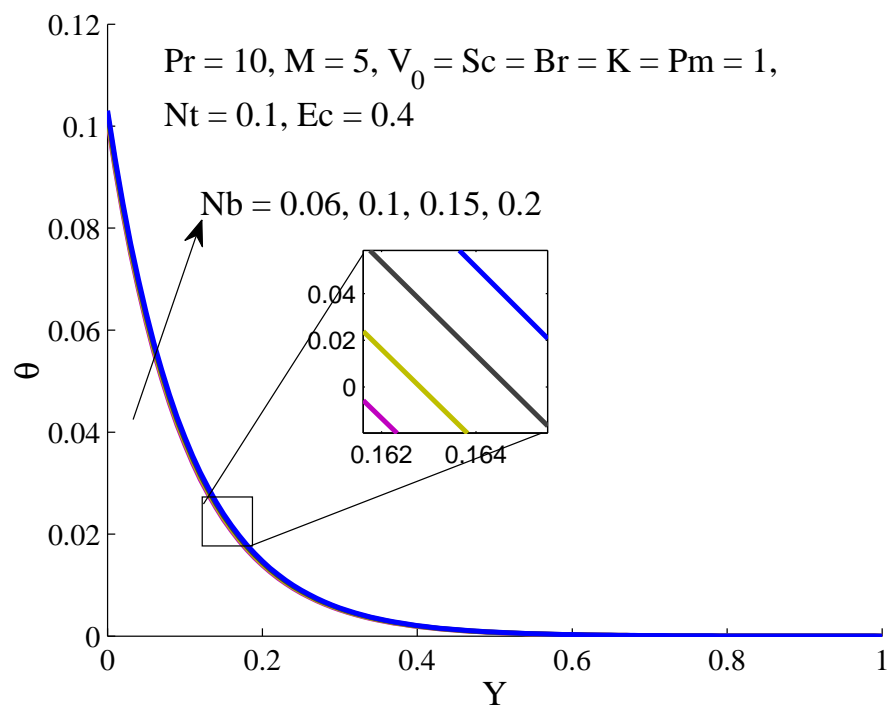
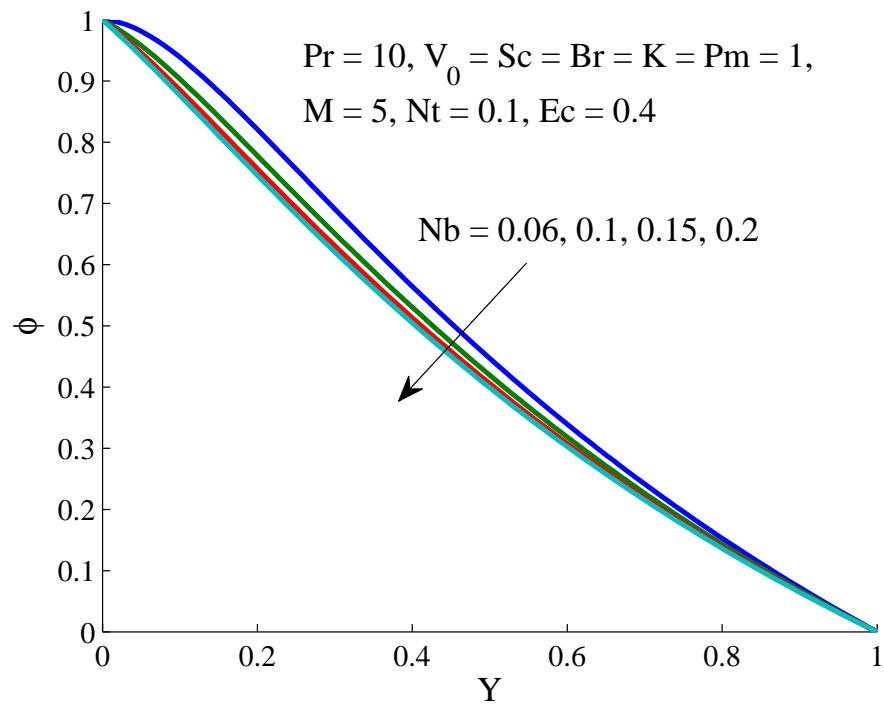
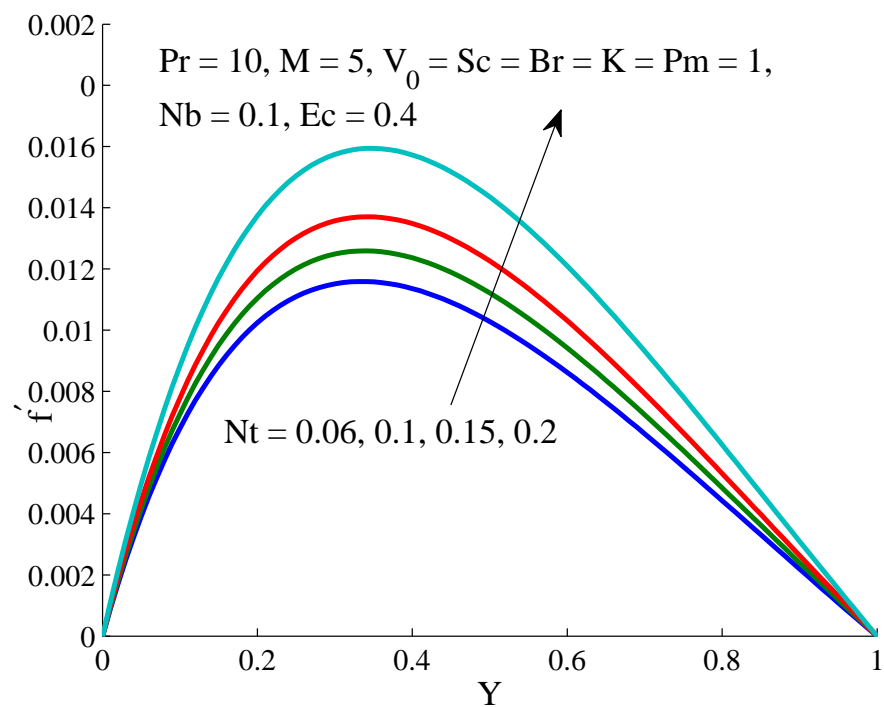


FIGURE 5.17: Impact of Schmidt number Sc on the temperature.

FIGURE 5.18: Impact of Schmidt number Sc on the concentration.FIGURE 5.19: Impact of suction parameter V_0 on the velocity.

FIGURE 5.20: Impact of suction parameter V_0 on the angular momentum.FIGURE 5.21: Impact of suction parameter V_0 on the induced magnetic field.

FIGURE 5.22: Impact of suction parameter V_0 on the temperature.FIGURE 5.23: Impact of Brownian motion parameter Nb on the temperature.

FIGURE 5.24: Impact of Brownian motion parameter Nb on the concentration.FIGURE 5.25: Impact of thermophoresis parameter Nt on the velocity.

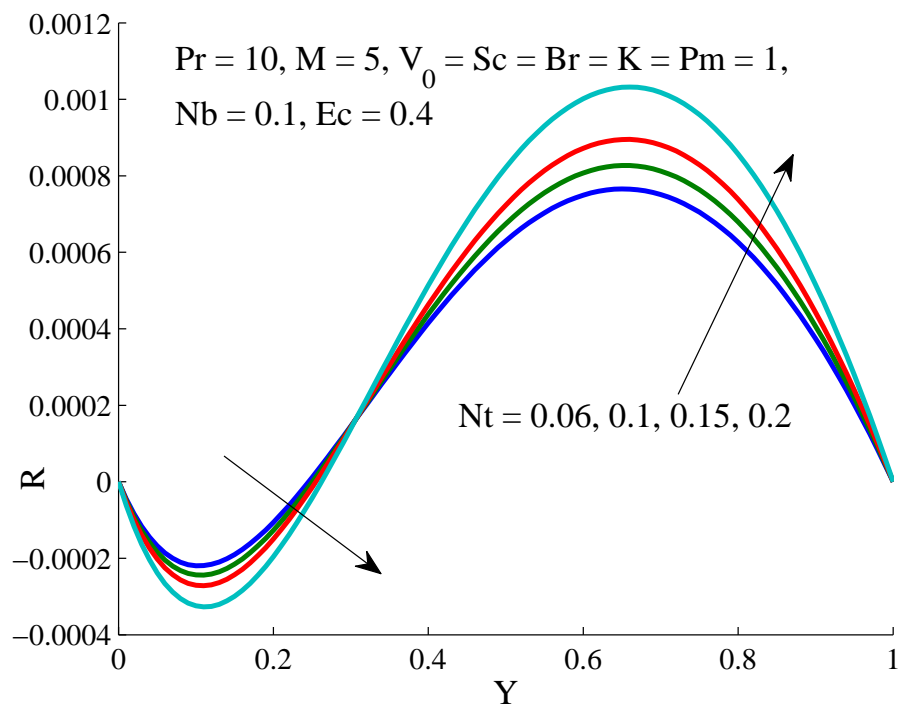


FIGURE 5.26: Impact of thermophoresis parameter N_t on the angular momentum.

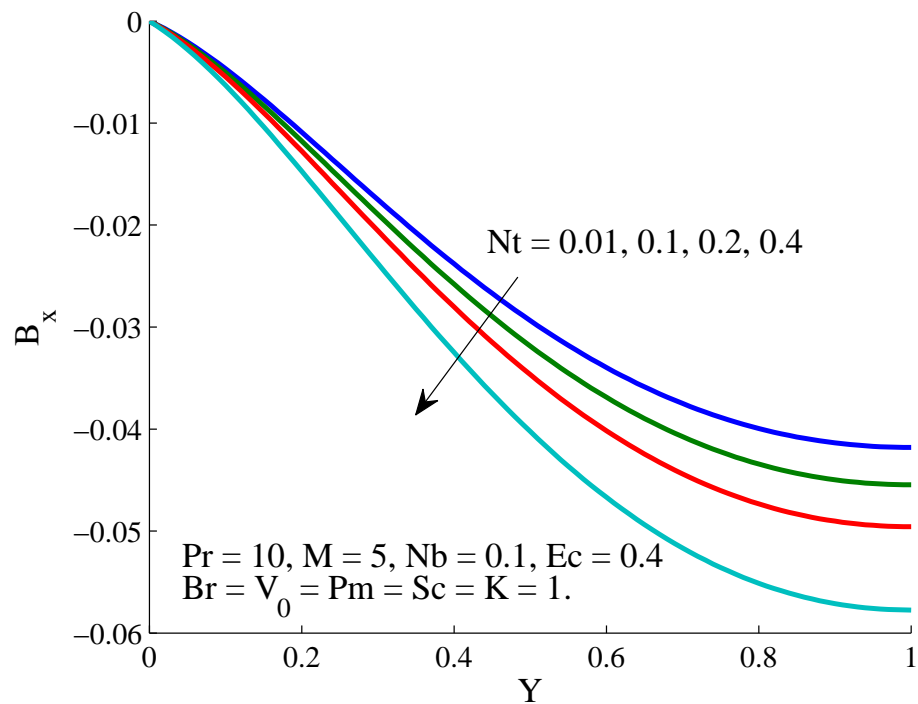


FIGURE 5.27: Impact of thermophoresis parameter N_t on the induced magnetic field.

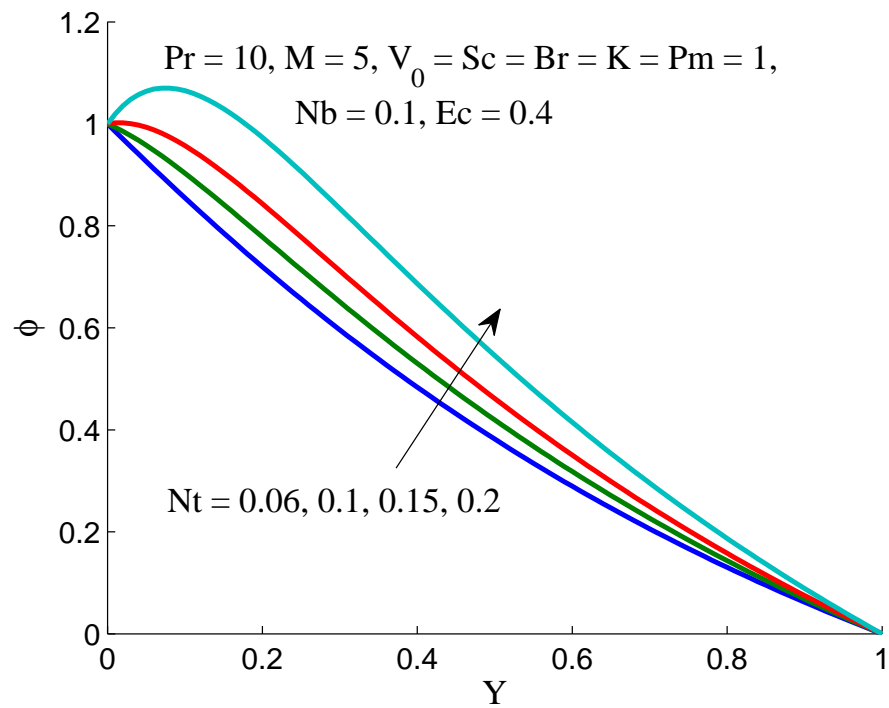


FIGURE 5.28: Impact of thermophoresis parameter Nt on the concentration.

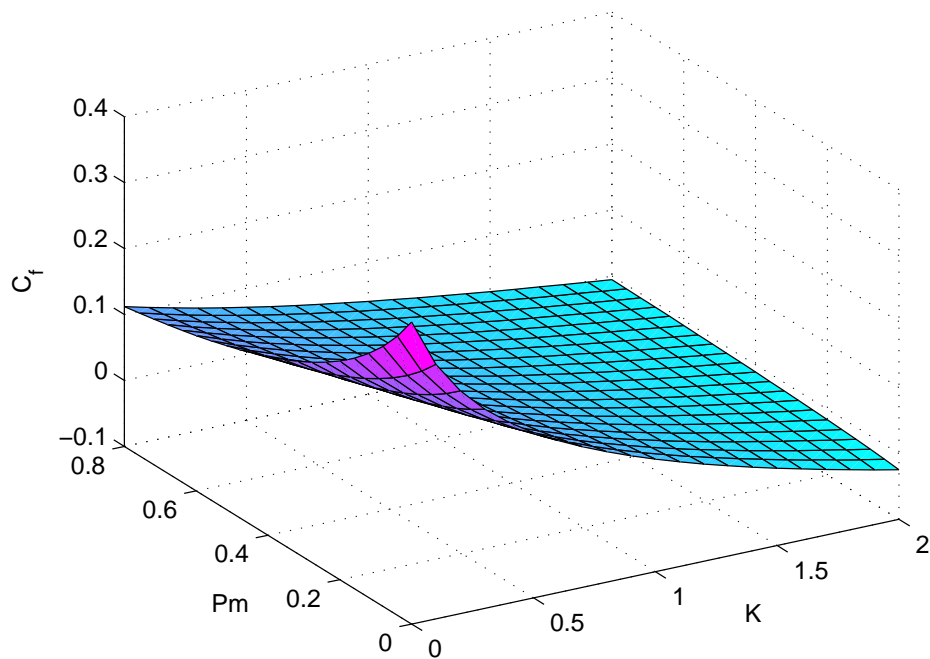


FIGURE 5.29: Skin friction as a function of Pm and K for $Pr = 10$, $M = 5$, $V_0 = 1$, $Nt = 0.1$, $Br = 1$, $Sc = 1$.

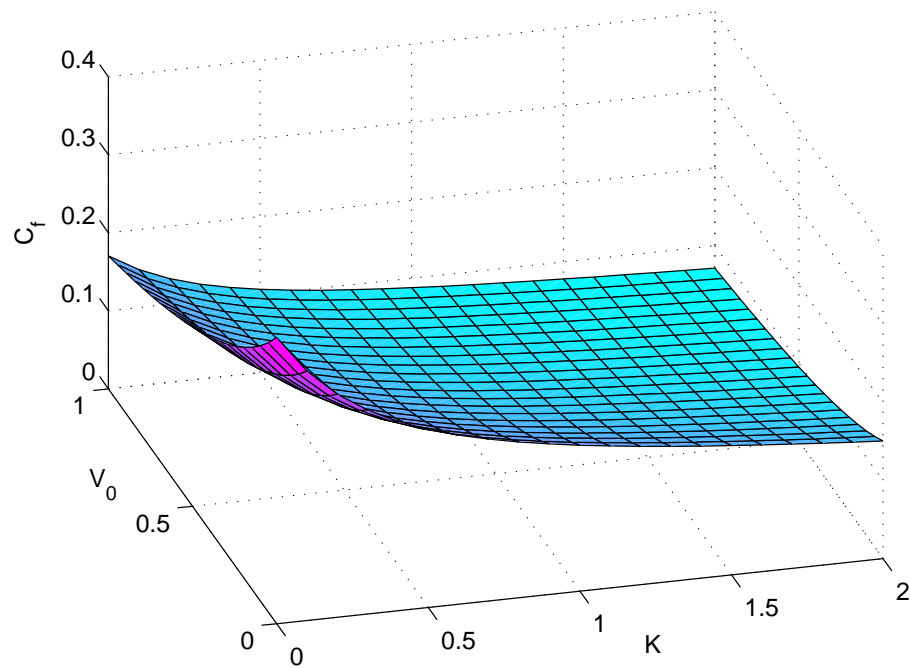


FIGURE 5.30: Skin friction as a function of Pm and V_0 for $Pr = 10$, $M = 5$, $K = 1$, $Nt = 0.1$, $Br = 1$, $Sc = 1$.

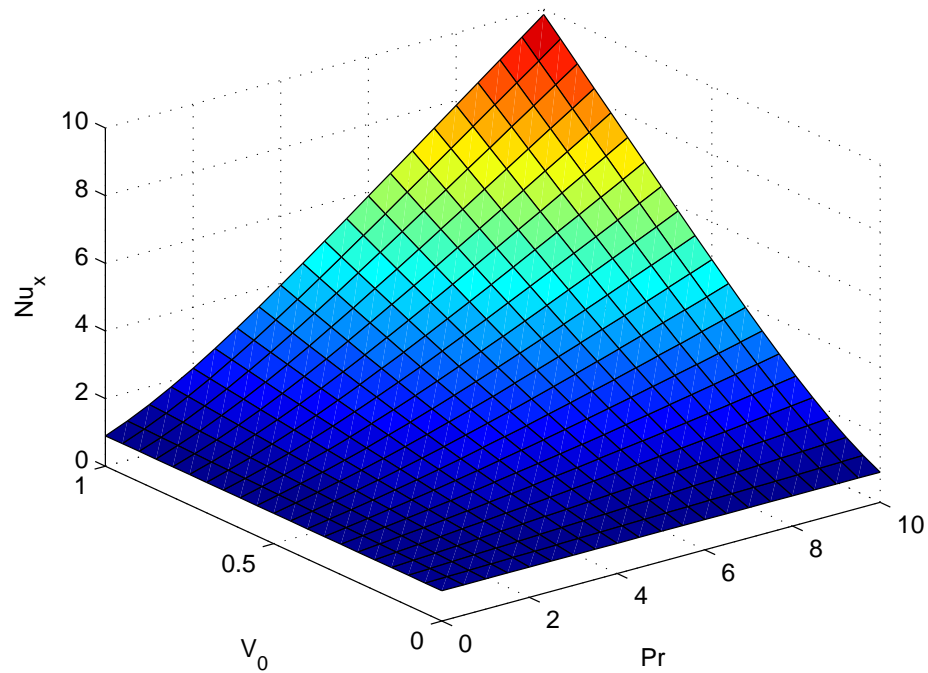


FIGURE 5.31: Nusselt number as a function of Pr and V_0 for $Pm = 1$, $M = 5$, $K = 1$, $Nt = 0.1$, $Br = 1$, $Ec = 0.4$, $Sc = 1$.

5.5 Conclusion

The present chapter throws light on the impact of the induced magnetic field coupled with microrotating particles within the composition of the nanofluids. The basis of the study was the theoretical analysis of the flow and heat transfer using Navier- Stokes equations, angular momentum equation along with the Maxwell equations of electromagnetism. The numerical scheme of Keller box is utilized to solve the nondimensional system. The main findings of the study can be summarized as follows.

- Hartmann number, magnetic Prandtl number and material parameter K reduce the fluid velocity and the skin friction.
- The suction velocity enhances the heat transfer rate in the nanofluids.
- The rising values of the buoyancy ratio increase the fluid velocity and the Nusselt number but causes a decrement in the temperature of the fluid.
- The heat transfer rate is found to increase for increasing values of the thermophoresis parameter while the random motion of the nanoparticles makes the heat transfer rate to reduce.
- Schmidt number enhancement results in shrinking of the concentration profile thickness.

Chapter 6

Conclusion and Future Work

6.1 Conclusion

In the present dissertation, the flow analysis of heat and mass transfer for different fluids is carried out. The single-phase models, that is Tiwari-Das and Buongiorno models are utilized for the flow analysis. Tiwari-Das model is considered in Chapter 3 and Buongiorno model is used in Chapters 4 and 5. This work is mainly focused on nanofluids. The effects of Lorentz forces, Joule heating and induced magnetic field are taken into account in different chapters. Both Newtonian and non-Newtonian nanofluids are used in Chapter 3 and Chapters 4 & 5 respectively. Cattaneo–Christov heat flux model is analyzed in Chapter 3. Micropolar fluid with nano-particles is taken into account in Chapters 4 and 5.

Governing PDEs are modeled for the boundary layer flow over the surface and in the boundary layer and are then converted to nondimensional ODEs. Finite difference method (Keller box method) is employed on these ODEs for the numerical solution. The change in velocity and thermal boundary layer is monitored for the variation in the physical parameters emerging in the ODEs with the help of graphs. The heat transfer in the boundary layer flow was investigated by calculating the values of Nusselt number. Sherwood number describes the mass transfer in the boundary layer flow. Skin friction coefficient was evaluated to find the drag force

at the surface. Some important and outstanding findings are summarized here.

- With an increase in the magnetic parameter, the velocity is reduced but the temperature of the system became higher.
- A rise in relaxation time parameter results in a fall in the temperature.
- For increasing volume fraction, temperature of the system decreases.
- High positive squeezing parameter values result in an increment in the velocity of the fluid and the temperature. For negative values of the squeezing parameter, the temperature and the velocity of the system both decrease.
- Brownian motion reduces the heat transfer rate and velocity of the fluid and the concentration of the fluid is also decreased.
- With an upsurge in the values of the thermophoresis parameter, the heat transfer rate increases and the concentration profile rises up.
- The growing Prandtl number decreases the temperature but augments the concentration profile near the wall.
- Schmidt number reduces the concentration profile and the concentration boundary layer thickness.
- The greater K affects positively on the velocity of the nanofluid near the wall, which in return reduces the effects of the angular velocity. However, as we move away from the wall, the linear velocity tends to decrease which results an increase in the angular velocity of the nanofluid.
- In case of shear thinning fluid as we increase the value of power-law index the temperature of the fluid decreases while the concentration is increased.
- With the growing values of the induced magnetic parameter the velocity and the skinfriction decreased whereas the temperature increases.
- Due to increase in the value of the bouncy ratio the velocity and the Nusselt number enhanced but the temperature of the fluid decreased.

- Growing Eckert number enhances the temperature.
- An enhanced suction velocity results in increase in the Nusselt number of the nanofluid due to the fact that because of the obstruction caused by the fluid flowing into the channel.

6.2 Future Work

The work in this dissertation can be extended in many directions. A few of them are listed below:

- Single phase nanofluid models are used in the present study, in place of these models two phase nanofluid models like Eulerian-Eulerian, mixture and Eulerian-Lagrangian can be used.
- Fluid models like Bird–Carreau model, Herschel–Bulkley model, Williamson fluid model, Maxwell fluid model, Jeffery model can also be opted.
- Different set of boundary conditions like convective and slip, porous plates can be used. Viscous dissipation, Soret and Dufour effects can also be considered.
- Water is considered as the base fluid in the present study. We can try other base fluids like kerosene oil, engine oil and ethylene glycol, as well.
- Nano-particles like ferrous oxides, titanium oxide and carbon nano tubes can be used in place of aluminum oxide and copper nano-particles to find their effect on the heat transfer rate.

Bibliography

- [1] H. Masuda, A. Ebata, K. Teramae, and N. Hishinuma, “Alteration of thermal conductivity and viscosity of liquid by dispersing ultra-fine particles. Dispersion of Al_2O_3 , SiO_2 and TiO_2 ultra-fine particles,” *Netsu Bussei*, vol. 7, no. 4, pp. 227–233, 1993.
- [2] S. U. S. Choi and J. A. Eastman, “Enhancing thermal conductivity of fluids with nanoparticles,” Argonne National Lab., IL (United States), Tech. Rep., 1995.
- [3] Y. Li, S. Tung, E. Schneider, S. Xi *et al.*, “A review on development of nanofluid preparation and characterization,” *Powder technology*, vol. 196, no. 2, pp. 89–101, 2009.
- [4] S. Peyghambarzadeh, S. Hashemabadi, M. Naraki, and Y. Vermahmoudi, “Experimental study of overall heat transfer coefficient in the application of dilute nanofluids in the car radiator,” *Applied Thermal Engineering*, vol. 52, no. 1, pp. 8–16, 2013.
- [5] M. Naraki, S. Peyghambarzadeh, S. Hashemabadi, and Y. Vermahmoudi, “Parametric study of overall heat transfer coefficient of CuO /water nanofluids in a car radiator,” *International Journal of Thermal Sciences*, vol. 66, pp. 82–90, 2013.
- [6] H. M. Ali, H. Ali, H. Liaquat, H. T. B. Maqsood, and M. A. Nadir, “Experimental investigation of convective heat transfer augmentation for car radiator using ZnO -water nanofluids,” *Energy*, vol. 84, pp. 317–324, 2015.

- [7] H. M. Ali, M. D. Azhar, M. Saleem, Q. S. Saeed, and A. Saieed, "Heat transfer enhancement of car radiator using aqua based magnesium oxide nanofluids." *Thermal Science*, vol. 19, no. 6, 2015.
- [8] M. Elias, I. Mahbubul, R. Saidur, M. Sohel, I. Shahrul, S. Khaleduzza-man, and S. Sadeghipour, "Experimental investigation on the thermo-physical properties of Al_2O_3 nanoparticles suspended in car radiator coolant," *International Communications in Heat and Mass Transfer*, vol. 54, pp. 48–53, 2014.
- [9] B. P. S. Tomar and A. Tripathi, "Experimental study of heat transfer of a car radiator with nano fluid- Al_2O_3 water mixture as coolant," *International Journal of Advanced Research in Science, Engineering and Technology*, vol. 2, no. 9, pp. 830–7, 2015.
- [10] M. Ebrahimi, M. Farhadi, K. Sedighi, and S. Akbarzade, "Experimental investigation of force convection heat transfer in a car radiator filled with sio 2–water nanofluid," *International Journal of Engineering, Transactions B: Applications*, vol. 27, no. 2, pp. 333–340, 2014.
- [11] S. A. M. Mehryan, M. Izadi, and M. A. Sheremet, "Analysis of conjugate natural convection within a porous square enclosure occupied with micropolar nanofluid using local thermal non-equilibrium model," *Journal of Molecular Liquids*, 2017.
- [12] A. Hussanan, M. Z. Salleh, I. Khan, and S. Shafie, "Convection heat transfer in micropolar nanofluids with oxide nanoparticles in water, kerosene and engine oil," *Journal of Molecular Liquids*, vol. 229, pp. 482–488, 2017.
- [13] H. Hashemi, Z. Namazian, and S. A. M. Mehryan, "Cu-water micropolar nanofluid natural convection within a porous enclosure with heat generation," *Journal of Molecular Liquids*, vol. 236, pp. 48–60, 2017.
- [14] K. L. Hsiao, "Micropolar nanofluid flow with MHD and viscous dissipation effects towards a stretching sheet with multimedia feature," *International Journal of Heat and Mass Transfer*, vol. 112, pp. 983–990, 2017.

- [15] K. Mehmood, S. Hussain, and M. Sagheer, “Mixed convection in alumina-water nanofluid filled lid-driven square cavity with an isothermally heated square blockage inside with magnetic field effect: Introduction,” *International Journal of Heat and Mass Transfer*, vol. 109, pp. 397–409, 2017.
- [16] S. Hussain, K. Mehmood, and M. Sagheer, “MHD mixed convection and entropy generation of water–alumina nanofluid flow in a double lid driven cavity with discrete heating,” *Journal of Magnetism and Magnetic Materials*, vol. 419, pp. 140–155, 2016.
- [17] H. Xu, S. J. Liao, and I. Pop, “Series solution of unsteady boundary layer flows of non-Newtonian fluids near a forward stagnation point,” *Journal of non-Newtonian Fluid Mechanics*, vol. 139, no. 1-2, pp. 31–43, 2006.
- [18] A. Postelnicu and I. Pop, “Falkner–Skan boundary layer flow of a power-law fluid past a stretching wedge,” *Applied Mathematics and Computation*, vol. 217, no. 9, pp. 4359–4368, 2011.
- [19] A. Ishak, Y. Y. Lok, and I. Pop, “Stagnation-point flow over a shrinking sheet in a micropolar fluid,” *Chemical Engineering Communications*, vol. 197, no. 11, pp. 1417–1427, 2010.
- [20] A. Malvandi and D. D. Ganji, “Analytical study on accelerating falling of non-spherical particle in viscous fluid,” *International Journal of Sediment Research*, vol. 29, no. 3, pp. 423–430, 2014.
- [21] S. A. Moshizi, A. Malvandi, D. D. Ganji, and I. Pop, “A two-phase theoretical study of Al_2O_3 –water nanofluid flow inside a concentric pipe with heat generation/absorption,” *International Journal of Thermal Sciences*, vol. 84, pp. 347–357, 2014.
- [22] A. Malvandi, “The unsteady flow of a nanofluid in the stagnation point region of a time-dependent rotating sphere,” *Thermal Science*, vol. 19, no. 5, pp. 1603–1612, 2015.

- [23] Y. Xuan and Q. Li, "Heat transfer enhancement of nanofluids," *International Journal of Heat and Fluid Flow*, vol. 21, no. 1, pp. 58–64, 2000.
- [24] Y. R. Sekhar, K. V. Sharma, R. T. Karupparaj, and C. Chiranjeevi, "Heat transfer enhancement with Al_2O_3 nanofluids and twisted tapes in a pipe for solar thermal applications," *Procedia Engineering*, vol. 64, pp. 1474–1484, 2013.
- [25] J. Albadr, S. Tayal, and M. Alasadi, "Heat transfer through heat exchanger using Al_2O_3 nanofluid at different concentrations," *Case Studies in Thermal Engineering*, vol. 1, no. 1, pp. 38–44, 2013.
- [26] R. Dharmalingam, K. K. Sivagnanaprabhu, B. S. Kumar, and R. Thirumalai, "Nano materials and nanofluids: An innovative technology study for new paradigms for technology enhancement," *Procedia Engineering*, vol. 97, pp. 1434–1441, 2014.
- [27] C. S. K. Raju, N. Sandeep, and V. Sugunamma, "Unsteady magneto-nanofluid flow caused by a rotating cone with temperature dependent viscosity: A surgical implant application," *Journal of Molecular Liquids*, vol. 222, pp. 1183–1191, 2016.
- [28] R. S. R. Gorla and A. J. Chamkha, "Natural convective boundary layer flow over a nonisothermal vertical plate embedded in a porous medium saturated with a nanofluid," *Nanoscale and Microscale Thermophysical Engineering*, vol. 15, no. 2, pp. 81–94, 2011.
- [29] A. J. Chamkha, S. Abbasbandy, A. M. Rashad, and K. Vajravelu, "Radiation effects on mixed convection about a cone embedded in a porous medium filled with a nanofluid," *Meccanica*, vol. 48, no. 2, pp. 275–285, 2013.
- [30] C. R. Reddy, P. V. S. N. Murthy, A. J. Chamkha, and A. M. Rashad, "Soret effect on mixed convection flow in a nanofluid under convective boundary condition," *International Journal of Heat and Mass Transfer*, vol. 64, pp. 384–392, 2013.

- [31] P. S. Reddy and A. J. Chamkha, "Soret and Dufour effects on MHD convective flow of Al_2O_3 -water and TiO_2 -water nanofluids past a stretching sheet in porous media with heat generation/absorption," *Advanced Powder Technology*, vol. 27, no. 4, pp. 1207–1218, 2016.
- [32] P. S. Reddy, P. Sreedevi, and A. J. Chamkha, "MHD boundary layer flow, heat and mass transfer analysis over a rotating disk through porous medium saturated by Cu -water and ag-water nanofluid with chemical reaction," *Powder Technology*, vol. 307, pp. 46–55, 2017.
- [33] O. Mahian, L. Kolsi, M. Amani, P. Estellé, G. Ahmadi, C. Kleinstreuer, J. S. Marshall, M. Siavashi, R. A. Taylor, H. Niazmand *et al.*, "Recent advances in modeling and simulation of nanofluid flows-part i: Fundamentals and theory," *Physics reports*, vol. 790, pp. 1–48, 2019.
- [34] Y. Ding and D. Wen, "Particle migration in a flow of nanoparticle suspensions," *Powder Technology*, vol. 149, no. 2-3, pp. 84–92, 2005.
- [35] O. Mahian, L. Kolsi, M. Amani, P. Estellé, G. Ahmadi, C. Kleinstreuer, J. S. Marshall, M. Siavashi, R. A. Taylor, H. Niazmand *et al.*, "Recent advances in modeling and simulation of nanofluid flows-part i: fundamental and theory," *Physics reports*, 2018.
- [36] Z. Zhang and Q. Chen, "Comparison of the eulerian and lagrangian methods for predicting particle transport in enclosed spaces," *Atmospheric environment*, vol. 41, no. 25, pp. 5236–5248, 2007.
- [37] P. Davidson, "An introduction to magnetohydrodynamics (cambridge university press, cambridge, 2001)."
- [38] M. Sheikholeslami, M. Rashidi, and D. Ganji, "Effect of non-uniform magnetic field on forced convection heat transfer of Fe_3O_4 -water nanofluid," *Computer Methods in Applied Mechanics and Engineering*, vol. 294, pp. 299–312, 2015.
- [39] A. Kabeel, E. M. El-Said, and S. Dafea, "A review of magnetic field effects on flow and heat transfer in liquids: present status and future potential for

- studies and applications,” *Renewable and Sustainable Energy Reviews*, vol. 45, pp. 830–837, 2015.
- [40] B. M’hamed, N. A. C. Sidik, M. N. A. W. M. Yazid, R. Mamat, G. Najafi, and G. Kefayati, “A review on why researchers apply external magnetic field on nanofluids,” *International Communications in Heat and Mass Transfer*, vol. 78, pp. 60–67, 2016.
- [41] A. Dogonchi, K. Divsalar, and D. Ganji, “Flow and heat transfer of MHD nanofluid between parallel plates in the presence of thermal radiation,” *Computer Methods in Applied Mechanics and Engineering*, vol. 310, pp. 58–76, 2016.
- [42] P. Ariel, “A numerical experiment in the simulation of MHD flow of a power law fluid through a duct,” *Computer methods in applied mechanics and engineering*, vol. 106, no. 3, pp. 367–380, 1993.
- [43] L. M. Monzon and J. Coey, “Magnetic fields in electrochemistry: The kelvin force. a mini-review,” *Electrochemistry Communications*, vol. 42, pp. 42–45, 2014.
- [44] A. Afifah, S. Syahrullail, and N. Sidik, “Magnetoviscous effect and thermomagnetic convection of magnetic fluid: A review,” *Renewable and Sustainable Energy Reviews*, vol. 55, pp. 1030–1040, 2016.
- [45] F. Mabood, W. Khan, and A. M. Ismail, “MHD flow over exponential radiating stretching sheet using homotopy analysis method,” *Journal of King Saud University-Engineering Sciences*, vol. 29, no. 1, pp. 68–74, 2017.
- [46] M. Rashidi, S. Bagheri, E. Momoniat, and N. Freidoonimehr, “Entropy analysis of convective MHD flow of third grade non-newtonian fluid over a stretching sheet,” *Ain Shams Engineering Journal*, vol. 8, no. 1, pp. 77–85, 2017.
- [47] A. Raptis, “Effects of thermal radiation on the MHD flow past a vertical plate,” *Journal of Engineering Thermophysics*, vol. 26, no. 1, pp. 53–59, 2017.

- [48] R. Kandasamy, R. Dharmalingam, and K. S. Prabhu, "Thermal and solutal stratification on MHD nanofluid flow over a porous vertical plate," *Alexandria engineering journal*, vol. 57, no. 1, pp. 121–130, 2018.
- [49] H. F. Öztop, A. Sakhrieh, E. Abu-Nada, and K. Al-Salem, "Mixed convection of MHD flow in nanofluid filled and partially heated wavy walled lid-driven enclosure," *International Communications in Heat and Mass Transfer*, vol. 86, pp. 42–51, 2017.
- [50] A. H. P. Skelland, "Non-newtonian flow and heat transfer (book on quantitative relationships for non-newtonian systems, considering classification and fluid behavior of materials with anomalous flow properties)," *New York, John Wiley and Sons, INC., 1967. 469 P*, 1967.
- [51] J. D. Anderson, "Ludwig prandtl's boundary layer," *Physics Today*, vol. 58, no. 12, pp. 42–48, 2005.
- [52] F. Pinto and M. Meo, "Design and manufacturing of a novel shear thickening fluid composite (stfc) with enhanced out-of-plane properties and damage suppression," *Applied Composite Materials*, vol. 24, no. 3, pp. 643–660, 2017.
- [53] A. C. Eringen, "Theory of micropolar fluids," *Journal of Mathematics and Mechanics*, pp. 1–18, 1966.
- [54] V. K. Stokes, "Couple stresses in fluids," *The Physics of Fluids*, vol. 9, no. 9, pp. 1709–1715, 1966.
- [55] J. D. Lee and A. C. Eringen, "Wave propagation in nematic liquid crystals," *The Journal of Chemical Physics*, vol. 54, no. 12, pp. 5027–5034, 1971.
- [56] J. D. Lee and A. C. Eringen, "Boundary effects of orientation of nematic liquid crystals," *The Journal of Chemical Physics*, vol. 55, no. 9, pp. 4509–4512, 1971.
- [57] S. J. Allen and K. A. Kline, "A theory of mixtures with microstructure," *Zeitschrift für angewandte Mathematik und Physik ZAMP*, vol. 20, no. 2, pp. 145–155, 1969.

- [58] K. A. Kline and S. J. Allen, “The relationship of pressure gradient to blood velocity based on a continuum theory of blood,” *Journal of Biomechanics*, vol. 2, no. 3, pp. 313–318, 1969.
- [59] T. Ariman, “On the analysis of blood flow,” *Journal of Biomechanics*, vol. 4, no. 3, pp. 185–192, 1971.
- [60] J. J. Shu and J. S. Lee, “Fundamental solutions for micropolar fluids,” *Journal of Engineering Mathematics*, vol. 61, no. 1, pp. 69–79, 2008.
- [61] P. Muthu, B. V. K. Rathish, and P. Chandra, “A study of micropolar fluid in an annular tube with application to blood flow,” *Journal of Mechanics in Medicine and Biology*, vol. 8, no. 4, pp. 561–576, 2008.
- [62] J. Chen, C. Liang, and J. D. Lee, “Theory and simulation of micropolar fluid dynamics,” *Proceedings of the Institution of Mechanical Engineers, Part N: Journal of Nanoengineering and Nanosystems*, vol. 224, no. 1-2, pp. 31–39, 2010.
- [63] M. Z. Haque, M. M. Alam, M. Ferdows, and A. Postelnicu, “Micropolar fluid behaviors on steady MHD free convection and mass transfer flow with constant heat and mass fluxes, Joule heating and viscous dissipation,” *Journal of King Saud University-Engineering Sciences*, vol. 24, no. 2, pp. 71–84, 2012.
- [64] I. L. Animasaun, “Melting heat and mass transfer in stagnation point micropolar fluid flow of temperature dependent fluid viscosity and thermal conductivity at constant vortex viscosity,” *Journal of the Egyptian Mathematical Society*, vol. 25, no. 1, pp. 79–85, 2017.
- [65] P. J. Pritchard and J. W. Mitchell, *Fox and McDonald’s introduction to fluid mechanics*. John Wiley & Sons, 2016.
- [66] M. C. Potter and E. P. Scott, *Thermal sciences: An introduction to thermodynamics, fluid mechanics, and heat transfer*. Brooks/Cole Publishing Company, 2004.

- [67] J. Fourier, “Théorie analytique de chaleur. chez firmin didot, père et fils,” 1822.
- [68] C. Christov, “On frame indifferent formulation of the maxwell–cattaneo model of finite-speed heat conduction,” *Mechanics Research Communications*, vol. 36, no. 4, pp. 481–486, 2009.
- [69] J. Buongiorno, “Convective transport in nanofluids,” *Journal of heat transfer*, vol. 128, no. 3, pp. 240–250, 2006.
- [70] N. Akmal, M. Sagheer, S. Hussain, and A. Kamran, “Investigation of free convection in micropolar nanofluid with induced magnetic field,” *The European Physical Journal Plus*, vol. 134, no. 5, p. 235, 2019.
- [71] R. K. Tiwari and M. K. Das, “Heat transfer augmentation in a two-sided lid-driven differentially heated square cavity utilizing nanofluids,” *International Journal of heat and Mass transfer*, vol. 50, no. 9-10, pp. 2002–2018, 2007.
- [72] M. Levin and M. Miller, “Maxwell a treatise on electricity and magnetism,” *Uspekhi Fizicheskikh Nauk*, vol. 135, no. 3, pp. 435–441, 1981.
- [73] D. M. Kalyon, “Perry’s chemical engineers’ handbook.” *Chemical Engineering*, vol. 104, no. 12, p. 12, 1997.
- [74] Y. Xuan and W. Roetzel, “Conceptions for heat transfer correlation of nanofluids,” *International Journal of heat and Mass transfer*, vol. 43, no. 19, pp. 3701–3707, 2000.
- [75] H. Schlichting and K. Gersten, *Boundary-layer theory*. Springer, 2016.
- [76] T. Cebeci and P. Bradshaw, *Physical and computational aspects of convective heat transfer*. Springer Science & Business Media, 2012.
- [77] L. C. Woods, “The thermodynamics of fluid systems,” *Chemical Physics*, 1975.
- [78] F. P. Incropera, A. S. Lavine, T. L. Bergman, and D. P. DeWitt, *Fundamentals of heat and mass transfer*. Wiley, 2007.

- [79] M. Bahiraei, “Impact of thermophoresis on nanoparticle distribution in nanofluids,” *Results in Physics*, vol. 7, pp. 136–138, 2017.
- [80] A. Bejan, “The method of entropy generation minimization,” in *Energy and the Environment*. Springer, 1999, pp. 11–22.
- [81] H. B. Keller, “A new difference scheme for parabolic problems,” in *Numerical Solution of Partial Differential Equations–II*. Elsevier, 1971, pp. 327–350.
- [82] N. Muhammad, S. Nadeem, and T. Mustafa, “Squeezed flow of a nanofluid with cattaneo–christov heat and mass fluxes,” *Results in Physics*, vol. 7, pp. 862–869, 2017.
- [83] A. Dogonchi and D. Ganji, “Impact of cattaneo–christov heat flux on MHD nanofluid flow and heat transfer between parallel plates considering thermal radiation effect,” *Journal of the Taiwan Institute of Chemical Engineers*, vol. 80, pp. 52–63, 2017.
- [84] A. Dogonchi and D. Ganji, “Investigation of MHD nanofluid flow and heat transfer in a stretching/shrinking convergent/divergent channel considering thermal radiation,” *Journal of Molecular Liquids*, vol. 220, pp. 592–603, 2016.
- [85] M. Khan *et al.*, “On cattaneo–christov heat flux model for carreau fluid flow over a slendering sheet,” *Results in Physics*, vol. 7, pp. 310–319, 2017.
- [86] K. Gangadhar, K. Ramana, O. D. Makinde, and B. R. Kumar, “Mhd flow of a carreau fluid past a stretching cylinder with cattaneo–christov heat flux using spectral relaxation method,” in *Defect and Diffusion Forum*, vol. 387. Trans Tech Publ, 2018, pp. 91–105.
- [87] S. Eswaramoorthi, M. Bhuvaneshwari, S. Sivasankaran, and O. D. Makinde, “Heterogeneous and homogeneous reaction analysis on mhd oldroyd-b fluid with cattaneo–christov heat flux model and convective heating,” in *Defect and Diffusion Forum*, vol. 387. Trans Tech Publ, 2018, pp. 194–206.
- [88] M. Zubair, Z. Shah, S. Islam, W. Khan, and A. Dawar, “Study of three dimensional darcy–forchheimer squeezing nanofluid flow with cattaneo–christov

- heat flux based on four different types of nanoparticles through entropy generation analysis,” *Advances in Mechanical Engineering*, vol. 11, no. 5, p. 1687814019851308, 2019.
- [89] K. G. Kumar, M. G. Reddy, M. Sudharani, S. Shehzad, and A. J. Chamkha, “Cattaneo–christov heat diffusion phenomenon in reiner–philippoff fluid through a transverse magnetic field,” *Physica A: Statistical Mechanics and Its Applications*, vol. 541, p. 123330, 2020.
- [90] W. Ibrahim and G. Gadisa, “Finite element solution of nonlinear convective flow of oldroyd-b fluid with cattaneo-christov heat flux model over nonlinear stretching sheet with heat generation or absorption,” *Propulsion and Power Research*, vol. 9, no. 3, pp. 304–315, 2020.
- [91] S. Hussain, S. E. Ahmed, and T. Akbar, “Entropy generation analysis in MHD mixed convection of hybrid nanofluid in an open cavity with a horizontal channel containing an adiabatic obstacle,” *International Journal of Heat and Mass Transfer*, vol. 114, pp. 1054–1066, 2017.
- [92] M. Mustafa, T. Hayat, and S. Obaidat, “On heat and mass transfer in the unsteady squeezing flow between parallel plates,” *Meccanica*, vol. 47, no. 7, pp. 1581–1589, 2012.
- [93] J. Sui, P. Zhao, Z. Cheng, L. Zheng, and X. Zhang, “A novel investigation of a micropolar fluid characterized by nonlinear constitutive diffusion model in boundary layer flow and heat transfer,” *Physics of Fluids*, vol. 29, no. 2, p. 023105, 2017.
- [94] A. Kamran, S. Hussain, M. Sagheer, and N. Akmal, “A numerical study of magnetohydrodynamics flow in Casson nanofluid combined with Joule heating and slip boundary conditions,” *Results in physics*, vol. 7, pp. 3037–3048, 2017.
- [95] M. Mustafa, “MHD nanofluid flow over a rotating disk with partial slip effects: Buongiorno model,” *International Journal of Heat and Mass Transfer*, vol. 108, pp. 1910–1916, 2017.

-
- [96] M. Bilal, M. Sagheer, S. Hussain, and Y. Mehmood, “MHD stagnation point flow of williamson fluid over a stretching cylinder with variable thermal conductivity and homogeneous/heterogeneous reaction,” *Communications in Theoretical Physics*, vol. 67, no. 6, p. 688, 2017.
- [97] M. Sheikholeslami and H. B. Rokni, “Nanofluid two phase model analysis in existence of induced magnetic field,” *International Journal of Heat and Mass Transfer*, vol. 107, pp. 288–299, 2017.
- [98] O. Abdulaziz and I. Hashim, “Fully developed free convection heat and mass transfer of a micropolar fluid between porous vertical plates,” *Numerical Heat Transfer, Part A: Applications*, vol. 55, no. 3, pp. 270–288, 2009.